

MASS FLOW AND TEMPERATURE MEASUREMENTS
IN THE FLUE OF A WOODBURNING APPLIANCE

by

Robert M. Bell

Thesis submitted to the Graduate Faculty
of the Virginia Polytechnic Institute and State University
in partial fulfillment of the requirements for the degree of
MASTER OF SCIENCE
IN
MECHANICAL ENGINEERING

APPROVED:


D. R. Jaasma, Chairman


H. L. Wood


T. E. Diller

February 1985
Blacksburg, Virginia

5655
V855
1985
B444
C-2

ACKNOWLEDGEMENTS

The author gives special thanks to Dr. Dennis R. Jaasma for his time and guidance in conducting this research. The author would also like to thank T. E. Diller and H. L. Wood for serving on his committee.

The author would like to thank my wife, Kim, whose love and patience made this goal possible and my family for their support and continuous encouragement.

The support of this project by the Department of Energy under the direction of Mr. Dan Lim is greatly appreciated.

TABLE OF CONTENTS

	<u>Page</u>
ABSTRACT	
ACKNOWLEDGEMENTS	ii
TABLE OF CONTENTS	iii
LIST OF FIGURES	v
LIST OF TABLES	viii
NOMENCLATURE	ix
1. INTRODUCTION	1
2. LITERATURE REVIEW	4
2.1 Methods for Flow Rate Measurements	4
2.2 Suitable Measurement Techniques	8
2.2.1 Tracer Techniques	8
2.2.2 Pitot Array	19
2.2.3 Scale-Based Method	22
2.3 Temperature Measurement	23
2.4 Summary	26
3. EXPERIMENTAL METHODS	28
3.1 General Set-up	28
3.2 Temperature Measurement Systems	31
3.2.1 Thermocouple Array	31
3.2.2 Suction Pyrometer	33
3.2.3 Thermopile	35
3.3 Flow Measurement Systems	36
3.3.1 CO Tracer System	36
3.3.2 Pitot Array Set-up	38
3.3.3 Scale-Based Method	42
3.3.4 General Set-up of the Flow System	45
3.4 Test Procedures	47
3.4.1 Temperature Measurement Procedure	47
3.4.2 Flow Rate Measurement Procedure	48
3.5 Calculation Procedures	51
3.5.1 CO Tracer Flow Rate Calculation	51
3.5.2 Pitot Array Flow Rate Calculation	53
3.5.3 Scale-Based Flow Rate Calculation	54
3.5.4 CO ₂ Tracer and the Thermal Mass Flowmeter Flow Rate Calculation	56

TABLE OF CONTENTS (continued)

	<u>Page</u>
4. RESULTS	61
4.1 Temperature Measurements	61
4.1.1 Burn Rates	61
4.1.2 Temperature Profiles	64
4.1.3 Heat Loss Measurement	73
4.2 Flow Rate Measurements	80
5. DISCUSSION	88
5.1 Temperature Profiles	88
5.2 Flow Measurements	97
5.2.1 CO Tracer	108
5.2.2 Pitot Array	111
5.2.3 Scale-Based Method	112
6. CONCLUSIONS	113
7. RECOMMENDATIONS	115
8. REFERENCES	116
9. APPENDIX A CALIBRATION PROCEDURES	119
A.1 Calibration of the Pitot Array	119
A.2 Calibration of Dilution Tunnel Orifice	126
10. APPENDIX B EXTERNAL ERROR ANALYSIS	129
11. APPENDIX C TEMPERATURE ANALYSIS	135
C.1 Temperature Modeling	135
C.2 Bulk Temperature Calculation	138
12. APPENDIX D FLOW MEASUREMENT DATA	139
VITA	146

LIST OF FIGURES

<u>Figure</u>		<u>Page</u>
1	Dilution Tunnel	12
2	Stove and Flue Gas Handling System Used in Tests	29
3	Schematic of the Shenandoah R-76LC Stove	30
4	Schematic of 16 Thermocouple Array	32
5	Schematic of Suction Pyrometer Measuring Position	34
6	Sampling Train for CO Tracer System	37
7	Top View of Pitot Array	39
8	Side View of Pitot Array	40
9	Sampling Train for Scale-Based Method	43
10	Set-up of Flow Measuring Systems	46
11	Mass-Time History of Fuel Charge from Scale Readings for Run 1	62
12	Mass-Time History of Fuel Charge from Scale Readings for Run 2	63
13	Temperature Profile Recorded Near the Beginning of Run 1	65
14	Temperature Profile Recorded Near the Middle of Run 1	66
15	Temperature Profile Recorded Near the End of Run 1	67
16	Temperature Profile Recorded Near the Beginning of Run 2	68
17	Temperature Profile Recorded Near the Middle of Run 2	69
18	Temperature Profile Recorded Near the End of Run 2	70
19	Average Stack Temperature History for Run 1	71
20	Average Stack Temperature History for Run 2	72

LIST OF FIGURES (continued)

<u>Figure</u>		<u>Page</u>
21	The Effect of a Change in Stack Temperature on the Radial Temperature Difference for Run 1	74
22	The Effect of a Change in Stack Temperature on the Radial Temperature Difference for Run 2	75
23	Mass-Time History from Scale Readings for Run 3	77
24	Stack Temperature History for Run 3	77
25	Mass-Time History from Scale Readings for Run 4	78
26	Stack Temperature History for Run 4	78
27	Mass-Time History from Scale Readings for Run 5	79
28	Stack Temperature History for Run 5	79
29	Comparison of Stack Flows Measured During Run 3	82
30	Comparison of Stack Flows Measured During Run 4	83
31	Comparison of Stack Flows Measured During Run 5	84
32	Comparison of Stack Flows for Run 4 With a Recalculated Scale-Based Flow	86
33	Comparison of Stack Flows for Run 5 With a Recalculated Scale-Based Flow	87
34	Comparison of Aspirated and Non-Aspirated Thermocouple Readings	93
35	Comparison of Measured and Calculated Temperature Differences	95
36	Comparison of Aspirated and Non-Aspirated Fine Gage Thermocouple Readings	96
37.	The Effect of Stack CO Concentrations on Flow Measurements	99
38.	The Effect of Dilution Tunnel CO Concentrations on Flow Measurements	100
39	The Effect of Temperature on Flow Measurements	102
40.	The Effect of Stack Reynolds Number on Flow Measurements	103

LIST OF FIGURES (continued)

	<u>Page</u>
41 Calibration Data of Pitot Array	121

LIST OF TABLES

<u>Table</u>	<u>Page</u>
I. Sensitivities of Potential Stack Flow Rate Measurement Methods to Uncertainties in Flue Gas Properties	5
II. Heat Loss Through Insulated Stove Pipe Section	76
III. Calculated Error in Sensible Energy Loss Using the Centerline Stack Temperature	89
IV. Sensitivity of Scale-Based Flow to Concentration Measurement Errors	105
V. Comparison of "Instantaneous" Burn Rates Measured for Run 4	107
A.1 Initial Pitot Array Calibration Data	122
A.2 Post Run 3 Pitot Array Calibration Data	123
A.3 Post Run 4 Pitot Array Calibration Data	124
A.4 CO Analyzer Calibration Curve Equations	125
D.1 Summary of Flow Measurements from Run 3	140
D.2 Summary of Flow Measurements from Run 4	141
D.3 Summary of Flow Measurements from Run 5	142
D.4 Raw Data of Run 3	143
D.5 Raw Data of Run 4	144
D.6 Raw Data of Run 5	145

NOMENCLATURE

a	moles of wood, kmol
A	cross-sectional area or surface area, m ²
C	calibration coefficient (dimensionless)
C _p	specific heat of flue gas, kJ/kg K
e	uncertainty in the independent variables
E _E	uncertainty in the measurement
F	moles of ambient water per mole of dry ambient room air
\bar{h}	enthalpy of a gas, kJ/kmol
j	moles of water, kmol
J ₀	zeroth order Bessel function of the first kind
k	thermal conductivity, w/mK
m	mass, kg
\dot{m}	mass flow rate, kg/s
MW	molecular weight, kg/kmol
\dot{n}	molar flow rate, kmol/s
P _w	moles of water per mole of dry wood
P	ambient pressure, kPa
\dot{Q}	heat flux, W
R	gas constant, kJ/kg K
\bar{R}	universal gas constant, 8.3143 kJ/kmol
R _w	inner radius of flue pipe, 7.62 cm
S	moles of CO ₂ per mole of dry room air
t	time, s
T	temperature, K
u	velocity in stack, m/s

U_c	heat transfer coefficient, W/m^2K
V_{OUT}	output voltage, volts
V	volume, m^3
x	distance, m

Subscripts

A	room air
AVE	average
b	bulk temperature
DA	dry air
DP	calibration coefficient of pitot array
DT	dilution tunnel
I	entering control volume
IN	heat input
IR	injection rate
m	positive displacement meter
O	out of control volume
OS	outer surface of insulation
OR	dilution tunnel orifice
OUT	heat loss
PA	pitot array
RM	room
S	stack
SUP	from supply bottle
T	target meter
T_m	thermal mass flow meter
w	stack wall

wd wood

Greek Symbols

β ratio of diameters

α thermal diffusivity, m^2/s

Δ difference

ρ density, kg/m^3

λ separation constant

θ, τ, ψ functions as defined in text

σ Stefan-Boltzmann constant, $5.76 \times 10^{-8} \text{ W/m}^2 \text{ K}^4$

ϵ emissivity of outer stack surface

Miscellaneous

[x] mole fraction of x

1. INTRODUCTION

The use of wood stoves for residential heating has been increasing over the past several years. This increased use of wood stoves has caused significant concern about increased air pollution. Development of improved emissions and efficiency measurement methods will allow the development of improved stoves.

Room calorimetry is used as the standard for measuring the energy efficiency of stoves. Unfortunately, this method is expensive and few wood stove manufacturers can afford it. For this reason, flue loss methods which are generally less expensive are attractive.

Flue loss methods measure either directly or indirectly the following instantaneous losses:

1. Sensible energy loss due to the flue gases being at a higher temperature than the ambient.
2. Chemical energy loss from incomplete combustion.
3. Latent energy loss due to water existing as a vapor in the flue gas. This loss is included since the higher heating value of wood is used.

The instantaneous efficiency of the stove can then be determined from measurement of these three losses and the instantaneous energy input.

This project is part of a larger project which has an overall objective to develop an accurate flue loss method. An accurate flue loss method is needed since many of the traditional flue loss methods have unknown accuracies.

The "WHA (Wood Heating Alliance) Test Protocol" [1] is the most common flue loss method used. However, there have been many questions

raised concerning the accuracy of the assumptions as well as some of the measurement techniques used in this protocol. In particular, the methods of measuring the stack flow and stack temperature have unknown accuracy.

In the WHA Protocol, the stack flow rate is calculated from a computational algorithm. The algorithm uses the following assumptions:

1. Uniform burning of the fuel (the fuel remains at a constant elemental composition throughout the burn)
2. The stack flow is gaseous and includes only CO, CO₂, O₂, H₂O, CH₄, and N₂
3. Steady state operation exists
4. Trace elements are neglected.

The flow measurement errors due to these assumptions are unknown.

The WHA protocol uses one shielded thermocouple in the center of the stack to measure the average stack temperature for purposes of evaluating flue gas properties as well as the "instantaneous" sensible energy loss. The question concerning the flue gas temperature measurement is whether the magnitude of the error due to the lack of averaging is significant.

In another test protocol being developed by a group of independent laboratories, an unshielded thermocouple is used to measure the stack temperature. This measurement method has raised questions about whether the errors due to using unshielded thermocouples are significant.

The purpose of this study is to evaluate the accuracy of the temperature and flow rate measurement methods used for wood stoves. In this study, an unshielded thermocouple array is used to measure radial

temperature profiles in real time. Temperature profile data will be used to assess the error due to the WHA Protocol's lack of averaging. Tests were run to quantify the radiation errors of using unshielded thermocouples and to determine if finer gage thermocouples can be used to give accurate measurements without radiation shielding.

A review of various flow measurement methods was performed to evaluate the suitability of these methods for measuring the stack flow rate. Based on the review, three techniques were believed to be suitable for stack flow measurements. The first technique uses a proprietary pitot array, designed by Shelton Energy Research^{*}, which measures the average velocity in the stack. The second technique uses the CO in the flue gas as a tracer to determine the stack flow. The third technique uses an algorithm similar to the WHA algorithm to compute the stack flow. A comparison between the three flow measurement techniques is conducted for several tests in which the stack flow was measured simultaneously by each technique.

^{*}Shelton Energy Research, Santa Fe, NM

2. LITERATURE REVIEW

2.1 Methods for Flow Rate Measurement

Flow rate measurement of the flue gases from wood stoves can be very difficult. The flue gases are heavily laden with particulates, are of time-varying composition, and are corrosive. Temperatures of up to 600°C can occur in the flue pipe. Mass flow rates are unsteady and typically under 0.02 kg/s. Gas velocities are on the order of 1 m/s.

A successful flow rate measurement method will be able to work in dirty flows, measure small flow rates, tolerate hot temperatures, and not obstruct the gas flow to the extent of altering the natural draft operation of the stove. A list of potentially successful flow rate measurement methods considered is shown in Table I. These methods were evaluated based on their ability to work in the stack environment and their dependence on gas composition, temperature, and viscosity of the flue gas in measuring the flow rate. A discussion of the various methods believed not to be suitable for the flue flow measurement follows. The methods believed to be suitable are discussed in Section 2.2.

The ordinary pitot-static tube is not suitable for stack flow measurements due to buoyancy effects in the tube. The buoyancy effects occur because the static pressure tube surrounds the total pressure tube and acts as a thermal insulator. If the gas stream temperature increases, then the gas temperature increase in the total pressure tube will lag that of the static pressure tube. The temperature increase lag causes a pressure differential due to density differences in the

Table I. Sensitivities of Potential Stack Flow Rate Measurement Methods to Uncertainties in Flue Gas Properties

MEASUREMENT	SENSITIVITY LEVELS (PERCENT)				COST (3)
	VISCOSITY ¹	GAS TEMPERATURE ²	GAS COMPOSITION ³	RANGEABILITY ⁴	
Gas Tracer (CO, CO ₂)	0	0	1.3	% CO > 0.03 mol % % CO ₂ > 0.5 mol %	4000-8000
Pitot Array	1.9	3	1.1	$\Delta P > 0.025$ Pa	4000
Orifice ($\beta=0.75$)	2.4	3	1.1	$Re_D > 400$	4000
Conventional Pitot-Static Tube	0	90	1.1	$\Delta P > 0.025$ Pa	3000-4000
WHA Algorithm	0	0	1.3	$\Delta M_{fuel} > 100g$	4000-15000
Target Meter ($\beta_T=0.333$)	2.6	3	1.1	$Re_D > 1000$	1200
Thermal Mass flowmeter	0	2	6.3	$\Delta T > 10^{\circ}C$	900
Dilution Tunnel Temperature Measurement	0	2	10*	$T_{stack} - T_{ROOM} > 40^{\circ}C$	600
Vortex Meter	NA	NA	NA	$Re_D > 3,000$	1500
Hot Wire Anemometer	6.5	8.9**	2.5	$T < 125^{\circ}C$	1500

NA - Not Applicable due to Rangeability

1 - Change in viscosity of 10% (change in pipe Reynolds number from 2250 to 2500)

2 - Change in stack temperature of 200°C to 250°C

3 - Change in flue gas composition of 20% H₂O, 15% CO₂, 2% CO, 4% O₂, 59% N₂ to 5% H₂O, 5% CO₂, 0.4 CO, 15.2% O₂, 74.8% N₂

4 - Recommended operating range expressed in terms of the most influential factor of a particular method.

* - Specific heat of air vs. specific heat of flue gas at 400 K

** - Based on thermal conductivity of air

tubes. This error can be significant compared to the actual differential pressure. For example, in work conducted as part of a larger project, negative differential pressures were measured with conventional pitot-static probes [2].

An orifice in the stack would not be suitable for stack flow measurements. To keep the obstruction of the gas flow to a minimum, an orifice with a beta ratio (ratio of orifice diameter to pipe diameter) of approximately 0.75 would be needed. The flow coefficient for such an orifice has a strong dependence on viscosity for pipe Reynolds numbers below 6000. For example, the discharge coefficient for a square-edge orifice with a beta of 0.75 changes 2.4 percent for a change in the pipe Reynolds number from 2250 to 2500. The discharge coefficient is also affected by thermal expansion of the orifice plate which could account for a one percent change in the orifice area. Particulate accumulation on the orifice must also be considered since it will affect the discharge coefficient.

A vortex flow meter works on the principle of relating the vortex-shedding frequency of a blunt body in the flow stream to the velocity of the flow. The coefficient relating the vortex-shedding frequency to the velocity changes only 5 percent for pipe Reynolds numbers between 3000 and 10,000. However, for pipe Reynolds numbers below 3000 the vortex-shedding phenomena is no longer constant and the repeatability of the meter deteriorates rapidly. Reynolds numbers in the stack vary between 1000 and 4000 during a burn cycle and therefore the vortex meter is unsuitable for stack flow measurements.

A target meter consists of a circular disk, i.e. a target, which is attached to a support rod and placed in the flow stream. The meter works on the principle of relating the velocity of the gas to the force exerted on the target. The coefficient relating the force to the velocity is a function of the pipe Reynolds number and the target diameter. For example, the coefficient of a 5 cm target meter in a 15 cm diameter duct changes 2.6 percent for pipe Reynolds numbers between 2250 and 2500. The change in the coefficient decreases if a larger diameter target is used but then flow obstruction becomes a problem. Another problem with using the target meter is particulate build-up on the target. If the target is mounted in a vertical pipe, any particulate build-up on the target will result in changing the force-flow calibration of the meter. Assuming 50 g of organic condensibles per kilogram of wood are produced and 10 percent collects on the stack, the amount of particulate build-up for a 14 kg charge is 2.9×10^{-6} kg/cm². If a 5 cm diameter target collects the same amount of particulates per area as the stack, the additional force due to accumulation one side of the target is 5.8×10^{-4} N. Assuming stagnation of the flow occurs over the whole target, the force on the target for a mass flow of 0.006 kg/s at 200°C is 7.05×10^{-4} N. This indicates that particulate build-up on the target may cause a 20 percent error in the flow measurement. Thus the target meter is believed not to be suitable for stack flow measurements.

2.2 Suitable Measurement Techniques

Based on the review of potential methods in section 2.1 it appears that only three methods are suitable. The following sections discuss the fundamental principles and review the literature presently available on these three methods.

2.2.1 Tracer Techniques

Tracer methods are non-intrusive, work in dirty flows, can give real time flow measurements, and can measure small flow rates. A tracer method can use either inherent tracers, natural added tracers, or unnatural added tracers. Inherent tracers are tracers that already exist in the flow. Natural added tracers are tracers that are inherent in the flow but are added to the flow and unnatural added tracers do not exist in the flow and therefore must be added to the flow.

ADDED TRACERS

One can inject a known amount of a gas into the flow and measure the concentration downstream of the injection point. The flow rate can be determined by:

$$\dot{m} = \dot{n}_{IR} MW \frac{[TR]}{[DTR]} \quad (1)$$

where

- \dot{m} = mass flow rate, kg/s
- \dot{n}_{IR} = injection rate of tracer, kmol/s
- [TR] = mole fraction of injected tracer (wet basis)

[DTR] = mole fraction of tracer in flow stream (wet basis)

MW = molecular weight of the flow stream, kg/kmol

Tiegs [3] used this method for measuring the flow rate of the flue gases from a wood stove. The tracer gas, sulfur dioxide, was metered through a rotameter before being injected in the stack. The concentration of SO_2 in the flue gas was measured 8-10 diameters downstream of the injection point to allow adequate mixing to occur. Flow rates predicted by the tracer did not agree with other flow rate measurements taken during the tests. Compared to the other flow rate measurements, the SO_2 tracer flow rates were 1 to 100 percent higher for the first stove tested and 1 to 9 percent lower for the second stove tested. Tiegs believed that this difference in flow predictions was caused by either interference of flue gas with SO_2 concentration measurements or SO_2 reacting with the flue gas. Interference in the SO_2 measurement would cause an underestimate of the flow rate and the SO_2 reacting with the flue gas would cause an overestimation of the flow rate. Another possible source of overestimation of the flow rate is the fact that SO_2 is water soluble and a portion of the SO_2 may have been removed while passing through the condenser prior to reaching the analyzer.

Another tracer method by Tiegs uses a helium tracer to calculate the stack flow. The helium tracer was injected in the stack at a measured flow rate. Downstream of the injection site a sample was taken from the stack and the CO , CO_2 , O_2 , and H_2O were removed from the sample leaving only N_2 and He in the sample gas. The He concentration was

determined by thermal conductivity measurements and thus the N_2 concentration of the sample could be determined. The air flow rate was calculated using the concentration data of N_2 and He along with the He injection rate. Stack measurements of CO, CO_2 , and O_2 , are used to calculate the air to fuel ratio. The stack flow could then be determined with knowledge of the air-fuel ratio, and the air flow rate. A series of tests to verify the helium tracer had not yet been performed. The helium tracer method has an advantage over the SO_2 tracer method in that helium is inert and will not react with the flue gas. However, this method would not work well during unsteady stack conditions where the flow and gas concentrations were changing rapidly unless time-averaged samples are used.

Staab, et al. [4] assessed a tracer system presently being used for measuring motor vehicle exhaust flow rates. Motor vehicle exhaust is similar to flue gas since both are time varying in composition, corrosive, hot, and dirty. Staab wanted a flow measurement system that could work in dirty flows, measure on a real time basis, have a fast time response to flow changes, and measure small flow rates. The tracer gas, CO_2 , was also present in the exhaust gas and therefore required two concentration measurements. The CO_2 concentration was measured both upstream and downstream of the injection probe. The flow rate can be determined with the two CO_2 concentration measurements and the injected CO_2 flow rate.

INHERENT TRACERS

Another method of using a tracer is one in which the tracer gas is inherent to the flow. A dilution tunnel (a hood and duct which collect air and the emissions) is required for this tracer method. A schematic of a dilution tunnel is shown in Fig. 1. The flow rate of the stack can be related to the dilution tunnel flow rate by the conservation equation of the tracer.

$$\dot{n}_S [\text{TR}]_S + \dot{n}_A [\text{TR}]_A = \dot{n}_{\text{DT}} [\text{TR}]_{\text{DT}} \quad (2)$$

where

\dot{n}_S = molar flow rate of the stack, kmol/s

\dot{n}_A = molar flow rate of the air drawn into the dilution tunnel,
kmol/s

\dot{n}_{DT} = molar flow rate of the dilution tunnel, kmol/s

$[\text{TR}]_S$ = mole fraction of the tracer in the stack (wet basis)

$[\text{TR}]_{\text{DT}}$ = mole fraction of the tracer in the dilution tunnel (wet
basis)

$[\text{TR}]_A$ = mole fraction of the tracer in room air (wet basis)

The stack flow rate can be calculated if the dilution tunnel flow rate and the concentrations in both ducts are measured. The tracer concentrations can be measured either on a wet or dry basis. (A dry basis concentration measurement is one in which the water in the flue gas has been removed prior to the concentration measurement and therefore gives a higher concentration indication than the actual tracer concentration in the ducts.) If a dry basis concentration is used,

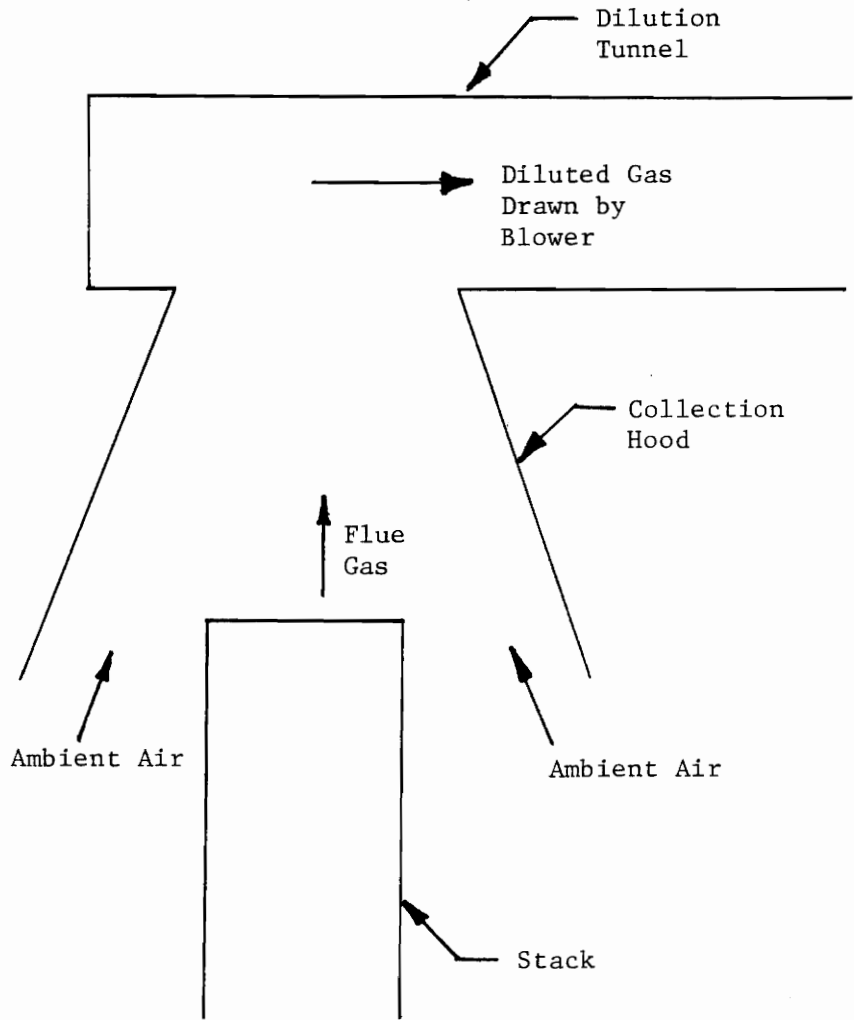


Figure 1. Dilution Tunnel

accurate knowledge of the water concentration in the stack and dilution tunnel is required to correct to a wet basis. The water concentration in the dilution tunnel would be different than the stack due to the dilution process. If wet basis concentrations are used, then no water corrections are necessary on the concentration measurements. Macumber and Jaasma [5] used this method to measure the flue gas flow rates from a coal stove. The tracer, CO_2 , was chosen due to its concentration levels being high enough (even when diluted in the dilution tunnel) to allow accurate measurement with the same gas analyzer used for stack concentration measurements. The CO_2 concentrations of the stack and the dilution tunnel were measured on a dry basis and therefore required correction to a wet basis. Their correction from a dry to a wet basis was based on the assumption that all the hydrogen in the coal formed water. This assumption was not totally correct since hydrocarbons were also formed from the hydrogen in the coal. Another assumption made was that the ambient CO_2 which was drawn into the dilution tunnel was negligible compared to the dilution tunnel CO_2 concentrations. The validity of this assumption depends on the CO_2 levels in the dilution tunnel and the accuracy desired in the flow rate measurements. For example, if the stack and dilution tunnel CO_2 levels were 14 and 1.4 percent, respectively, then neglecting an ambient CO_2 concentration of 0.033 percent would result in a 2.4 percent error in calculating the stack flow.

Heat is another type of tracer that may be used to measure the flow rate of the flue gas. An electric heater, which gives a known energy input to the flue gas, along with measurement of the gas temperature

upstream and downstream of the heater can be used to measure the quantity $\dot{m}c_p$ (product of mass flow rate and specific heat) of the gas. The heater should be designed for uniform heating of the gas stream or adequate distance allowed for bulk mixing before the post-heater temperature is taken. The advantage of the electric heat tracer method over a gas tracer method for evaluating the sensible energy loss of a stove is that the heat tracer can measure the $\dot{m}c_p$ product directly. The disadvantages of this method are accurate measurement of the temperature difference across the heater may be hampered by a nonuniform temperature profile in the stack and keeping the heat losses in the heater section to a minimum may be difficult due to the high temperatures.

One of the earliest reports on an electric heat tracer (known sometimes as a Thomas meter) is by Thomas [6]. His meter consisted of a heater and two thermometers made of resistance wire. One thermometer was placed upstream of the heater and the other was placed downstream of it. A 1°C temperature difference was maintained between the thermometers. The energy required to accomplish this is directly proportional to $\dot{m}c_p$ product of the gas. The meter was tested simultaneously against a pitot traverse and a venturi meter. The test results showed that all three meters agreed within 4 percent of the average flow measured over a flow range of 1 to 2.5 kg/s. Heat losses between the heater and the downstream thermometer were not a problem in this application since the gas temperatures were nearly the same as the ambient temperature and a small temperature rise was used.

Since the work by Thomas, many different thermal flowmeters were developed--mostly for the fields of biomedical science (blood flow

rates) and biology (sap flow rates). Zinsmeister [7] gives a detailed mathematical analysis of several types of flowmeters as well as their applications. Zinsmeister mentions that thermal flow meters give erratic results when used in flows that are in the transition region between laminar and turbulent. No explanation was given for the cause of this erratic behavior. However, this may be an important point since stack flows are in the transition region. Another problem with thermal flow meters is slow response to sudden changes in flow rates. However, this problem may be avoided by proper design of the meter as demonstrated by Richards and Kuether [8] who designed a probe to sense pulsatile blood flow.

The "rate of heat loss" flowmeter has been used by Barnett and Shea [9] to measure stack flows from wood stoves. The heat loss of the sensing element determines its mean temperature and thus the resistance of the element which in turn can be related to the velocity of the flow. Barnett and Shea used a Kurtz 440 air flow meter and then a Teledyne Hasting Raydist PCI-30 flow meter. Both meters use the heat loss principle to measure the velocities. The meters needed to be placed high in the stack due to the temperature limit of the meter being around 77°C. After several months of testing, they concluded that the Kurtz meter was not acceptable for flue gas flow measurements because of the frequent break downs encountered with the meter. Later, the Hasting meter was tried and tested to determine the sensitivity of the meter to condensed flue gas droplets. These tests showed that the meter was insensitive to the levels of condensed droplets found in flue gas. The results of these tests are questionable. The meter output is a function

of the thermal conductivity of the gas and therefore should have varied as the condensed gas droplet level changed. A disadvantage of the meter was that it needed to be checked for creosote build-up every half hour and cleaned as required since particulate build-up changes the calibration. The accuracy of the meter would depend on calibrating the meter with a gas whose thermal conductivity is similar to that of flue gas. Also, if mass flow is required then the velocity of the single point measurement must be related to the average velocity in the duct which requires knowledge of the velocity profile.

The boundary-layer thermal flow meter developed by Laub [9] relates the mass flow to the heat necessary to maintain a constant temperature difference in the boundary layer and has the advantage of being non-intrusive to the flow. The governing equation relating the heat input to the mass flow differs for laminar and turbulent flow and requires the use of two different coefficients. This would make the boundary-layer flow meter difficult to use for stack flow measurements, since it is unclear whether turbulent or laminar flow exists.

Another heat tracer method that can be used to measure the stack flow does not require an electrical heater. The method relates the flow rate of the stack, dilution tunnel, and ambient air drawn into the tunnel by an energy balance. If the stack, collection hood, and dilution tunnel as shown in Fig. 1 are insulated, then an energy balance could be written as:

$$\dot{n}_S \bar{h}_S + \dot{n}_A \bar{h}_A = \dot{n}_{DT} \bar{h}_{DT} \quad (3)$$

where

\dot{n}_A = the molar flow rate of air drawn into the dilution tunnel,
kmols/

\bar{h}_S = enthalpy of flue gas, kJ/kmol

\bar{h}_a = enthalpy of room air drawn into the dilution tunnel,
kJ/kmol

\bar{h}_{DT} = enthalpy of gas in dilution tunnel, kJ/kmol

The continuity equation relating the molar flow rates can be solved for \dot{n}_{DT} and substituted into Eq. (3)

$$\dot{n}_S \bar{h}_S + \dot{n}_A \bar{h}_A = (\dot{n}_S + \dot{n}_A) \bar{h}_{DT} \quad (4)$$

Assuming the specific heat of the flue gas and ambient air to be constant, Eq. (4) can be written as:

$$\dot{n}_S \bar{c}_{PS} (T_S - T_{DT}) + \dot{n}_A \bar{c}_{PA} (T_A - T_{DT}) = 0 \quad (5)$$

where

\bar{c}_{PS} = molar specific heat of stack gas, kJ/kmol K

\bar{c}_{PA} = molar specific heat of ambient air, kJ/kmol K

If the specific heat of ambient air and flue gas are assumed to be equal, then Eq. (5) can be simplified to:

$$\dot{n}_S T_S + \dot{n}_A T_A = \dot{n}_{DT} T_{DT} \quad (6)$$

where

T_S = the stack temperature, K

T_{DT} = the dilution tunnel temperature, K

T_A = ambient air temperature, K

Equation (6) assumes that the heat loss to the room and the kinetic energies are negligible along with that of the specific heats of the three flows are equal. The assumption that the specific heats are equal is not totally correct since the specific heat of the flue gas would be different than air and this difference would depend on the flue gas composition. For example, flue gas with 20 percent H_2O , 15 percent CO_2 , 2 percent CO , 4 percent O_2 , and 59 percent N_2 would have a specific heat of 32.7 kJ/kmol·K compared to 29.3 kJ/kmol·K for air at 400 K. This would result in a 10 percent error in the flow measurement.

The continuity equation relating the molar flow rates can be written and solved for \dot{n}_A . Substitution of the continuity equation into Eq. (6) gives the stack flow.

$$\dot{n}_S = \dot{n}_{DT} \left(\frac{T_{DT} - T_A}{T_S - T_A} \right) \quad (7)$$

The dilution tunnel molar flow rate can be measured with an orifice plate or a pitot-static tube, and the temperatures can all be measured.

This method depends on measuring the temperature differences accurately. Generally, the temperature difference between the stack and ambient will be greater than 40°C so a 2°C measurement error accounts for only a 5 percent error or less in the stack flow. However, the temperature difference between the dilution tunnel and ambient will be much smaller, generally on the order of 5 to 10°C. Therefore, a 2°C measurement error would cause a 20 to 40 percent error in the measured stack flow. If thermocouples are used to measure the differential temperatures, a thermopile arrangement would have the advantage of giving a larger output signal for a given differential temperature than if only one thermocouple had been used to measure each temperature.

The only literature found on this method was by Butcher and Ellenbecker [11]. They used this heat tracer method to determine the dilution ratio of flue gas to ambient air in the dilution tunnel during coal and wood stove particulate studies. The temperatures of the stack, dilution tunnel, and ambient air were recorded. Since only the dilution ratio (ratio of ambient air to stack emissions) was of interest to them, measurement of the dilution tunnel flow rate was not necessary.

2.2.2 Pitot Array

Literature on the use of a pitot array (a group of inter-connected static pressure and inter-connected total pressure tubes connected to one transducer) for flow rate measurements is scarce. Most flow rate measurements with pitot tubes are done using traverses. Since some errors that affect the traverse method also affect the pitot array both methods will be discussed.

A common pitot traverse method is based on equal area sampling points [12]. Burton [13] states that this method can easily miss the boundary layer flow profile and cause flow errors as high as 10 to 20 percent for boundary layers representing 5 percent of the stack diameter. Brown [14] evaluated four different traverse methods analytically, assuming various velocity profiles. The equal area method with 20 measurement points has an error of less than one percent in predicting the average velocity. Traverse methods depend on both constant flue gas properties and steady-state flow [12]. The traverse method cannot be used in wood combustion systems since the flow is unsteady.

One of the first pitot tube flow meters was developed by Preston [15]. The flow meter consisted of four total pressure pitot tubes equally spaced on the three-quarter radius of a circular duct. Static tubes were mounted on the wall of the duct at 90 degree intervals. Separate differential pressure readings were averaged to calculate the flow rate. The calibration factor (actual flow divided by indicated flow) of 0.992 varied ± 0.6 percent over a range of velocities between 100 and 450 feet per second. Use with velocities below 40 feet per second was not suggested due to low pressure differentials. The use of soot laden air streams was not recommended due to clogging problems with the pitot tubes.

Ma [16] also developed an averaging flow meter for air flow measurement. The flow meter consisted of two tubes perpendicular to each other with forty holes equally spaced across each of them. These two tubes were used to measure the average total pressure in the duct.

Four static pressure tubes were mounted on the circumference of the duct. The flow meter measured the mean velocity based on taking the square root of the fluid dynamic average of the velocity pressures. However, the mean velocity in a duct is normally calculated from the average of the square root of the differential pressure measured at each point. The error associated with this difference depends on the velocity profile. Calibration of the flow meter was done to express this error as well as other instrumental errors in the form of an experimental coefficient. This coefficient varied between 0.98 and 1.02 for a velocity range of 10 to 23 feet per second. Ma conducted various tests to see the effect on the flow meter performance and concluded that the major error in predicting the flow rate was due to swirling effects. Field tests of the flowmeter showed agreement within 3.5 percent compared to a pitot tube traverse in predicting air flow rates. However, tests in the laboratory showed the pitot traverse to be in error by 2 percent and, therefore, the actual flow rate of the field test could only be estimated.

Gasiorek [17] analyzed the accuracy of twelve inter-connected pitot-static tubes. Theoretical analysis of the system was performed to estimate the error caused by gas flow through the inter-connected pitot tubes. Gas flow through the interconnected pitot tubes would be caused by the static and/or the total pressure being different at each tube. Laminar flow was assumed in the pitot tubes and secondary losses as well as friction losses were included in the analysis. A relationship between the velocity pressure corresponding to the average velocity in the duct and the velocity pressure measured from the manifold was

derived. Data from the calibration test was used to provide necessary information for the analytical error prediction. Gasiorek concluded that the error due to flow occurring through the inter-connected pitot tubes (0.55% for a differential pressure of 183 Pa) was small for turbulent flow. This may not be true for laminar flow due to the steeper velocity profile which would tend to cause more flow through the interconnected tubes.

2.2.3 Scale-Based Method

In the scale-based method, the burning rate of the wood is modeled by the uniform burning assumption of the WHA algorithm. The uniform burning assumption implies that the fuel remains at a constant elemental composition throughout the burn and therefore releases the same proportions of C, H, and O atoms as existed in the as-fired fuel. This assumption along with the other assumptions stated for the WHA algorithm are used in the scale-based method to calculate the stack flow.

The efficiency-measurement sensitivity of this algorithm to concentration measurement errors and assumed elemental analysis of the wood efficiencies was investigated by Jaasma [18] and later by Shelton, et al. [19]. These studies included the sensitivity of the algorithm to measured CO, CO₂ and O₂ concentration and the assumed elemental analysis of the wood. However, the sensitivity of the algorithm for predicting flow rates was not investigated.

Hubble and Harkness [20] estimated mass flow rates by performing a carbon balance. The carbon balance they used had the same assumptions as the scale-based method but does not account for as many combustion

reactants and products. To determine the mass flow rate from a carbon balance, the mass of carbon burned in the wood is divided by the gas fraction of carbon in the stack over a certain time interval. Measurement of the wood burn rate required the uniform burning assumption of the WHA algorithm. The carbon burn rate can be calculated from knowledge of the wood burn rate along with the mass fraction of carbon in the wood. Hubble and Harkness assumed the carbon loss to hydrocarbons was negligible so that the CO and CO₂ concentrations gave the total carbon concentration in the stack. This assumption is not totally correct since carbon in hydrocarbons and particulates has been measured to account for 15 percent of the carbon in the fuel [21].

Tiegs [3] used a carbon balance method similar to that of Hubble and Harkness to measure stack flow but included an estimate of the hydrocarbon and particulate carbon. The stack flow was also determined using the WHA scale-based algorithm. Comparison of these two methods for determining the flow rate during operation of a stove showed that the carbon balance method predicted flow rates up to 34 percent higher than the scale-based method. Tiegs believed that the scale-based method was more accurate due to it accounting for more combustion reactants and products.

2.3 Temperature Measurement

According to the WHA Protocol for measuring the heating performance of wood stoves the flue gas temperature should be measured by a thermocouple shielded with two concentric tubes and placed in the centerline of the pipe 1.2 m above the stove breech [1]. This would

• give a good indication of the average flue temperature only if the radial temperature differences at this location were small. With the insulated flue walls being cooler than the flue gases, one would expect radial temperature differences to exist. Premixing the flow before measuring the temperature is one method that is used when temperature gradients are present in a duct [22], but the mixers may cause a flow restriction which is too large to use in woodstove flues. Another method used when large radial temperature differences are present is a thermocouple array, but the number of the thermocouples and the spacing of them depends on the magnitude of the differences and accuracy desired [23]. The bulk temperature could be evaluated from the array data if the velocity, density, and specific heat at each temperature measurement point is known. The specific heat and density can be evaluated based on the temperature and an assumed flue gas composition. However, little is known about the velocity profiles in the stack since the unsteady flow conditions prevent the use of traverses. Therefore, the bulk temperature can only be estimated since a velocity profile must be assumed.

Dutt [24] measured the bulk temperature in a circular duct using a platinum resistance sensor. These sensors measure an average temperature over the element length and therefore must be properly located if a single sensor is to measure the bulk temperature. By combining velocity and temperature profiles, the location where a single temperature measurement would give the bulk temperature of the flow was analytically predicted. However, Dutt did not recommend the use of a one point bulk temperature measurement with natural convection and low

Reynolds numbers due to the possibility of asymmetrical velocity and temperature profiles existing.

Real time temperature profile measurement from an array is possible through the use of a data acquisition system which rapidly reads the individual thermocouples. A data acquisition system is needed since the temperatures change too rapidly to allow manual data collection of temperature profiles. However, the use of a data acquisition system can lead to many possible errors in obtaining accurate temperature measurements. Mackenzie and Kehret [25] describe the most common sources of errors such as noise sources in the multiplexer and parasitic thermal effects. (Parasitic thermal effects are caused by junctions of various metals on the circuit board and are most likely to occur during instrument warmup.) Multiplexing should be wired using differential inputs to avoid ground loops. Multiplexer noise can be reduced by shielding.

Analytical modeling of the heat transfer phenomena in the stack could give insight to the stack temperature gradients for various operating conditions. A study conducted at Auburn University [26] used a computer code to predict inner and outer surface temperatures on an insulated wood stove chimney. A one-dimensional, transient heat conduction equation was solved using a finite-difference solution. Surface temperatures were calculated for a step change in the flue gas temperature of 27 to 537°C. Results of the calculations showed that both the inner and outer wall temperatures required approximately 45 minutes before reaching a steady state value. Depending on the thermal conductivity used for the chimney, heat losses through the chimney

varied between 8 and 50 percent of the energy convected up the stack for a given location. If heat losses are large then a cooler inner wall temperature can be expected, which may cause larger temperature gradients in the stack. The response time of the chimney to reach a steady state temperature is important since during this transient time the difference in the inner wall and the flue gas temperature is at its highest and thus the probability of large radial temperature differences existing is high.

2.4 Summary

Many flow measurement methods exist, but only a few appear to be suitable for flow rate measurement of flue gas from wood stoves. The scale-based and carbon balance methods are widely used although the assumptions used in these methods are known to be inaccurate, and the errors due to these assumptions in flow rate measurement are unknown. Simultaneous testing of these two methods with other flow measurement methods, i.e., tracer or pitot array methods, would be needed to estimate the errors due to the assumptions. Tracer methods have been used to measure the stack flow, although not all methods have been successful. Added tracers must be compatible with the flue gas or erroneous flow measurements will result. Inherent tracers have been used successfully, although concentrations were measured on a dry basis which required an estimate of the flue gas water concentrations. To avoid the possible errors due to estimating the water concentration, wet basis concentrations could be used. Heat tracers have been successfully used in other low-flow applications. Only one report was found that

used a heat tracer method, but the method was used to measure dilution ratios and not stack flows. The pitot array method has been used in air ventilating applications successfully and is just beginning to be used with wood stoves. The errors due to flow through the interconnected tubes of the pitot array was investigated and found to be small for the case of turbulent flow with a differential pressure of 183 Pa.

Measurement of the average flue temperature has mainly been done with only one thermocouple at the centerline of the flue. The literature suggests that the average temperature measurement should be performed with an array if the radial temperature differences are large. A thermocouple array could be used to measure the radial temperature differences to determine the errors of using only the centerline temperature.

3. EXPERIMENTAL METHODS

3.1 General Set-Up

The laboratory set-up for conducting the tests is shown in Fig. (2). A Shenandoah Manufacturing Co., Inc. stove (model R-76LC) was used and is shown schematically in Fig. (3). The stove is a radiant heater and has both primary and secondary air inlets. The stove outlet was connected to a 15 cm diameter (0.6 mm wall thickness) galvanized steel flue pipe. To prevent room air from infiltrating the stove pipe, the stove pipe sections were brazed together. The flue pipe extended 4 m above the stove and ended in the collection hood. A steel frame supported the stack and collection hood. The collection hood drew in room air and stove emissions at a dilution ratio of 4:1 to 20:1. This mixture was drawn through the dilution tunnel by a blower.

An electronic scale supported the stove and was used to measure the mass-time history of the combined weight of the stove, chimney, and fuel. Three low friction supports were used on the steel frame in an attempt to prevent thermal expansion and contraction of the stack from affecting the scale reading.

A 2.5 m flue pipe section was insulated with 8.9 cm thick fiberglass insulation. The insulated pipe section began 2.1 m above the electronic scale platform. The purpose of the insulation was to help develop a more uniform radial temperature profile at the top of the stack. By keeping the stack wall temperature elevated, the insulation also helped prevent water in the flue gas from condensing.

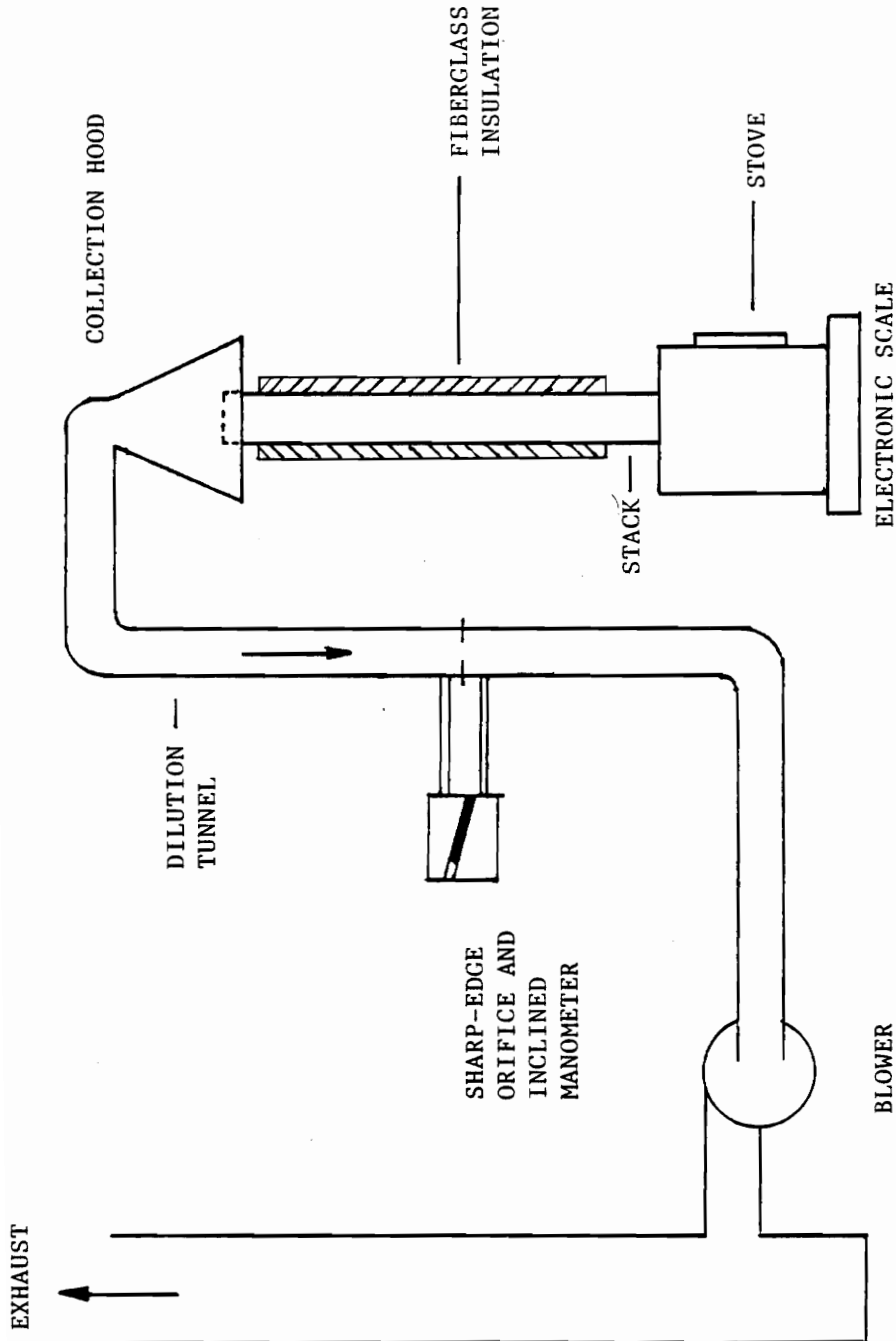


Figure 2. Stove and Flue Gas Handling System Used in Tests.

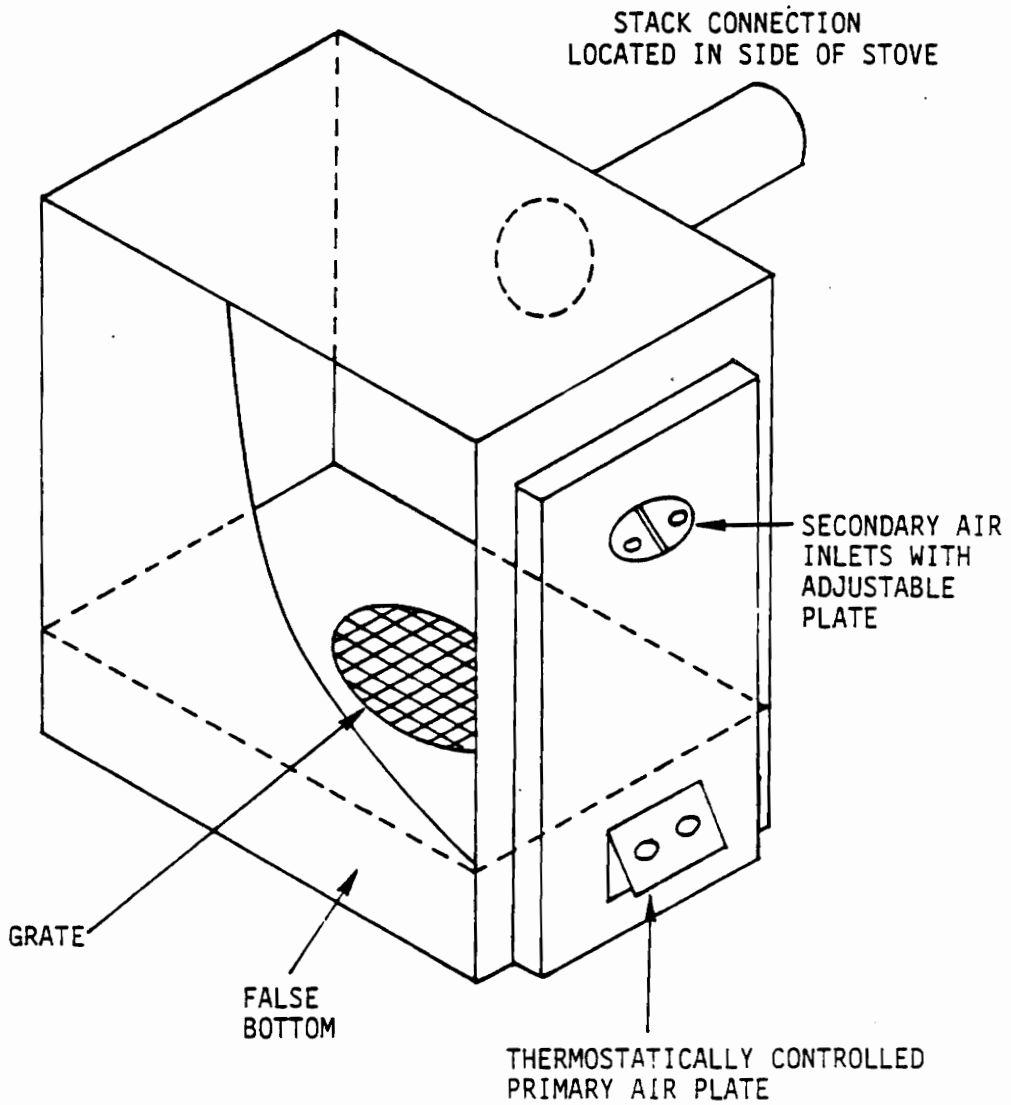


Figure 3. Schematic of the Shenandoah (R-76LC) Stove.

3.2 Temperature Measurement System

3.2.1 Thermocouple Array

A thermocouple array consisting of 16 thermocouples, the readings of which are individually recorded, is used to measure the instantaneous radial temperature profiles in the stack. The sixteen thermocouples are located in the stack 2.4 m above the electronic scale platform which the stove rests on. This location is presently being considered by ASTM as a standard location for measuring stack temperature.

A schematic of the thermocouple array is shown in Fig. (4). The array is constructed with 0.25 mm (10 mil) diameter, duplex, glass insulated, Chromel-Alumel (type K) thermocouple wire. Thermocouple beads are formed using an inert gas arc welder and range between 0.056 and 0.064 cm in diameter. The sixteen thermocouples are supported by two 6.4 mm diameter stainless steel rods placed perpendicular to each other in the flue pipe. Thermocouples are located at the centerline and at radii of 1.8, 3.5, 4.3, 5.2 and 6.0 cm from the centerline. The thermocouple at a radius of 4.3 cm (the mid-point between 3.49 and 5.24 cm) is used due to one rod having one less thermocouple than the other rod.

The junctions between the thermocouples and the ribbon cable are located 1.2 m from the array and were thermally shielded from the stove but exposed to the ambient surroundings. The junctions are at room temperature, which required the emf corresponding to the junction temperature to be added to the thermocouple voltages so that thermocouple tables referenced at 0°C could be used [23].

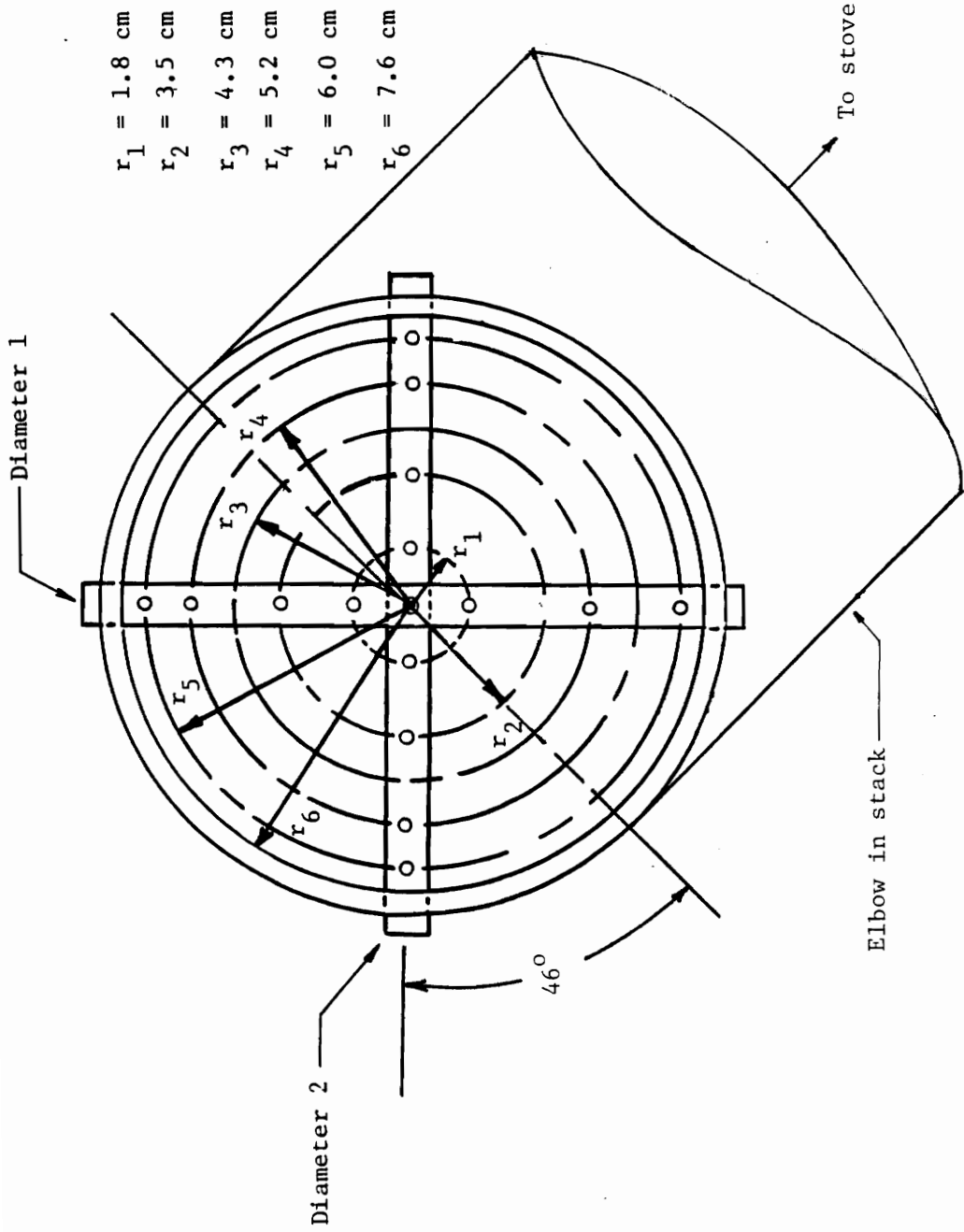


Figure 4. Schematic of 16 Thermocouple Array

An unshielded ribbon cable runs from this junction to the data acquisition system. An oscilloscope was used to check for noise on the unshielded cable. Noise in the 60 Hz and 1.4 MHz range was measured.

A fast analog to digital (A/D) converter with a programmable gain amplifier (Analog Devices RTI-1260) is used to read the thermocouple voltages. The gain on the converter is set at 100.

A machine language program combined with the fast A/D converter allows real time temperature profile measurements. A total of five readings of each thermocouple are taken in approximately 400 milliseconds. The thermocouples are read individually but all 16 thermocouples in the array are read once before another reading is taken. The five readings of each thermocouple are averaged and this average value is used for the temperature profile data. The averaging is done to reduce any noise that may be present in the thermocouple signal.

The voltage is converted to temperature using a third order polynomial curve fit [27]. To obtain better accuracy in the conversion, one curve was fit for the 0 to 600°C range and another for the 601° to 1000°C range.

3.2.2 Suction Pyrometer

A suction pyrometer is used as the standard to which the thermocouple measurement is compared. The suction pyrometer is positioned in the stack 5 cm above the thermocouple array at a radius of 1.8 cm from the centerline of the stack and is shown schematically in Fig. (5). The reading of the suction pyrometer is compared to the

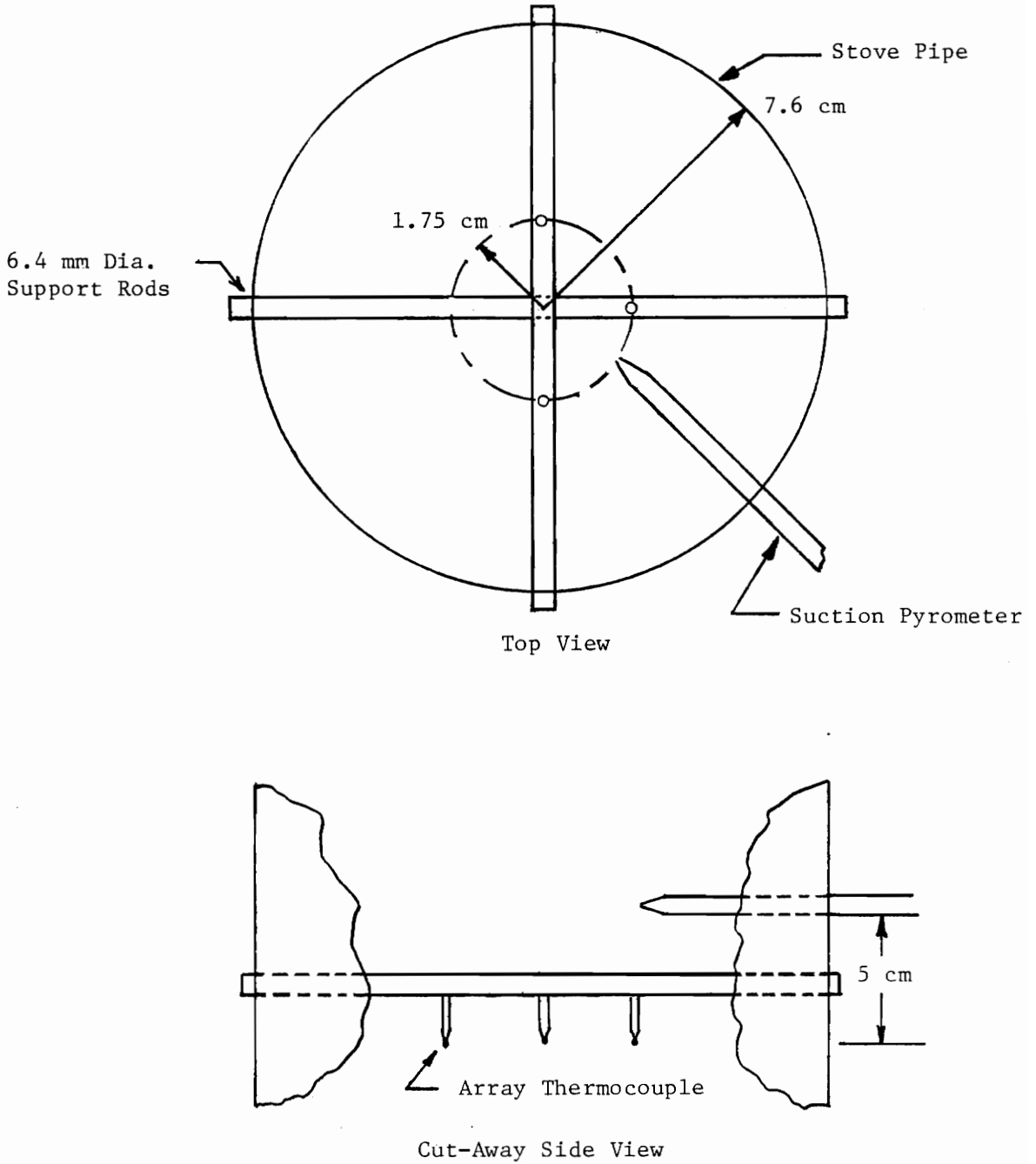


Figure 5. Schematic of Suction Pyrometer Measuring Position

average of the temperatures measured by the thermocouples on the 1.75 cm radius. The differences in the measurements is taken to be the radiation errors of the thermocouple measurement.

The pyrometer consists of a 0.076 mm (3 mil) diameter type-K thermocouple bead positioned near the 2 mm I.D. inlet of the pyrometer. The suction pyrometr is connected to the A/D converter via a disconnected thermocouple from the array. Thus, the suction pyrometer and the array thermocouples reference junctions are located together which would help prevent the reference junction temperatures from being different. A vacuum pump is used to pull the flue gas past the thermocouple bead. A fine gage thermocouple and an induced flow across the bead are used to make convection the dominant heat transfer mode for the thermcouple bead and thus the radiation error will be minimized.

3.2.3 Thermopile

A thermopile and the sixteen thermocouple array are used to measure the flue gas temperature drop through the insulated section. The thermopile is located 30 cm below the top of the insulated section and 2 m above the sixteen thermcouple array. The sixteen thermocouple array is located 30 cm above the beginning of the insulated pipe section.

The thermopile consists of four type-K thermocouples spaced 90 degrees apart on a radius of 1.8 cm from the centerline of the stack. The reference junctions of the thermopile are kept in an ice bath. The output of the thermopile is recorded on a strip chart recorder.

The thermopile reference junctions are in an ice bath and therefore the reference temperature does not need to be measured. The reference

junctions of the array are at ambient temperature and therefore the reference temperature needs to be measured. Any uncertainty in the measurement of the array reference temperature will result in an uncertainty in the temperature drop measurement. The uncertainty in the reference temperature measurement can be up to $\pm 2^{\circ}\text{C}$.

3.3 Flow Measurement Systems

3.3.1 CO Tracer System

The CO tracer system alternately measures the stack and dilution tunnel CO concentrations. The CO concentrations are to be measured on a wet basis and at a reduced pressure. This is a significant accomplishment since concentrations have normally been measured on a dry basis and at ambient pressure.

A schematic of the CO tracer system is shown in Fig. (6). The sample gas is drawn through either the stack or the dilution tunnel sample lines depending on which duct is being sampled. Water concentration in the flue gas is not expected to exceed 40 percent, and therefore both sample lines are kept at 75°C (the dew-point temperature for flue gas with 40 percent water). The sample gas is then filtered to prevent particulate contamination of the equipment in the system. The filters (one on each sample line) are located in a 75°C oven. The micro valve following the dilution tunnel filter is adjusted (as required) to allow the dilution tunnel and stack gas sampling rates to be equal. Two solenoid valves allow alternate sampling of the stack and the dilution tunnel. Following the solenoid valves is another micro valve which reduces the sample gas pressure from 96 kPa to 16 kPa. This reduction

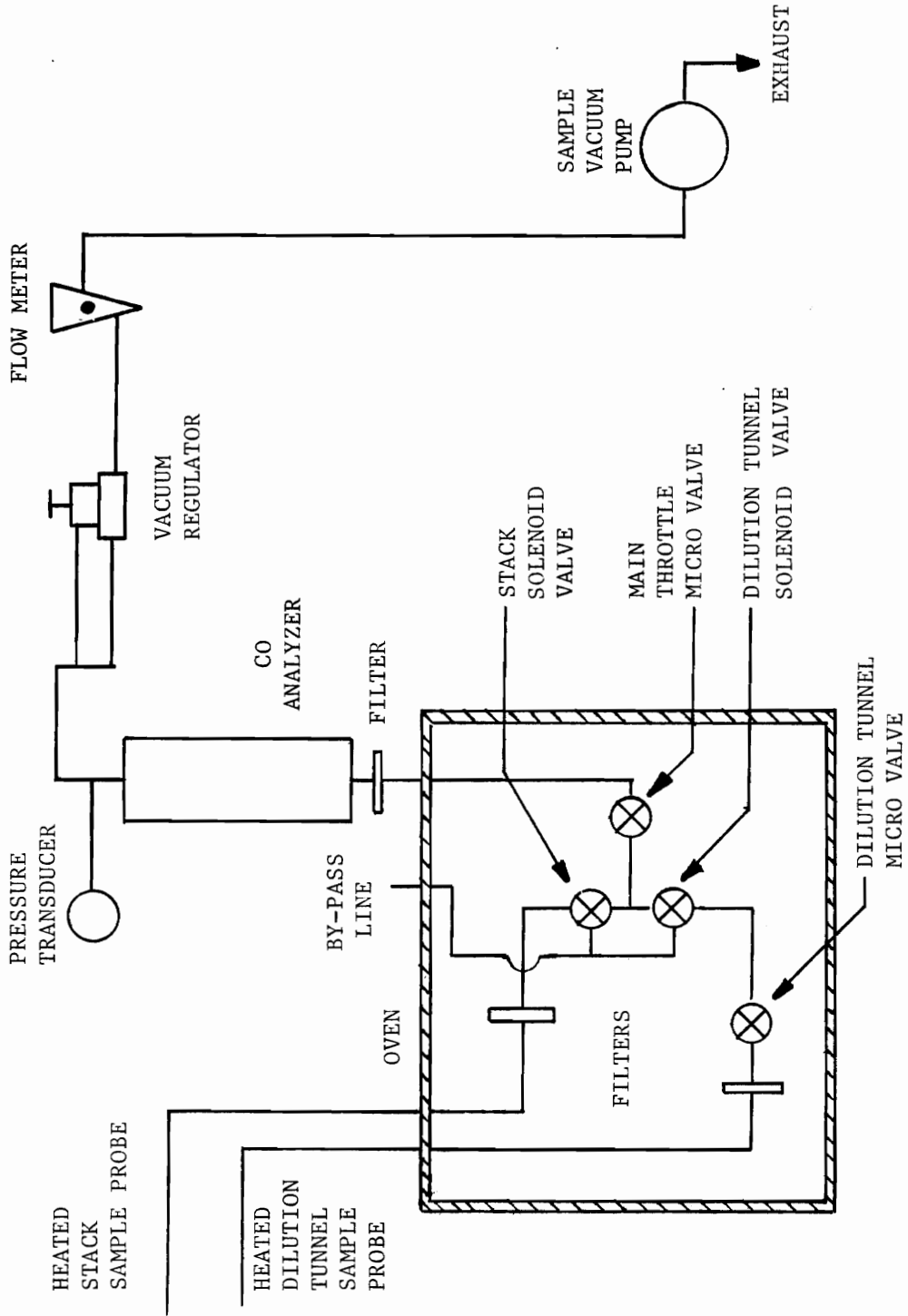


Figure 6. Sampling Train of CO Tracer System

in pressure allows the temperature of the gas to be lowered to 27°C before water condensation would begin.

The sample gas then passes through another heated line (kept at 37°C) to a filter. This filter catches any particulates still remaining in the sample gas before it enters the CO analyzer (Horiba Infrared Analyzer AIA-24(AS)). The pressure of the gas is measured on the outlet side of the analyzer by an absolute pressure transducer (Datametrics Barocel 600-A). A vacuum regulator (Conoflow GH20VT) is used to keep the system at the pressure for which the analyzer is calibrated. The instrument output is a function of the pressure in the analyzer and thus maintaining a constant pressure in the analyzer is essential. A rotameter located downstream of the analyzer is used during leak tests of the system to determine if there is flow when the probe tips are capped. A rotary vane vacuum pump (Gast 465) is used to pull the sample through the system and is used due to its ability to handle dirty flows. Although the pump runs at an elevated temperature, water and organics may condense in the pump due to the pressure of the gas increasing to 96 kPa before leaving the pump.

3.3.2 Pitot Array Set-Up

A proprietary pitot array designed by Shelton Energy Research consists of four static and twelve impact tubes and is used to measure the average velocity in the stack.

A schematic of the pitot array is shown in Figs. (7) and (8). The static tubes are located at a radius of 3.80 cm from the center of the stack. The impact tubes are positioned at radii of 3.18, 5.40 and 6.99

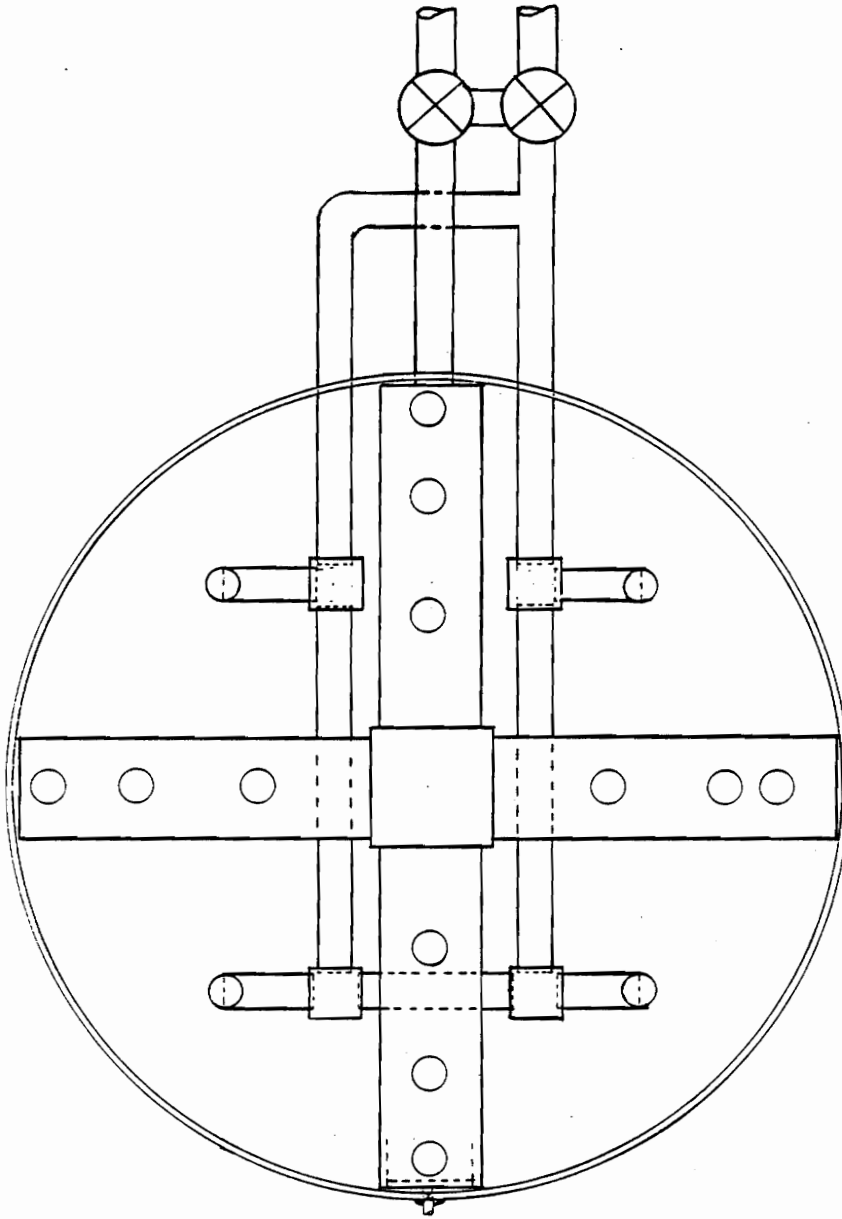


Figure 7. Top View of Pitot Array

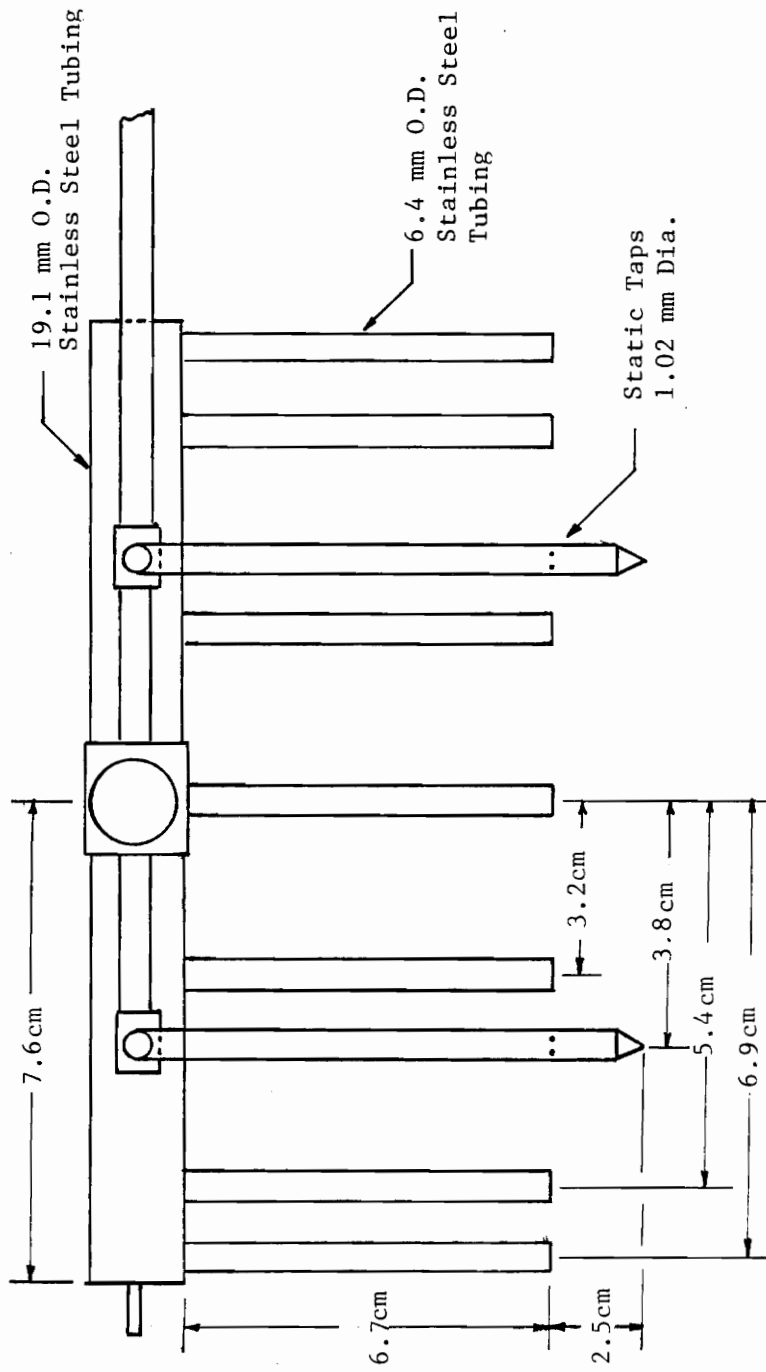


Figure 8. Side View of Pitot Array

cm from the centerline. The positions of the impact tubes are those specified by ASTM Code D3154-72 for equal area velocity profile traverses. The static and impact tubes measure their pressures in the same horizontal plane. The impact tubes are interconnected to allow measurement of the average total pressure. The static tubes are also interconnected to give an average static pressure. Unless a flat velocity profile exists, flow will occur through the impact tubes due to some tubes seeing a higher velocity head than others. The error due to the flow through the impact tubes will depend on the velocity profile in the stack. Analytical analysis by Gasiorek [17] showed the error due to flow through interconnected pitot-static tubes to be small but this was for turbulent flow. For a given mass flow rate in the stack, a laminar velocity profile would cause more flow through the impact tubes than a turbulent profile due to a steeper velocity profile. Calibration of the pitot array will account for this error only if the velocity profiles in the stack during calibration are similar to those in the stack when the stove is operating. Temperature profiles in the stack could cause buoyancy effects very similar to those mentioned in the pitot-static tube discussion. However, the buoyancy effects are minimized with the array since both the static pressure and impact pressure are average readings from several measurement points.

The differential pressure is measured using a capacitive pressure transducer (Datametrix Barocel 570-D). An electronic manometer is used to read the signal from the transducer. The transducer-manometer unit has five ranges but only the 0-0.75 and the 0-0.15 Pa ranges are used during the tests run. The transducer is mounted on a thermal base and

enclosed in a 46 by 61 by 30 cm temperature-controlled box. A temperature-controlled environment is used to reduce thermal zero drift. The box is mounted on the building wall to isolate the transducer from vibrations.

The pitot array is connected to the transducer by 6.4 mm O.D. tubing. The two tubes are twisted together and insulated (except near the valves and at the entrance to the temperature-controlled box) to help keep the lines at the same temperature. The two tubes run horizontally from the array to the transducer to prevent a pressure differential from developing if the lines are at different temperatures. Two valves are used to occasionally connect the ports of the transducer together (bypassing the array) for zeroing purposes.

3.3.3 Scale-Based Method

The scale-based method requires the "instantaneous" burn rate of the charge along with dry basis measurement of CO, CO₂, and O₂ concentrations. The "instantaneous" burn rate of the fuel is measured with an electronic scale and the gas concentrations are measured with three gas analyzers. A schematic of the gas sampling train used for the scale-based method is shown in Fig. (9). The sample gases are passed through a 0°C condenser and a filter to remove water and particulates before entering the sample bag. Due to the concentrations in the stack varying during the sampling interval, a 50 liter sample bag is used to collect a time-averaged flue gas sample. The desiccant tube removes any moisture left in the flue gas sample before it enters the O₂ analyzer (Horiba MPA-21A), the CO₂ analyzer (Horiba PIR 2000) and the CO analyzer

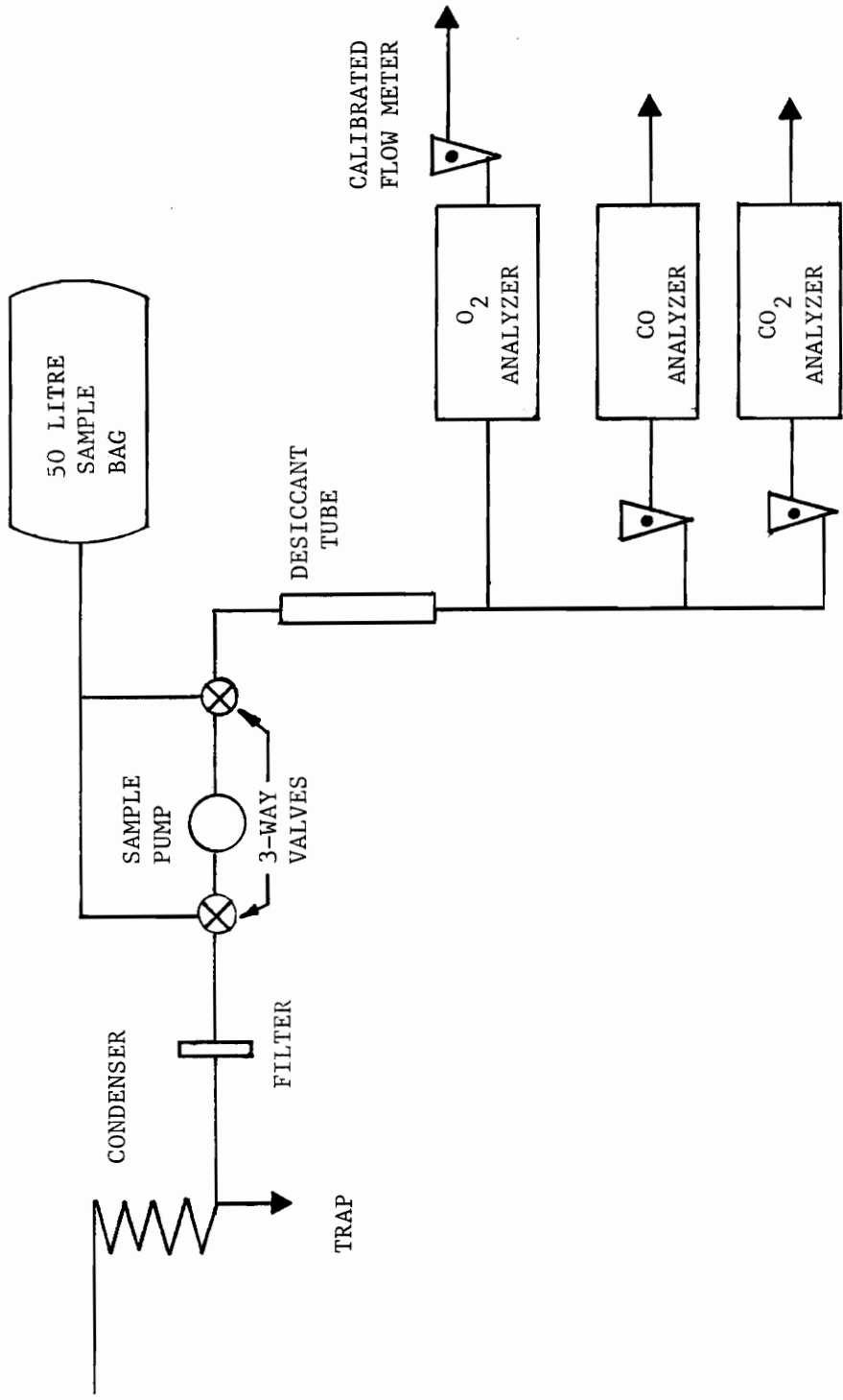


Figure 9. Sampling Train for Scale-Based Method

(Horiba PIR 2000). The flue gas leaving the analyzers is exhausted to the room.

3.3.4 General Set-Up of the Flow Systems

The set-up used for testing the flow rate measurement systems is shown in Fig. (10). The molar flow rate of the dilution tunnel is measured with a sharp-edged orifice. The pressure drop across the orifice is measured with a variable reluctance pressure transducer for some tests and with an inclined manometer for others. A type-K thermocouple, connected to a digital thermometer, is used to measure the gas temperature in the dilution tunnel. The stack temperature is measured using the centerline thermocouple of the array.

The CO tracer system is set up to keep the sample lines as short as possible. Short sample lines are needed to keep the pressure drop and response time of the sampling system to a minimum. The CO analyzer output is recorded on a strip chart recorder. The analyzer output during the tests varied between 7 and 0.5 volts and therefore the 0-10 and the 0-1 volt ranges on the strip chart recorder are used. The stack requires the 0-10 volt range and the dilution tunnel the 0-1 volt range. The ranges are manually switched when the CO tracer system is multiplexed.

The pitot array is located 3.2 m above the breech of the stove to allow the flue gas velocity and temperature gradients to become more uniform. The signal from the pitot tube transducer is electrically filtered to remove the noise before being recorded on a strip chart recorder. A filter with a time constant of 15 sec. is used.

The data recording for the scale-based method is done manually. This data includes the output of the analyzers, the scale reading at the beginning and end of the sampling interval, and the time period between

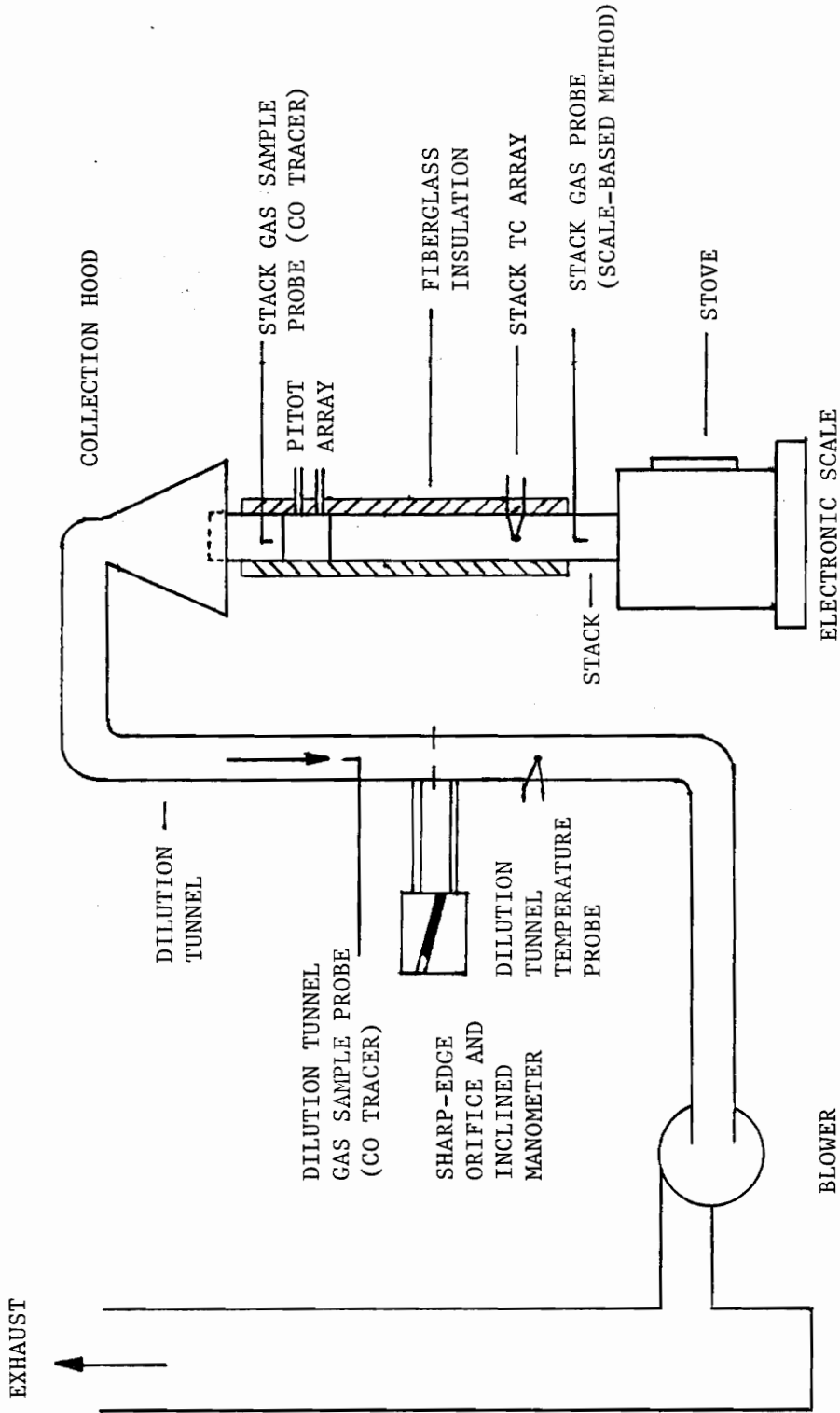


Figure 10. Set-Up of Flow Measuring Systems

the scale readings.

3.4 Test Procedures

3.4.1 Temperature Measurement Procedure

Temperature profiles of the flue gases in the stack were measured during test runs 1 and 2. The thermostat was set on low for the first run and high for the second run. During the low fire test the thermostat was set on high for the first hour to allow the fire to catch and then set to low.

Prior to array measurement of the temperature profiles, the zero and full scale points of the A/D converter were set using the proper calibration voltages. Next a software calibration was performed to correct biasing errors of the multiplexer. This calibration was performed using a low noise DC source (1.5 v battery) and a potentiometer to vary the input voltage. The voltage source was connected in turn to each of the 16 A/D channels. A multimeter was used to read the input voltage and this reading was then compared to the output of the data acquisition system in order to estimate the biasing error of the multiplexer. This was done over a 0-19 millivolt range and the correction factor was then applied to the temperature profile data.

The thermopile reference junctions were put in an ice bath. The strip chart recorder used to record the thermopile output was zeroed and allowed to run for the duration of the test.

The wood, red oak, was split so a portion could be used to evaluate the moisture content. The inclined manometer was zeroed and the blower on the dilution tunnel was turned on. The data acquisition system was

started and the electronic scale was zeroed prior to loading the stove. A kindling fire was started and after a sufficient coal bed was established (usually 3-4 kg) the main load of split oak (approximately 17 kg with 5 or 6 pieces averaging 63 cm long and 9 cm in diameter) was placed in the stove. The moisture content of the wood was determined by drying it at 100°C. It varied between 26 to 27 percent on a wet basis for the two runs.

Temperature data and scale readings were recorded with the data acquisition system for tests 1 and 2. Data were recorded once every minute during the kindling burn cycle since the stack temperature and the scale reading changed rapidly. Once the main load was placed in the stove, the time interval between data recordings was changed. Temperature data and scale readings were recorded every twenty-five minutes for a period of five minutes. During this five minute period, data was recorded at intervals of thirty seconds giving a total of ten stack temperature and scale readings.

3.4.2 Flow Rate Measurement Procedure

Stack flow rates were measured during runs 3, 4 and 5. All three methods were used during runs 4 and 5, but the scale-based method was not used during run 3. The three runs were generally conducted with a high fire thermostat setting although there were times during a test when the thermostat was adjusted to a lower setting. Flow data was taken when the CO stack readings were observed to change less than 0.2 volts over approximately a 15-30 second period. Fairly steady CO concentrations were needed so that the (multiplexed) stack and dilution

tunnel concentrations would be compatible (i.e., the dilution tunnel CO concentration differs from the stack CO concentration due to the dilution process only).

Prior to the flow rate testing, the wet basis CO analyzer was calibrated. This calibration was done at the operating pressure of the system (output signal of the pressure transducer at $6.00\text{v} \pm 0.01\text{v}$ which is approximately 16 kPa).

The pitot array and dilution tunnel orifice were calibrated using the methods described in Appendix A. Before each run, the filters of the CO tracer system were changed and the system was tested for leaks. Leak tests were performed by capping the probe tips and checking the rotameter for an indication of flow. Leaks upstream of the analyzer would cause errors in the concentration measurement and therefore leak checks were run before each test. After the leak test, the CO analyzer was zeroed and spanned. The sample line heaters and the oven were turned on and allowed to come up to 75°C . The CO, CO₂, and O₂ analyzers for the scale-based method were zeroed and spanned.

When the flow measurement systems were ready for testing, the dilution tunnel blower was turned on and a kindling fire was started. After a sufficient coal bed was established (usually 3-4 kg), the main load was added. The main load consisted of split oak (approximately 15 kg with 3 or 4 pieces averaging 11 cm in diameter and 63 cm in length). A quarter of each log was kept for the moisture content evaluation. The moisture content was determined by drying the wood at 100°C and varied between 24 and 25 percent on a wet basis for runs 3, 4, and 5.

After the main load was added, the pitot array transducer was zeroed and the CO tracer system began sampling. However, the pressure in the CO system did not remain constant, despite the vacuum regulator, when sampling first began. It is believed that the filters loading with particulates may have caused this problem. Once the CO tracer's pressure became steady, collection of the flow data from the three systems was begun. The beginning of each flow measurement was marked on the strip chart recorders used for recording the output of the pitot array and the CO tracer analyzer. The sample pump for the scale-based method was turned on to fill the sample bag. The scale was read and a stop watch was started (the time was needed to determine the burn rate during the sampling interval). The CO tracer system was manually multiplexed between the stack and the dilution tunnel every 1.5 to 2.0 minutes, which allowed more than enough time for the analyzer to reach its new reading. Each CO tracer flow measurement consisted of two stack and two dilution tunnel CO measurements. When the sample bag for the scale method was full, usually after 3 to 5 minutes, the sample pump was turned off and the stop watch was stopped. The scale was read and the sampling time interval was recorded. The end of the test was then marked on both strip chart recorders. The flue gas in the sample bag was pumped through the three analyzers and the output of each was manually recorded. The pitot array was zeroed once every hour to minimize zero drift errors of the transducer, which in an hour tended to be about 0.01 volts (1 percent of full scale).

Other data recorded during a test included the stack temperature, the dilution tunnel temperature, and the differential pressure across the dilution tunnel orifice.

At the end of a run, the analyzers were checked for drift at the zero and span points. The CO tracer sampling lines were disconnected from the stack and the dilution tunnel and room air was purged through the system for a period of 12-24 hours to thoroughly flush the system of flue gas before shutting it down. The blower on the dilution tunnel was allowed to run until the coal bed in the stove burned out.

The day following each test run the dilution tunnel orifice was calibrated (Appendix A.2) to check for any changes in the flow coefficient due to particulate build up on the orifice. The pitot array was also calibrated (Appendix A.1) to check for changes in the flow coefficient. (The flow coefficient of the pitot array is defined as the actual mass flow divided by the indicated mass flow.)

3.5 Calculation Procedures

3.5.1 CO Tracer Flow Rate Calculation

The CO tracer method relies on the conservation of CO, i.e., all the CO going up the stack will end up in the dilution tunnel if all the stack gas is drawn into the dilution tunnel. Since room air has a negligible amount of CO, the molar flow rate of CO in the stack and the dilution tunnel are equal and can be expressed by

$$[\text{CO}]_S \dot{n}_S = [\text{CO}]_{\text{DT}} \dot{n}_{\text{DT}} \quad (8)$$

where

$[CO]_S$ = mole fraction of CO in the stack (wet basis)

$[CO]_{DT}$ = mole fraction of CO in the dilution tunnel (wet basis).

Equation (8) gives

$$\dot{n}_S = \dot{n}_{OR} \frac{[CO]_{DT}}{[CO]_S} \quad (9)$$

The molar flow rate in the dilution tunnel is calculated by

$$\dot{n}_{DT} = \frac{C_{OR} A_{OR}}{MW_{DT}} \left[\frac{2 \Delta P_{OR} P}{RT_{DT}} \right]^{1/2} \quad (10)$$

where

C_{OR} = discharge coefficient of the orifice

A_{OR} = cross-sectional area of orifice, $4.56 \times 10^{-3} m^2$

MW_{DT} = molecular weight of gas in dilution tunnel, kg/kmol

P = ambient pressure, kPa

ΔP_{OR} = pressure differential across orifice, Pa

R = gas constant, kJ/kg K

T_{DT} = temperature of gas in dilution tunnel at orifice plate, K

The orifice discharge coefficient was determined by the calibration tests described in Appendix A.2. The choice of a 7.6 cm orifice gave a large enough dilution tunnel flow rate to entrain all the exhaust gases

from the stack yet a small enough dilution ratio to keep the CO concentration within measurable limits.

Equation (9) can be rearranged to give the stack flow in terms of a mass flow rate.

$$\dot{m}_S = \dot{n}_{DT} MW_S \frac{[CO]_{DT}}{[CO]_S} \quad (11)$$

where

MW_S = molecular weight of gas in the stack, 28.9 kg/kmol

The assumption of using the properties of air for the gas in the stack and in the dilution tunnel was reasonable since the molecular weight of flue gas is very close to 29 kg/kmol.

3.5.2 Pitot Array Flow Rate Calculation

The stack flow rate measured with the pitot array is determined by

$$\dot{m}_S = C_{DP} A_S \left[\frac{2\Delta P_{PA}}{RT_S} \right]^{1/2} \quad (12)$$

where

C_{DP} = calibration coefficient of the pitot array

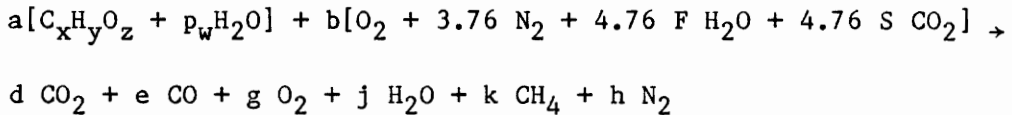
A_S = cross-sectional area of the stack, 0.0182 m²

ΔP_{PA} = pressure differential of the array, Pa

The discharge coefficient was determined by calibration tests described in Appendix A.1.

3.5.3 Scale-Based Flow Rate Calculation

The algorithm used to determine the stack flow rate was slightly different than the WHA algorithm. In the algorithm used, CO_2 and H_2O in room air was accounted for. Both are neglected in the WHA algorithm. Otherwise, the assumptions used in this algorithm were identical to those used in the WHA algorithm. The combustion equation is the following:



where the known quantities include

- F = moles of water per mole of dry CO_2 -free air in room air
 S = moles of CO_2 per mole of dry CO_2 -free air in room air
 p_w = moles of water per mole of dry wood

The quantities x , y , and z are chosen to give the wood a molecular weight of 1000 and to make the relative amounts of C, H, and O agree with the mass fractions of C, H, and O in the wood on a dry ash-free basis. Average mass fractions of 48.8 percent carbon, 5.8 percent hydrogen, and 45.4 percent oxygen were measured in the C-H-O analysis performed on the oak used in this study. Using these mass fractions, the quantities x , y , and z are calculated to be 40.7, 57.3, 28.4

respectively.

Solution of the combustion equation is necessary for determining the stack flow rate. Performing atom balances yields:

$$\text{H: } a(2p+y)+b(2(4.76)F)-2j-4k=0 \quad (14)$$

$$\text{O: } a(z+p)+b[4.76(F)+2+2(4.76)S]-2d-e-2g-j=0 \quad (15)$$

$$\text{N: } 3.76b-h=0 \quad (16)$$

$$\text{C: } ax+4.76(S)b-d-e-k=0 \quad (17)$$

The mole fractions d , e , and g are measured on a dry basis. This leaves five unknowns but only four equations, and thus an additional equation is needed. Assuming 100 moles of dry products as the basis of the solution gives:

$$d+e+g+k+h=100 \quad (18)$$

The solution of these five equations gives:

$$k = \frac{dC_1 - eC_2 + gC_3 - 126.6S(2z-y) + 106.38(1+4.76S)x}{(4.765 - 2.936)x + (1 + 1.266S)(y-2z)} \quad (19)$$

$$h = 100 - k - g - e - d \quad (20)$$

$$b = h/3.76 \quad (21)$$

$$a = \frac{(1+1.266S) - 126.6S + 1.266Sg}{x} \quad (22)$$

$$j = ap - 2k + 0.5ay + 4.76bF \quad (23)$$

where

$$\begin{aligned} C_1 &= (1 + 1.266S)(2z - y) - (5.0638 + 4.76S)x \\ C_2 &= (3.0638 + 4.76S)x + (y - 2z)(1 + 1.266S) \\ C_3 &= 1.266S(2z - y) - x(5.0638 + 4.76S) \end{aligned}$$

The stack flow can now be calculated by

$$\dot{m}_S = \left(\frac{\Delta m}{\Delta t}\right) \left(\frac{100 + j}{a}\right) \left(\frac{MW_S}{MW_{wd}}\right) \quad (24)$$

where

- Δm = change in mass during a measured time interval, kg
- Δt = time interval for the Δm measurement, s
- j = moles of water, kmol
- a = moles of wood, kmol
- MW_{wd} = molecular weight of wood, kg/kmol.

3.5.4 CO₂ Tracer and the Thermal Mass Flowmeter Flow Rate Calculations

Although not used in this study, the thermal mass flowmeter and the CO₂ tracer techniques are promising methods of stack flow measurement. Therefore, the flow rate calculations for these methods will be presented.

The stack flow rate calculation using the stack CO_2 as a tracer is very similar to the CO tracer method, the only difference being that the CO_2 in room air must be considered. The conservation equation for CO_2 relates the molar flow rate of the stack, the dilution tunnel, and the room air drawn into the dilution tunnel, and is given by:

$$\dot{n}_A [\text{CO}_2]_A + \dot{n}_S [\text{CO}_2]_S = \dot{n}_{\text{DT}} [\text{CO}_2]_{\text{DT}} \quad (25)$$

where

\dot{n}_A = molar flow rate of room air drawn into the dilution tunnel
(wet basis)

$[\text{CO}_2]_A$ = mole fraction of CO_2 in the room air (wet basis)

Since \dot{n}_{DT} and the concentrations are measured, there are only two unknowns (\dot{n}_A and \dot{n}_S). The overall continuity equation can be used to provide the needed additional equation:

$$\dot{n}_A + \dot{n}_S = \dot{n}_{\text{DT}} \quad (26)$$

Solving Eq. (26) for \dot{n}_A , substituting into Eq. (25) and solving for \dot{n}_S yields:

$$\dot{n}_S = \dot{n}_{\text{DT}} \frac{[\text{CO}_2]_{\text{DT}} - [\text{CO}_2]_A}{[\text{CO}_2]_S - [\text{CO}_2]_A} \quad (27)$$

The mass flow can be determined by:

$$\dot{m}_S = \dot{n}_{DT} MW_S \quad (28)$$

The molecular weight of the stack gas can be approximated by using properties of air or more accurately by using flue gas composition data.

The thermal mass flowmeter uses the energy input to a heater located in the flue gas along with measurement of the temperature rise across the heater to measure the $\dot{m}c_p$ product of the flue gas. The heat transfer from the electric heater to the gas will be mainly due to convection. Some of this energy input may be lost due to heat transfer or through the walls of the stack which will cause an error in the flow measurement. The first law written for a control volume around the meter section can be used to estimate the heat loss.

$$\dot{Q}_{in} = \dot{m}_S (h_o - h_i) - \dot{Q}_{OUT} \quad (29)$$

where

\dot{Q}_{in} = power input to heater, W

\dot{m}_S = mass flow of stack gas, kg/s

h_o = enthalpy of stack gas upstream of heater, J/kg

h_i = enthalpy of stack gas downstream of heater, J/kg

\dot{Q}_{OUT} = heat loss through stack walls, W

An energy balance on the insulated flue wall yields:

$$\frac{2\pi k \Delta x}{\ln(R_w/R_{OS})} [T_S - T_w] = U_c A_w [T_w - T_{Rm}] + \sigma A_w \epsilon_w [T_w^4 - T_{Rm}^4] \quad (30)$$

where

T_S = flue gas temperature at inner stack wall, K

k = thermal conductivity of insulation, W/mk

Δx = length of meter section, m

R_w = inner stack wall radius, cm

R_{OS} = radius of outer insulation surface, cm

U_c = heat transfer coefficient, W/m^2K

A_w = outer surface area of stack, m^2

T_{OS} = outer surface temperature of insulation, K

T_{Rm} = ambient temperature, K

σ = Stefan-Boltzman constant, $5.76 \times 10^{-8} W/m^2K^4$

ϵ = emissivity of outer stack surface.

Because Eq. 30 cannot be solved directly for T_w , an iterative procedure is required. Once T_w is found, the heat loss, \dot{Q}_{OUT} , can be determined. The heat loss will depend on the insulation used on the meter section and the surface area of the meter section. If the heat loss is nearly constant, then calibration of the meter is possible and Eq. (29) can be written as:

$$\dot{Q}_{in} = C_{TM} \dot{m}_s (h_o - h_i) \quad (31)$$

where

C_{TM} = Calibration factor

Assuming a constant specific heat over the temperature rise in the meter

section, then Eq. (31) can be solved for the $\dot{m}_s c_p$ product.

$$\dot{m}_s c_p = C_{TM} \frac{\dot{Q}_{in}}{\Delta T_{TM}} \quad (32)$$

where

\dot{Q}_{in} = power input to meter, watts

c_p = specific heat of gas stream, J/kg K

ΔT_{TM} = stream temperature rise across meter, K

If the mass flow is desired, then knowledge of the flue gas composition is necessary for evaluating the specific heat. The specific heat of the flue gas can be evaluated since the gas temperature is known and a gas composition can be estimated. The specific heat does not vary more than about 5 percent even for a large variation in flue gas composition and therefore the specific heat can be estimated with reasonable accuracy.

In order to measure the temperature rise across the meter, the average temperature upstream and downstream of the heater must be measured. This measurement of the average temperature would be easier to make if the temperature profile was flat. A analytical model was developed to determine if a reasonable-length insulated section of a flue pipe would be long enough to allow a flat temperature profile to develop. This model is described in Appendix C.

4. RESULTS

4.1 Temperature Measurements

The results of runs 1 (low fire setting) and 2 (high fire setting) are presented in the following sections.

4.1.1 Burn Rates

Plots of the scale readings are shown in Figs. (11) and (12). Times when the thermostat was adjusted or when the fire was stoked are indicated on these plots. The two tests were conducted on a hot-to-hot basis. The test interval began when the kindling coal bed weighed 20 percent of the main load, at which point the main load was added. The test interval ended when the main load coal bed returned to 20 percent of the initial main load weight. The burn rate over this test interval was the average burn rate for the test run and it can be determined from the change in fuel weight during the interval divided by the time period of the test interval. The average burn rates for test run 1 and 2 were 3.3 and 2.6 kg/hr respectively. These average burn rates were in the medium burn rate range. The "local" burn rates, i.e. the change in fuel weight during a time interval of about 30 minutes or less when data were taken, are obtained using a central difference technique. These burn rates were, in general, different than the average burn rate of the run. The times when the temperature profiles were measured are shown in Figs. (11) and (12). The burn rates during these temperature measurements varied between 5 and 1 kg/hr.

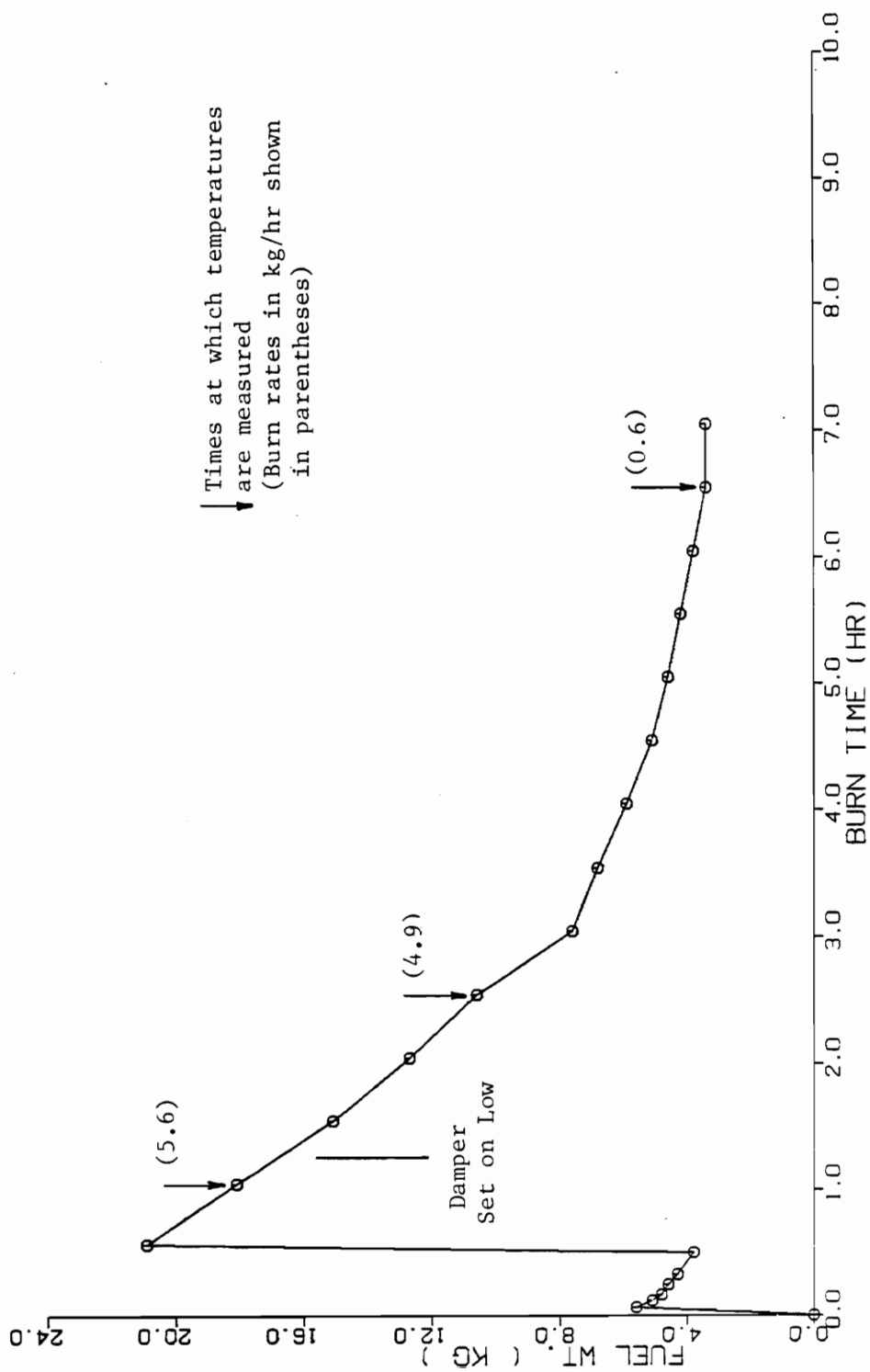


Figure 11. Mass-Time History from Scale Readings for Run 1

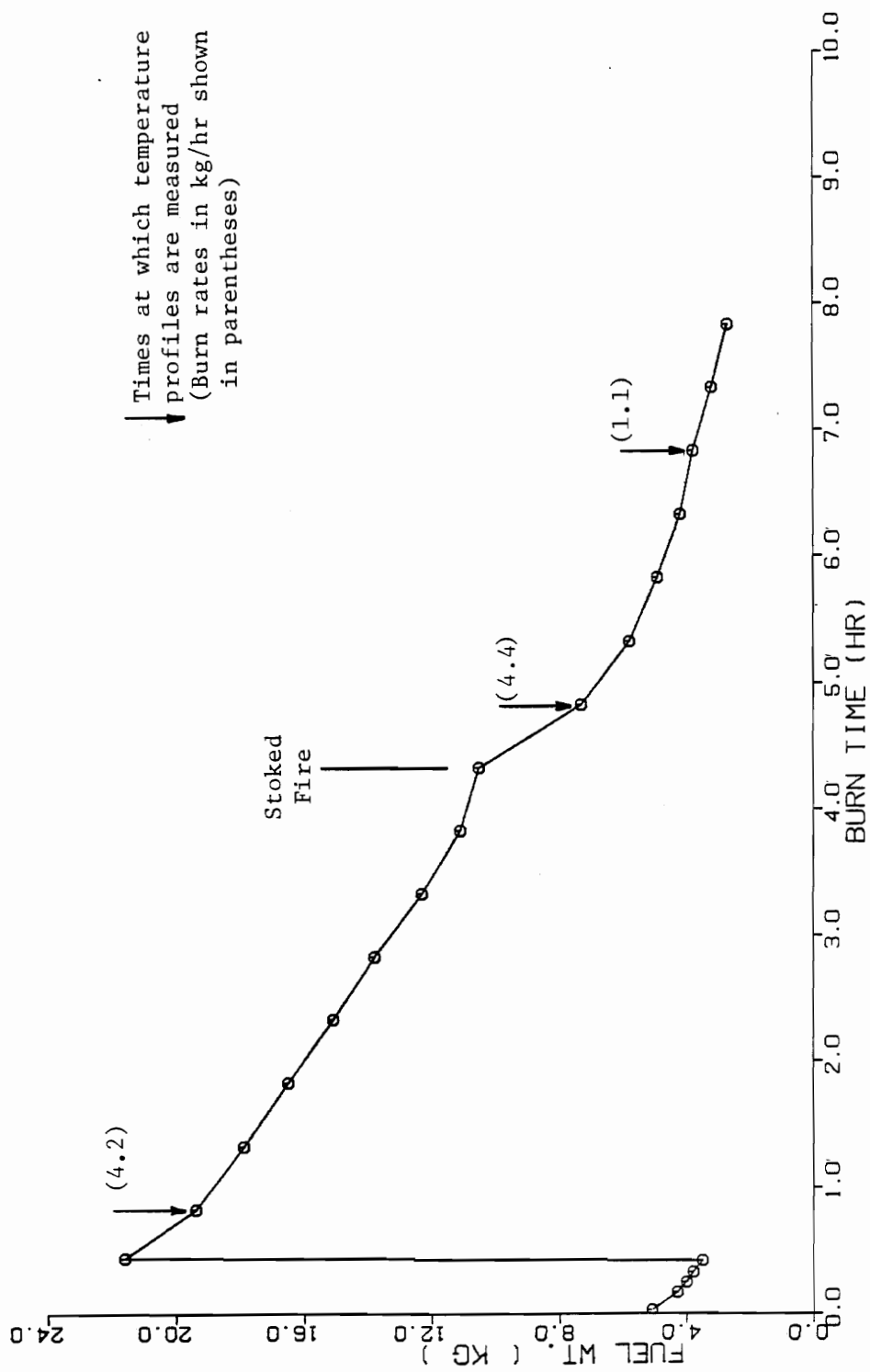


Figure 12. Mass-Time History from Scale Readings for Run 2

4.1.2 Temperature Profiles

The instantaneous temperature profiles were recorded at 25 minute intervals for a period of 5 minutes. During these 5 minute periods, the temperature profiles were recorded every thirty seconds. Temperature profiles were measured regardless of whether steady conditions existed in the stack. The profiles shown in Figs. (13-18) are those measured at approximately the beginning, middle, and the end of runs 1 and 2. Note that the profiles are plotted on an expanded temperature scale in order to show the profile in more detail. The time rate of change of the stack temperature shown on each figure is based on the area-average temperature of the profiles recorded during the 5 minute period. Each profile shown is typical of the others recorded during the five minute period.

Figures (19) and (20) show the area-weighted average temperature histories of the array for runs 1 and 2. The times when the temperature profiles of Figs. (13-18) were measured are indicated on these figures. The figures show that these temperature profiles were measured during times when the average temperature was changing rapidly with the exception of the last profile measurement of both runs. However, if one looks at just the average array temperature during the five minute period when these profiles were measured, the average array temperature changed less than 4°C except for the profile in Fig. (17) where it changed 15°C . Therefore, one can conclude that the temperature profiles were generally measured during fairly steady conditions in the stack even though the conditions appear to be changing rapidly in Figs. (19) and (20).

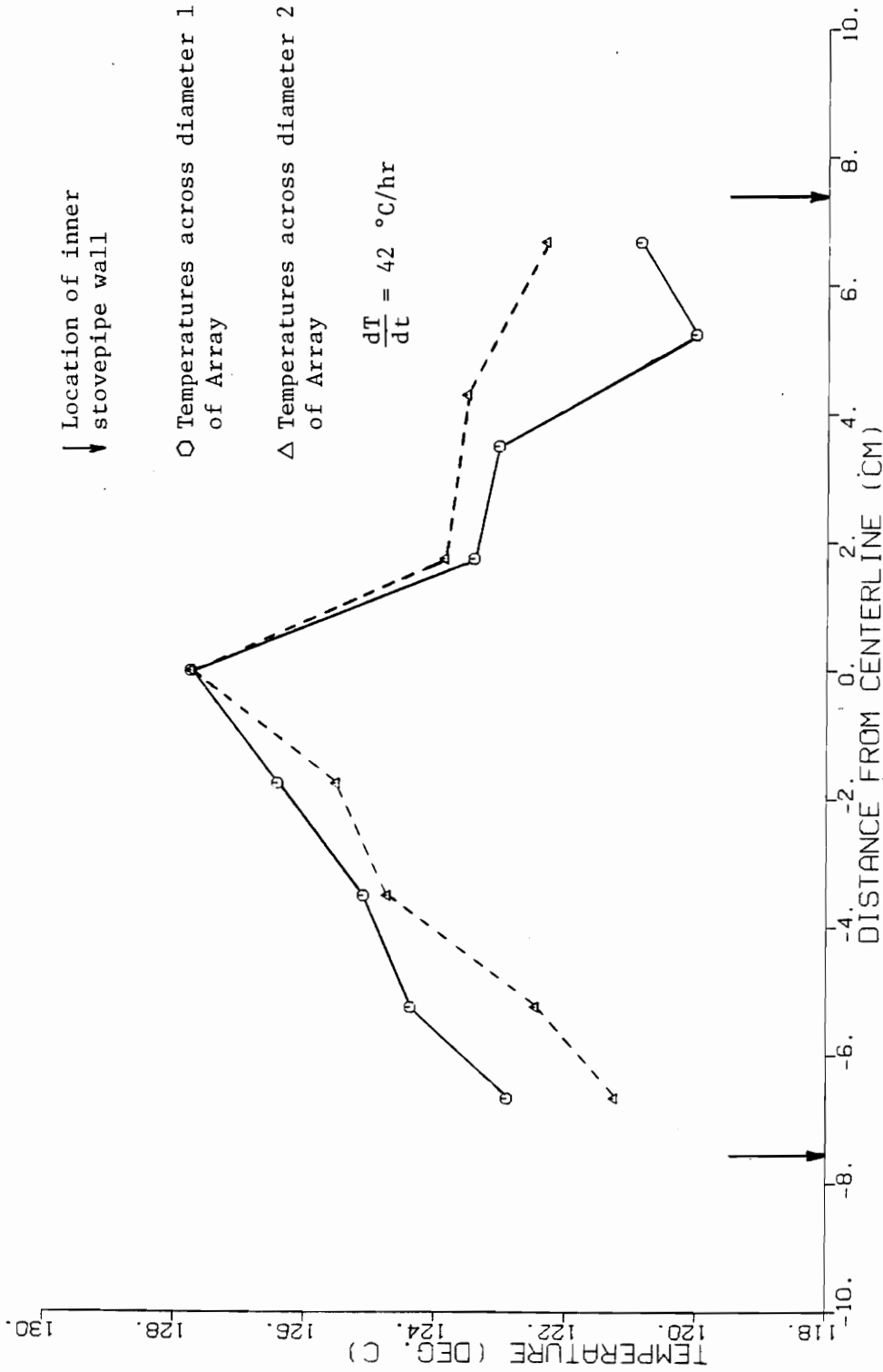


Figure 13. . Temperature Profile Recorded Near Beginning of Run 1

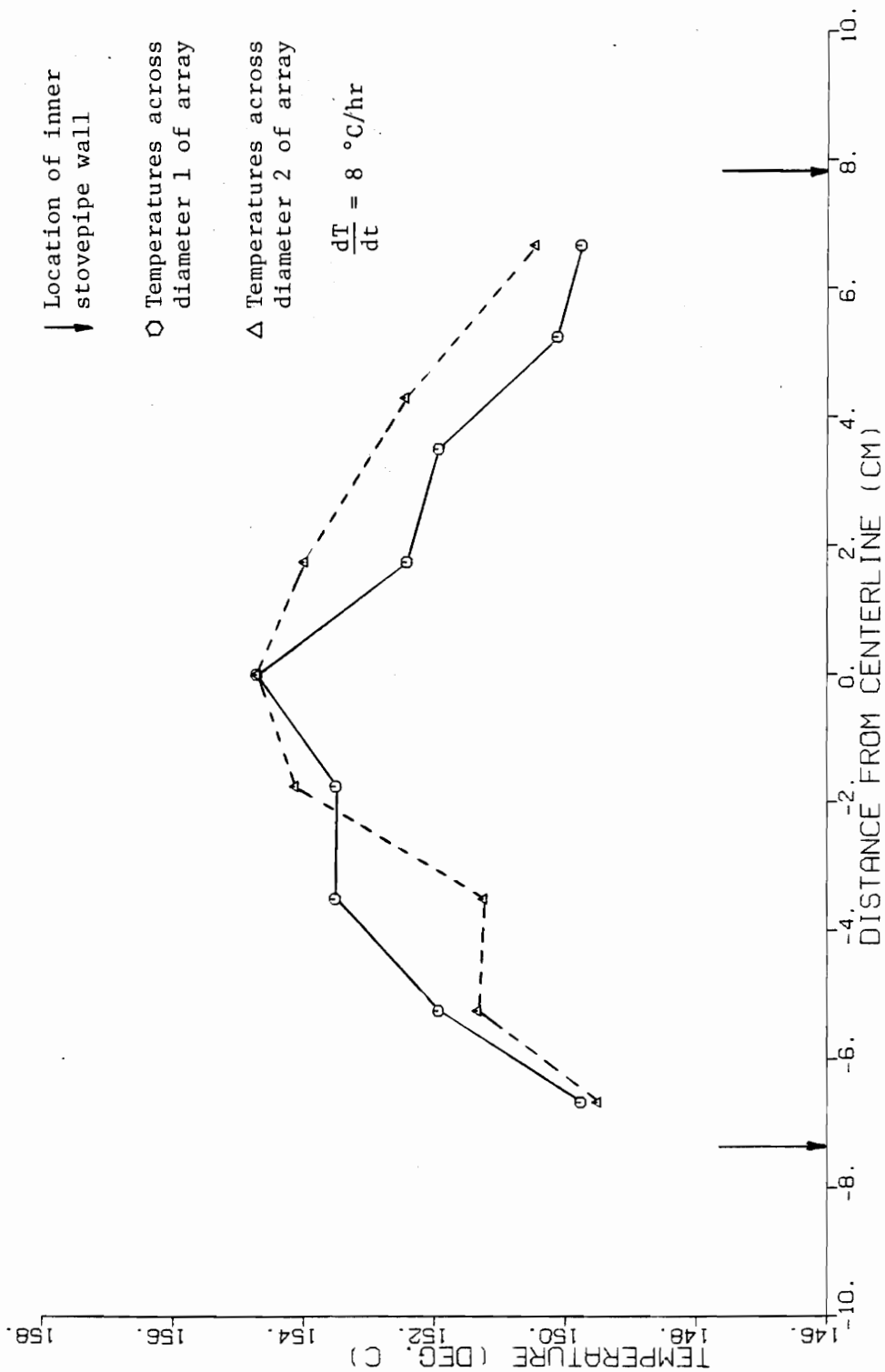


Figure 14. Temperature Profile Recorded Near the Middle of Run 1

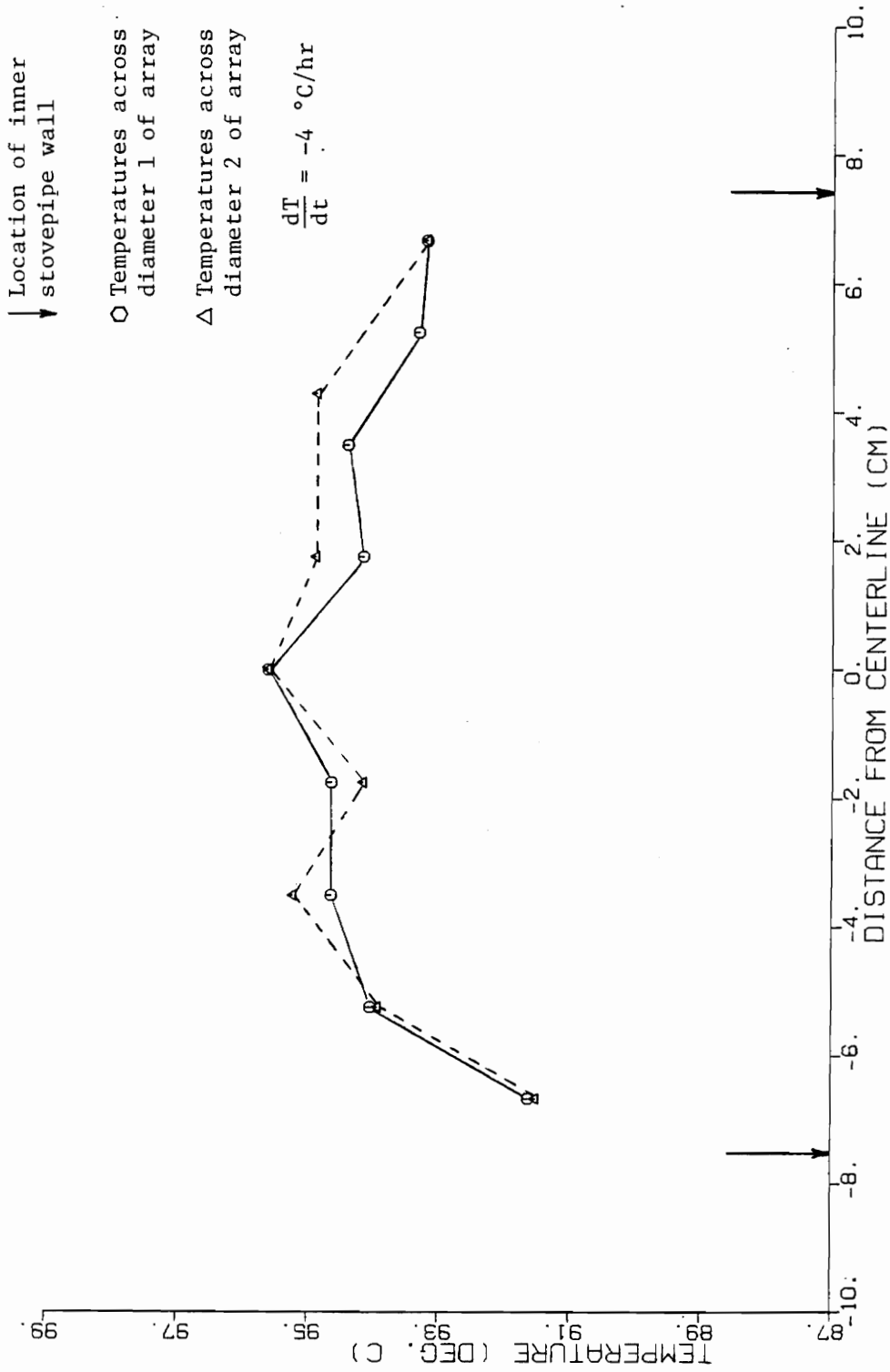


Figure 15. Temperature Profile Recorded Near the End of Run 1

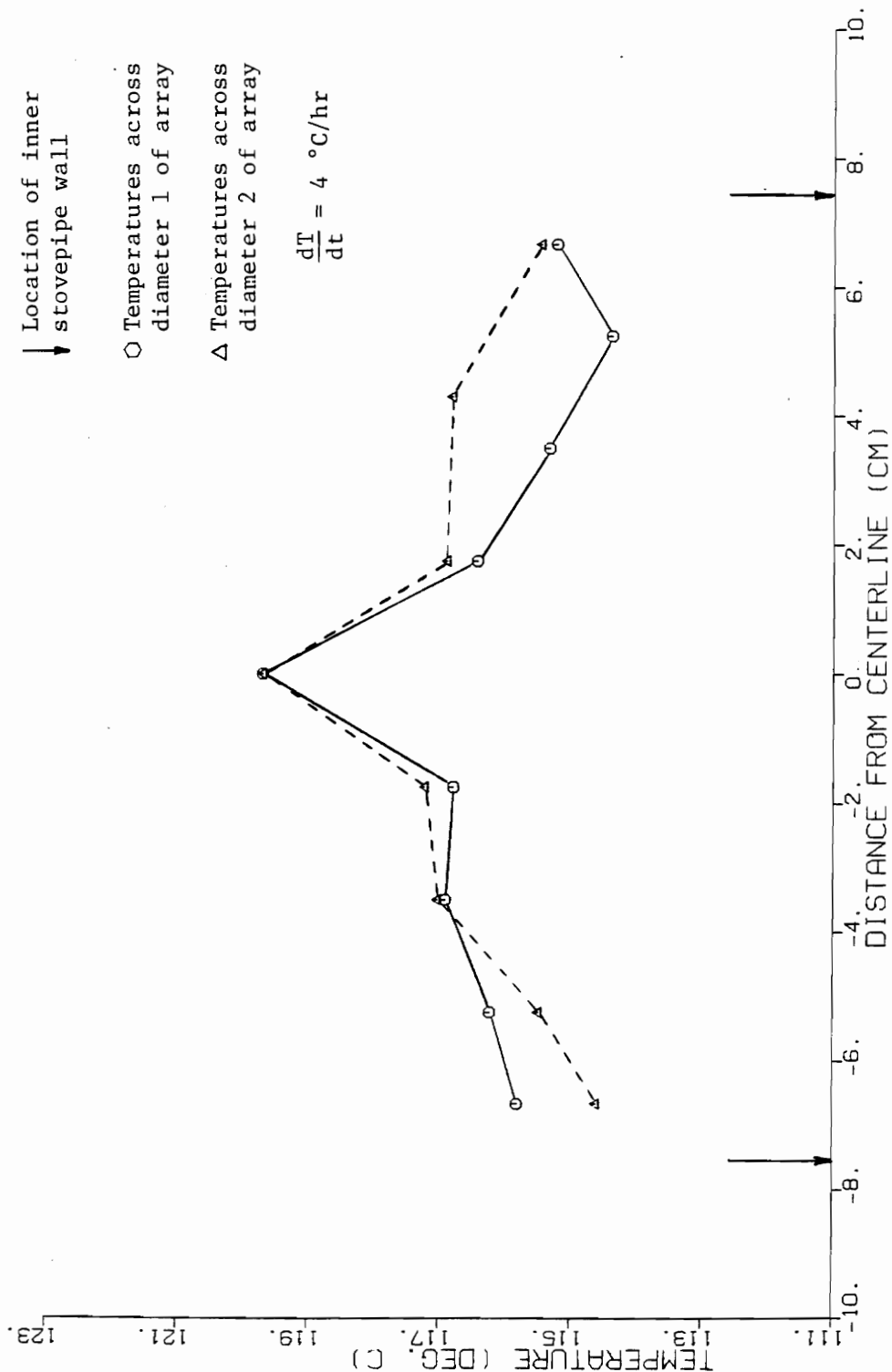


Figure 16. Temperature Profile Recorded Near the Beginning of Run 2

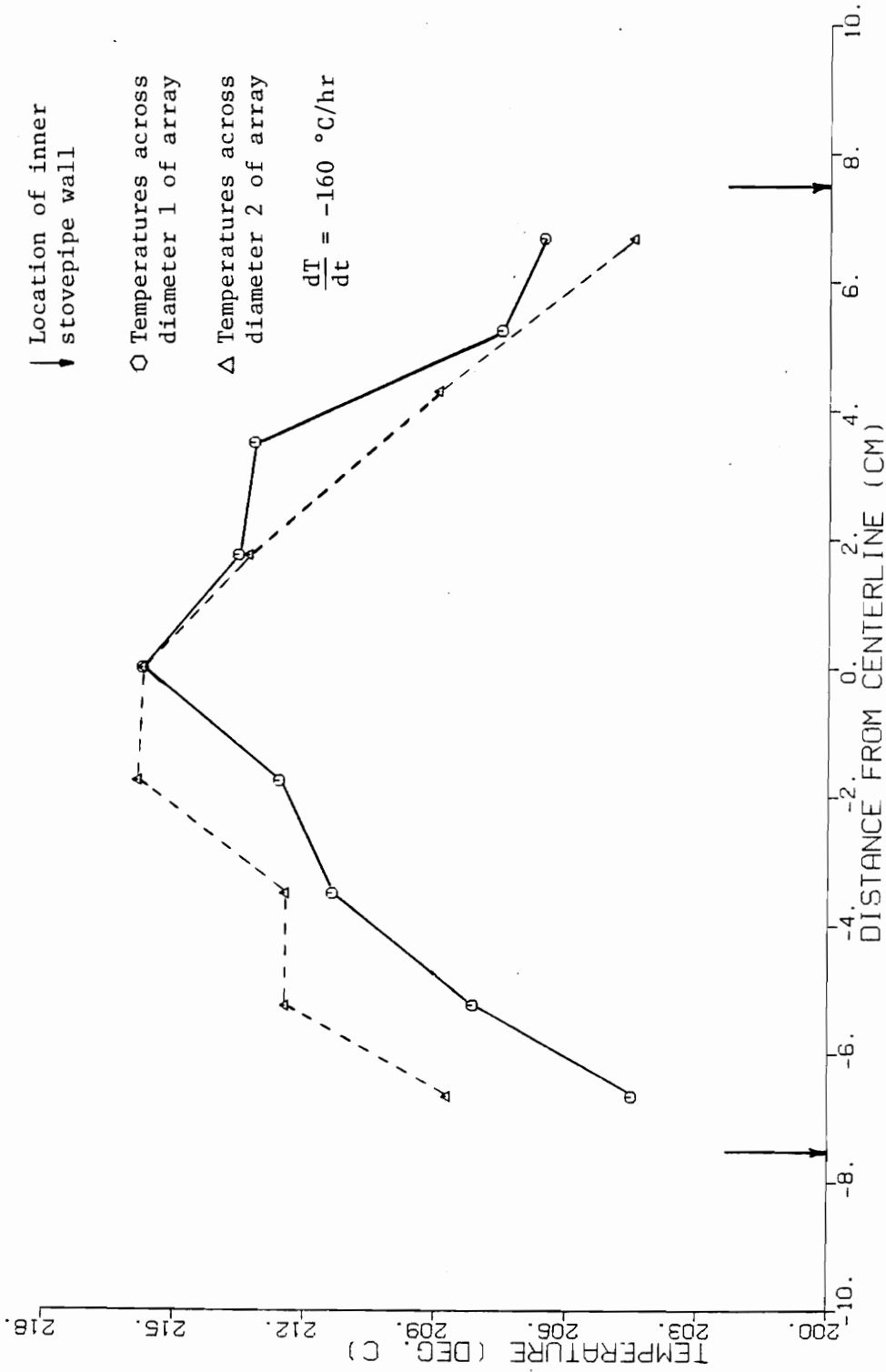


Figure 17. Temperature Profile Recorded Near the Middle of Run 2

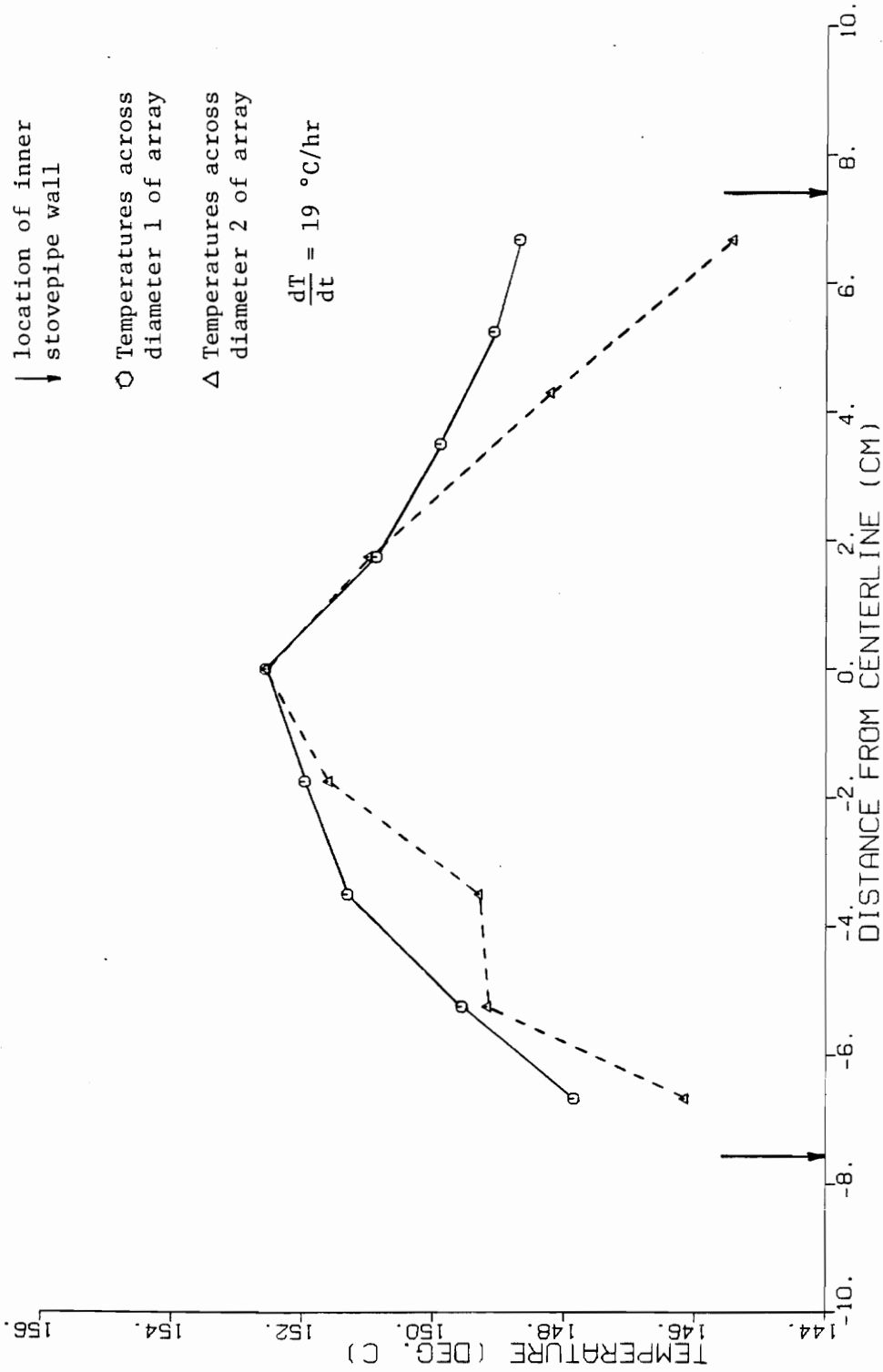


Figure 18. Temperature Profile Recorded Near the End of Run 2

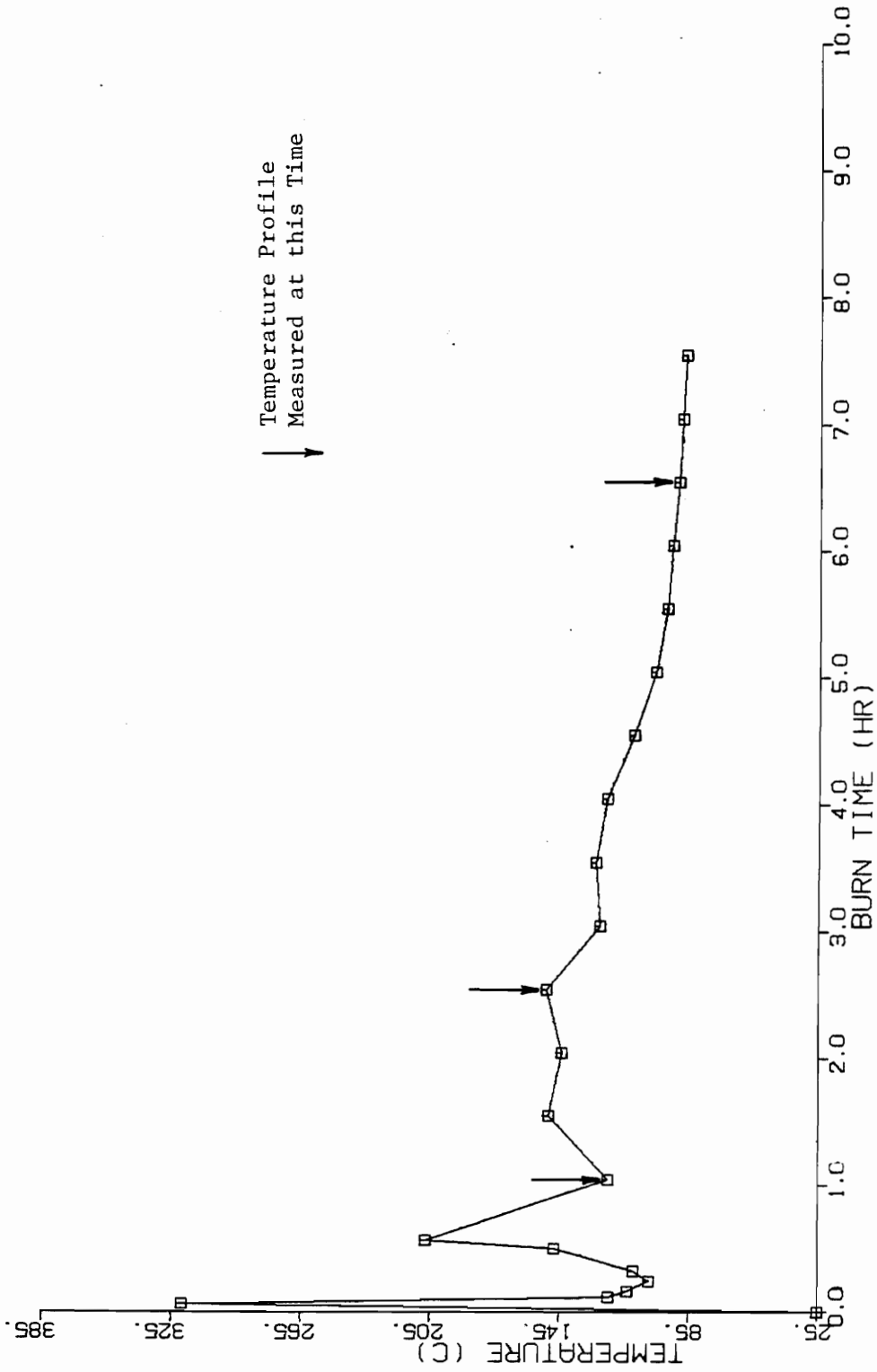


Figure 19. Average Stack Temperature History for Run 1

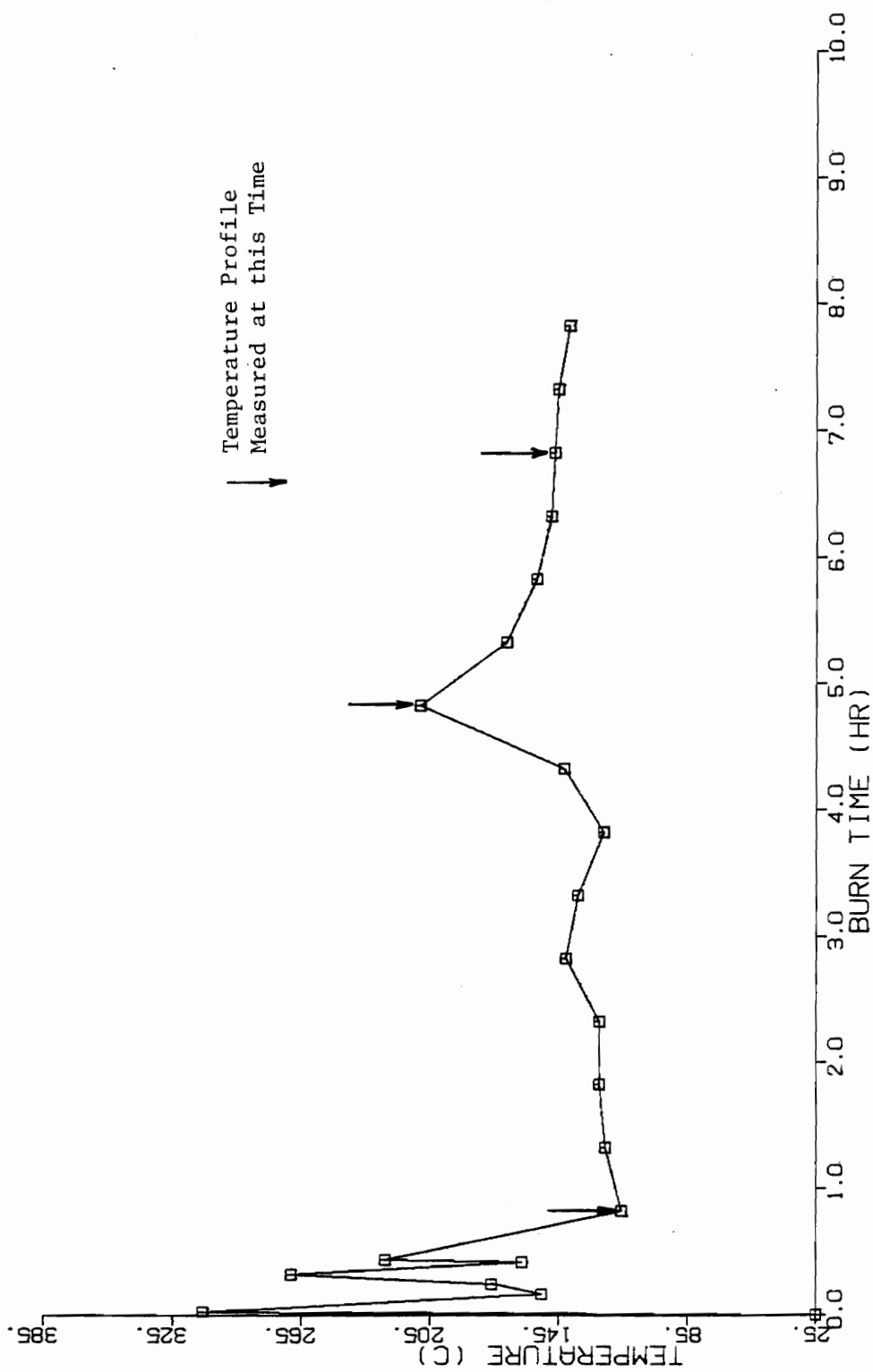


Figure 20. Average Stack Temperature History for Run 2

The radial temperature differences were caused by the wall temperature being cooler than the gas flow. The thermal mass of the stack slowed the response of the wall temperature to changes in the gas temperature and therefore the time rate of change of the average gas temperature might correlate with the radial temperature gradients in the stack. The time rate of change of the average stack temperature was approximated using the stack temperature measured by the thermopile (located 2m above the array) since it recorded the stack temperature on a continuous basis and the array did not. The time rate of change of the average temperature was then plotted versus the radial temperature variation. Figures (21) and (22) show that the magnitude of the radial temperature differences were generally around -1 to -5°C and did not change more than 5°C for large values of dT_{ave}/dt . Also, the slope of the temperature difference was always negative (temperature decreases as the radius increases). A positive temperature difference is theoretically possible if the gas cools rapidly enough that the insulated wall temperature remains hotter than the gas due to the stored energy in its thermal mass.

4.1.3 Heat Loss Measurement

The temperature drop of the flue gas through 2m of the insulated flue pipe section was measured during test runs 1 and 2 with the thermopile and the array. The temperatures measured by the 16 thermocouple array were area-weighted to give an average flue gas temperature.

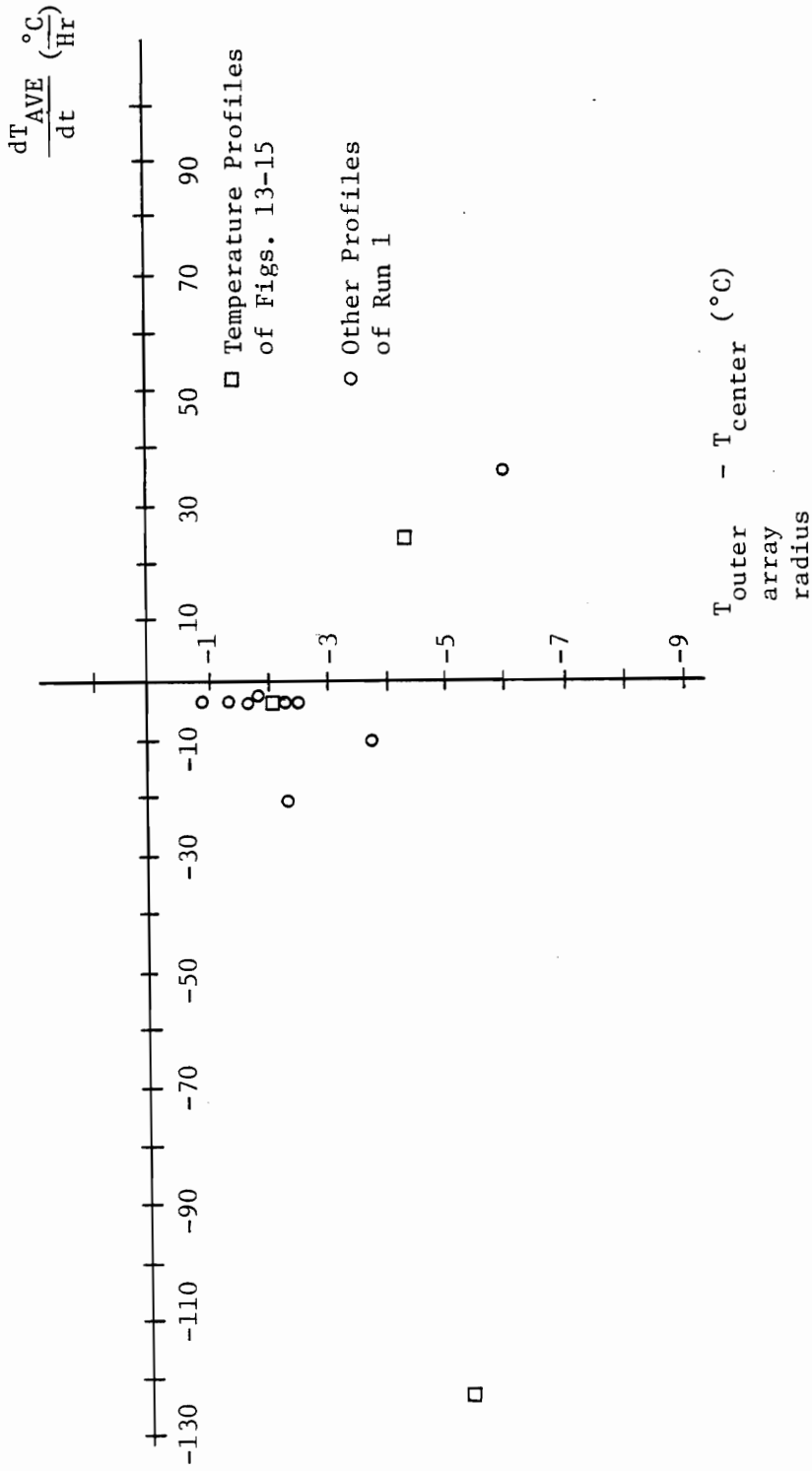


Figure 21. The Effect of a Change in Stack Temperature on the Radial Temperature Difference for Run 1.

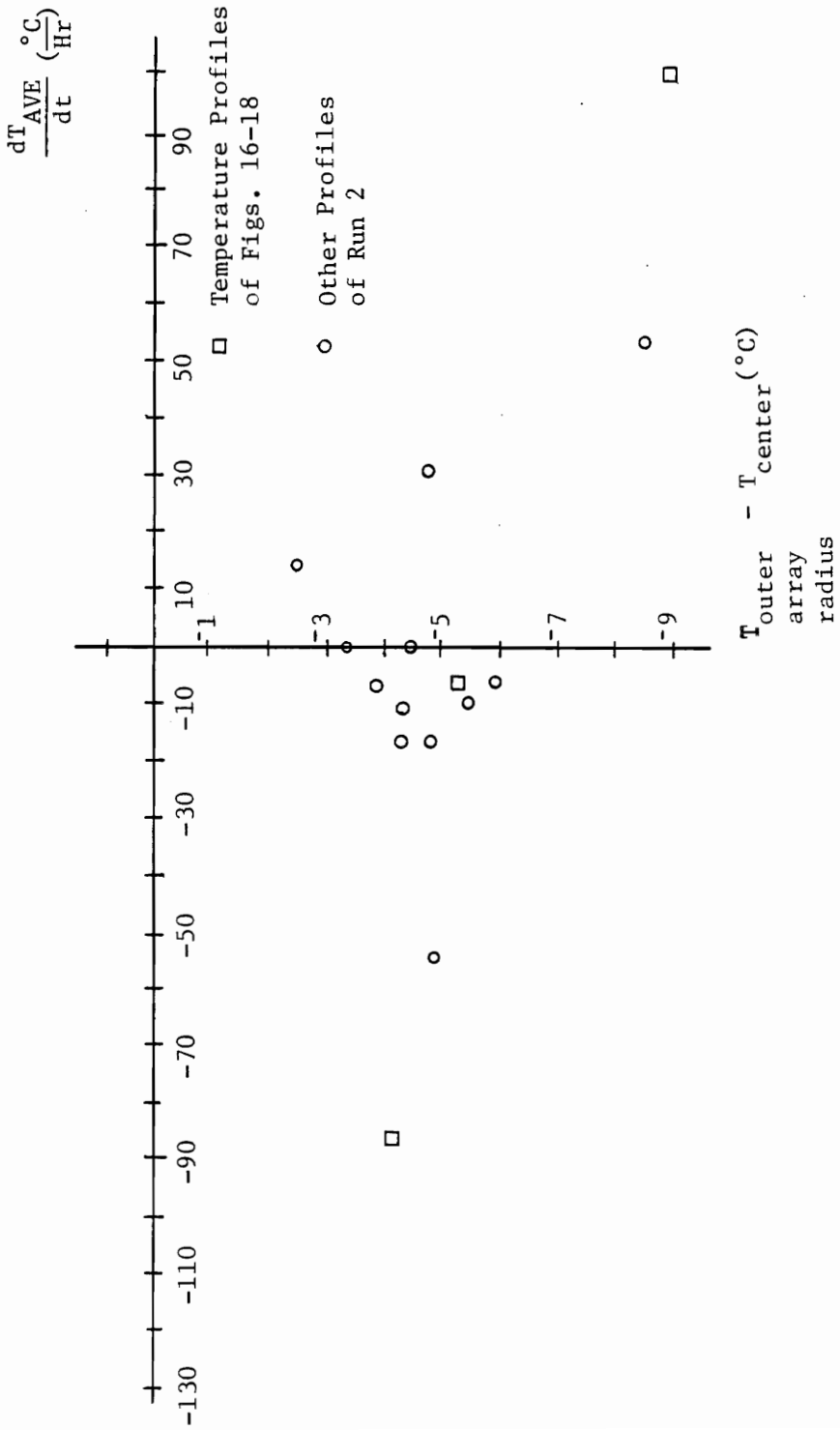


Figure 22. The Effect of a Change in Stack Temperature on the Radial Temperature Difference for Run 2.

Table II. Heat Loss Through 2m of Insulated Stove Pipe Section

Array Area-Averaged Temperature (°C)	Measured Temperature Drop (°C)	Heat Loss ¹ thru Stack Insulation (W)	Sensible Energy ² Flow Past Array ² (W)	Loss/Flow %
<u>Run 1</u>				
111	14	59	252	23
123	20	89	353	25
123	16	71	403	18
127	10	47	420	11
150	22	93	517	18
151	22	93	521	18
<u>Run 2</u>				
123	14	59	403	15
136	20	89	458	19
140	26	109	474	23
142	24	101	483	21
156	28	118	542	22
170	26	109	601	18

1. Based on $\dot{m} = 4$ g/s and $c_p = 1.05$ kJ/kg K

2. Based on an ambient temperature of 27°C

3. All measured drops have a ± 2 °C uncertainty due to measurement of the array reference junction temperature

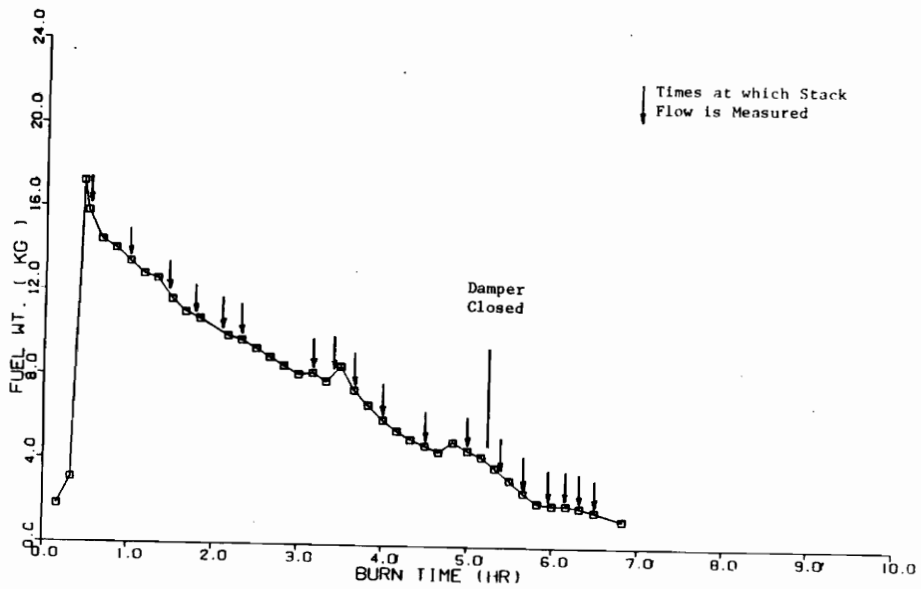


Figure 23. Mass-Time History from Scale Readings for Run 3

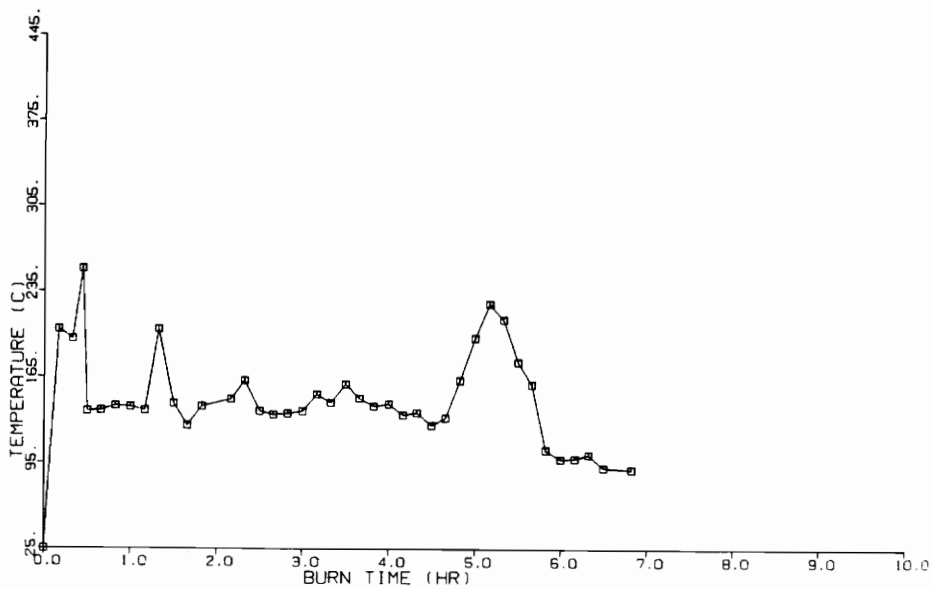


Figure 24. Stack Temperature History for Run 3

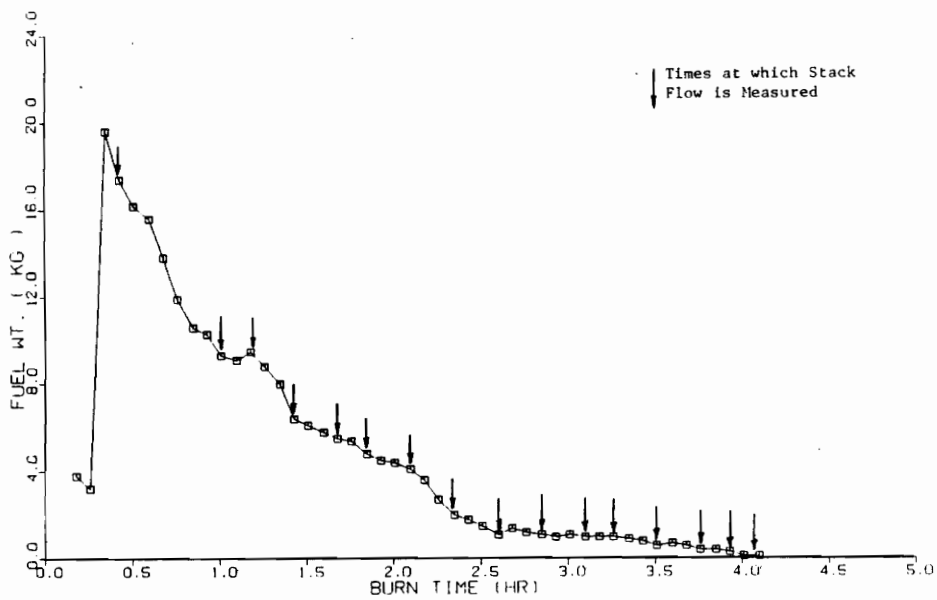


Figure 25. Mass-Time History from Scale Readings for Run 4.

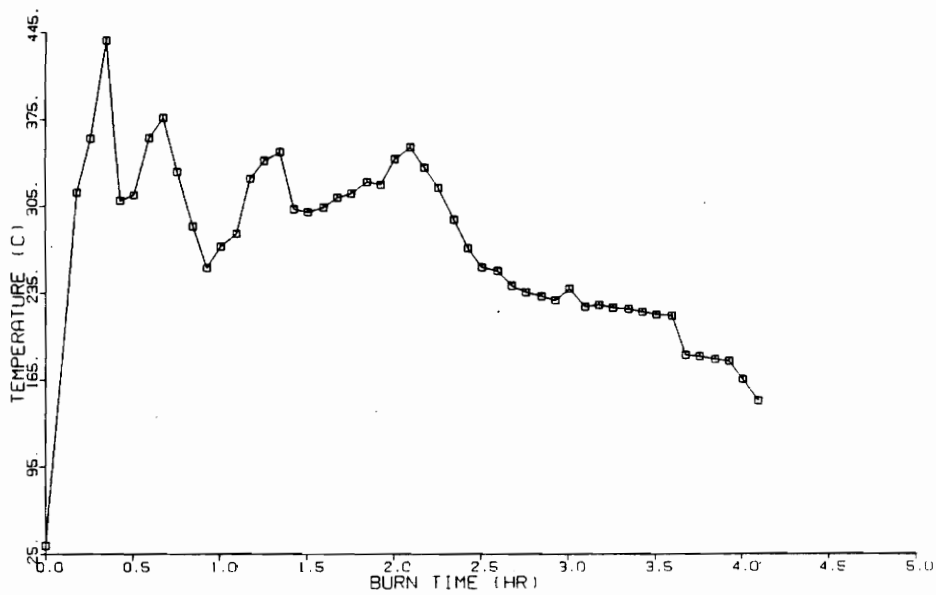


Figure 26. Stack Temperature History for Run 4

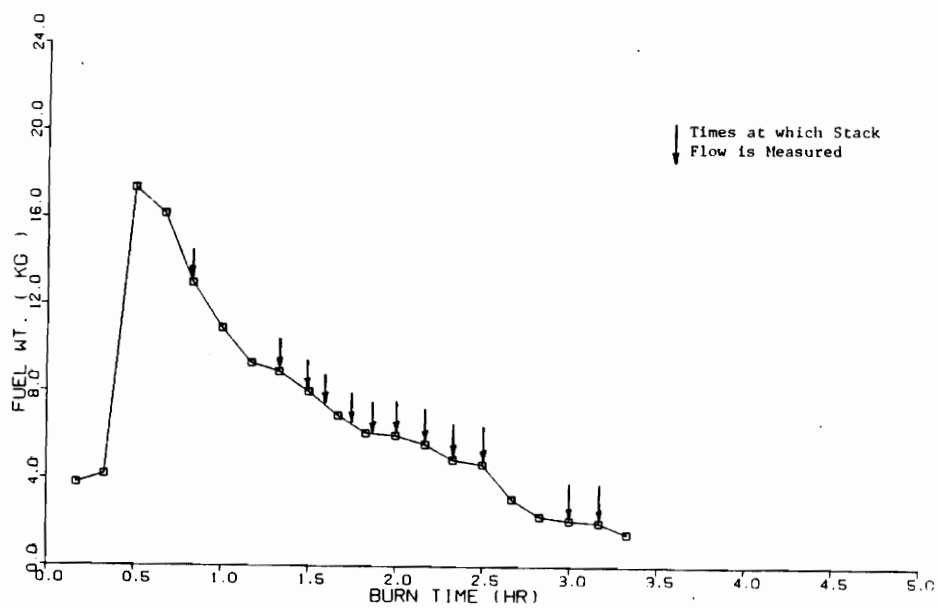


Figure 27. Mass-Time History from Scale Readings for Run 5

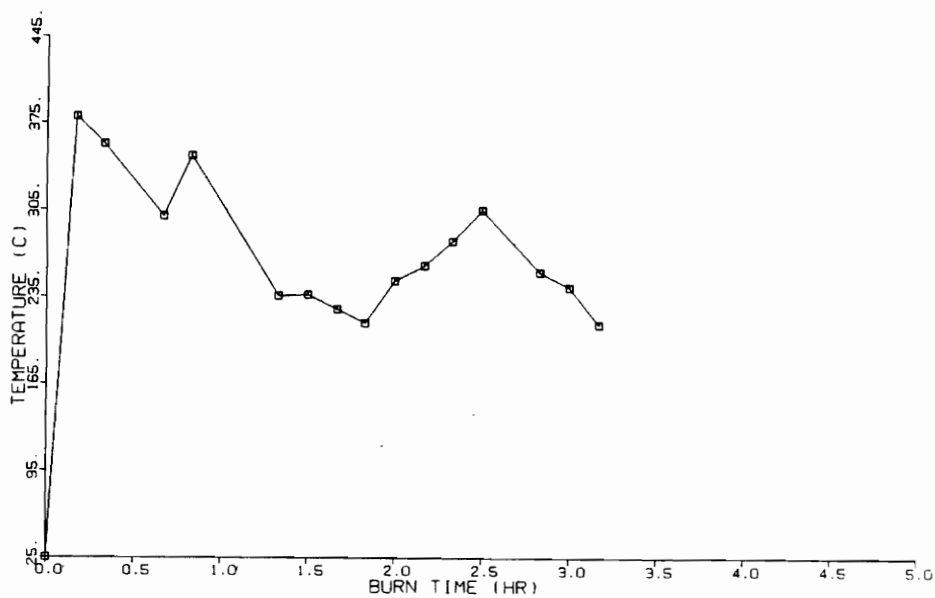


Figure 28. Stack Temperature History for Run 5

The heat loss through the insulated flue, i.e. the transfer of heat from the stack to the room, was calculated from the measured temperature drop. The heat losses were calculated for runs 1 and 2 using a specific heat of 1.05 kJ/kgK and a mass flow of 4 g/s (calculated using the average burn rate of runs 1 and 2 and a 10:1 air to fuel ratio) for the flue gas and are shown in Table (II). The sensible energy loss, i.e. the heat convected up the stack, is also shown in Table (II). A comparison of the two losses shows that the heat loss through the insulation varied between 11 and 25 percent of the sensible energy loss.

4.2 Flow Rate Measurement

Flow rate measurements were performed for runs 3, 4, and 5. Stack gas composition was not measured and thus the scale-based method was not used during run 3, even though the scale readings were recorded. The thermostat was set on high for test run 3 and was adjusted to a higher setting (beyond the high setting on the thermostat dial) for runs 4 and 5. Although high fire settings were used, the stack flow rate would decrease as the test progressed. This allowed both high and low flow measurements to be made during the same run.

The scale readings and stack temperatures for each run are shown in Figs. (23-28). The scale and temperature data were recorded with a data acquisition system except for test run 5 in which the data were recorded manually. This is the reason for fewer scale and temperature data in run 5 than in the other two runs. The times when the flow measurements were recorded is marked on the scale plots.

The average burn rate (over the hot-to-hot test interval) for test run 3 was 2.8 kg/hr, which was in the medium burn rate range. The average burn rate for test runs 4 and 5 was 8.8 and 7.5 kg/hr respectively, in the high fire range. As was the case for temperature tests (runs 1 and 2), the local burn rate at the time the flow measurements were taken would be different from the average burn rate for the run. Errors in the scale recordings can be observed in Figs. (23) and (25) where several times an increase in the weight of the fuel charge was recorded even though no additional fuel was added to the stove.

The stack temperature history for run 4 showed thermostatic cycling during the first hour of the run. Thermostatic cycling is typically noticed during high combustion rates when the stove temperature increases enough to cause the thermostat to close. The stove then cools to the point where the thermostat reopens and the cycle is repeated. Run 3 did not have thermostatic cycling due to the lower thermostat setting. Some thermostatic cycling may have occurred during run 5 but the data density is too sparse to conclude if it occurred.

The stack flow results are shown in Figs. (29-31). These results are also tabulated in Appendix D. The flow rate measurements were taken at discrete points during the run and therefore these figures do not give a continuous history of the stack flow. The pitot array and the CO tracer measurements represent the average stack flow for approximately a 5 minute interval. The scale-based measurements represent the average stack flow over a slightly shorter time interval of 3 to 5 minutes. Due to the noisy scale readings, the scale-based flow measurements did not

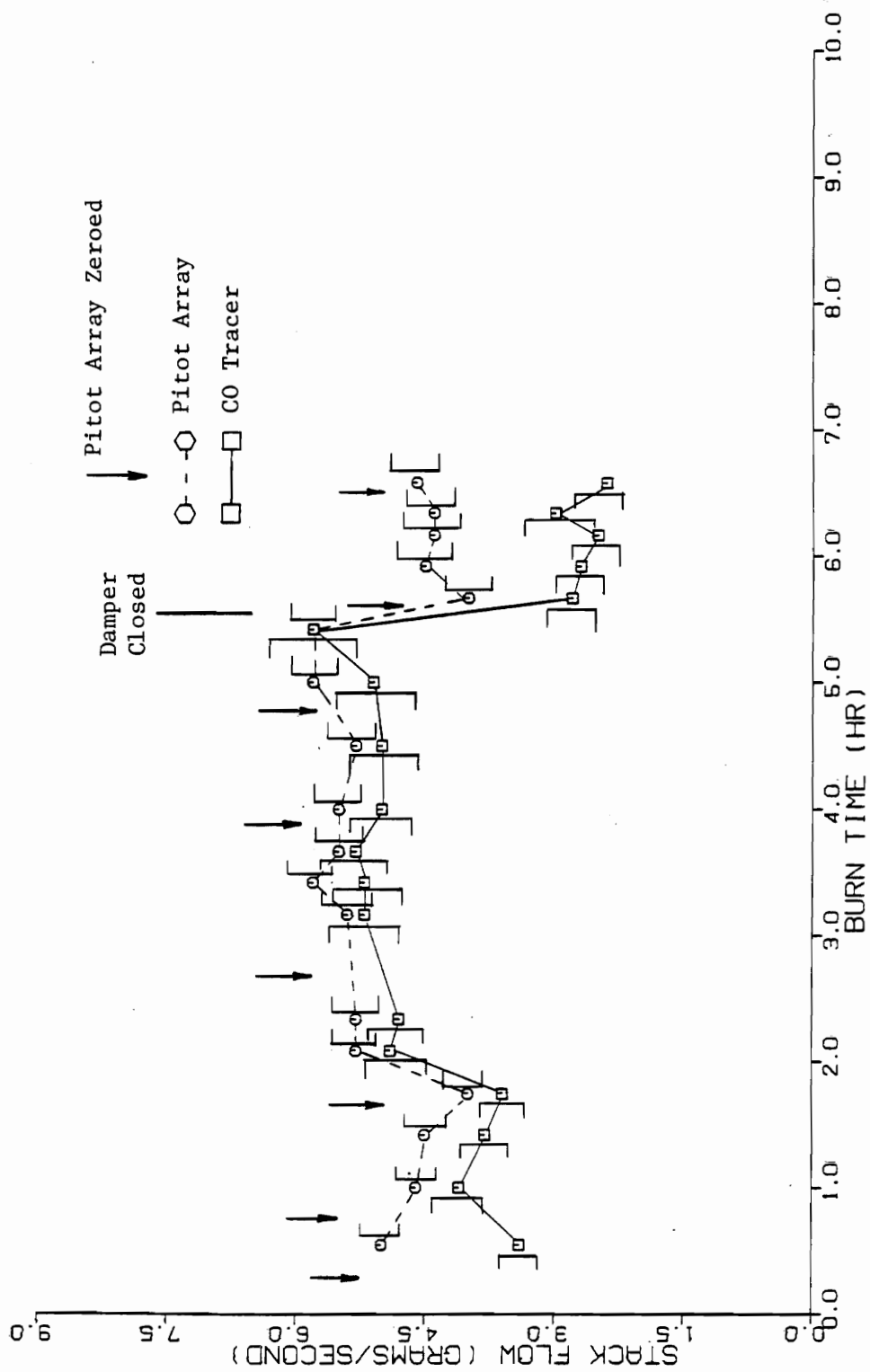


Figure 29. Comparison of Stack Flows Measuring During Run 3

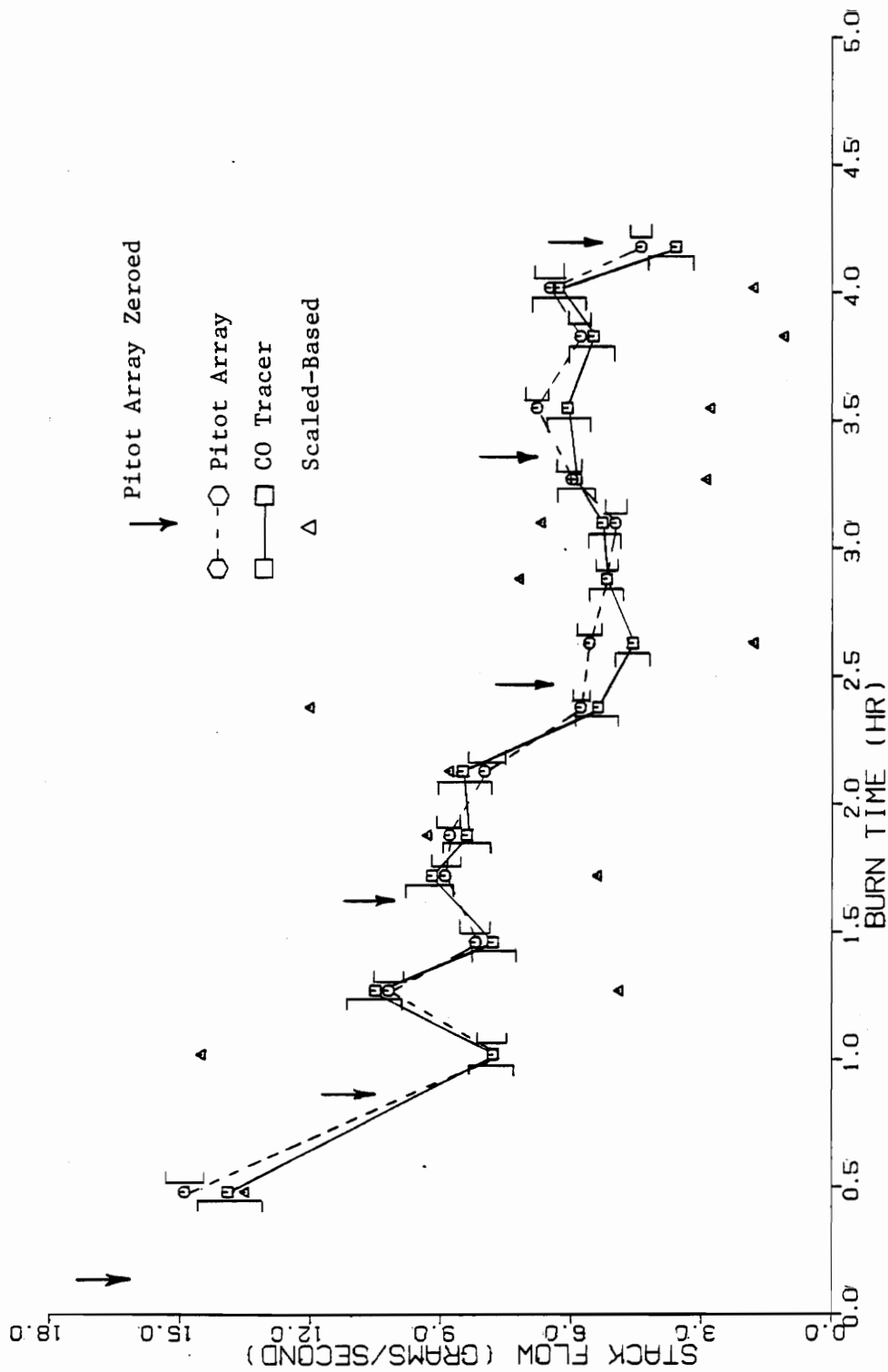


Figure 30. Comparison of Stack Flows Measured During Run 4

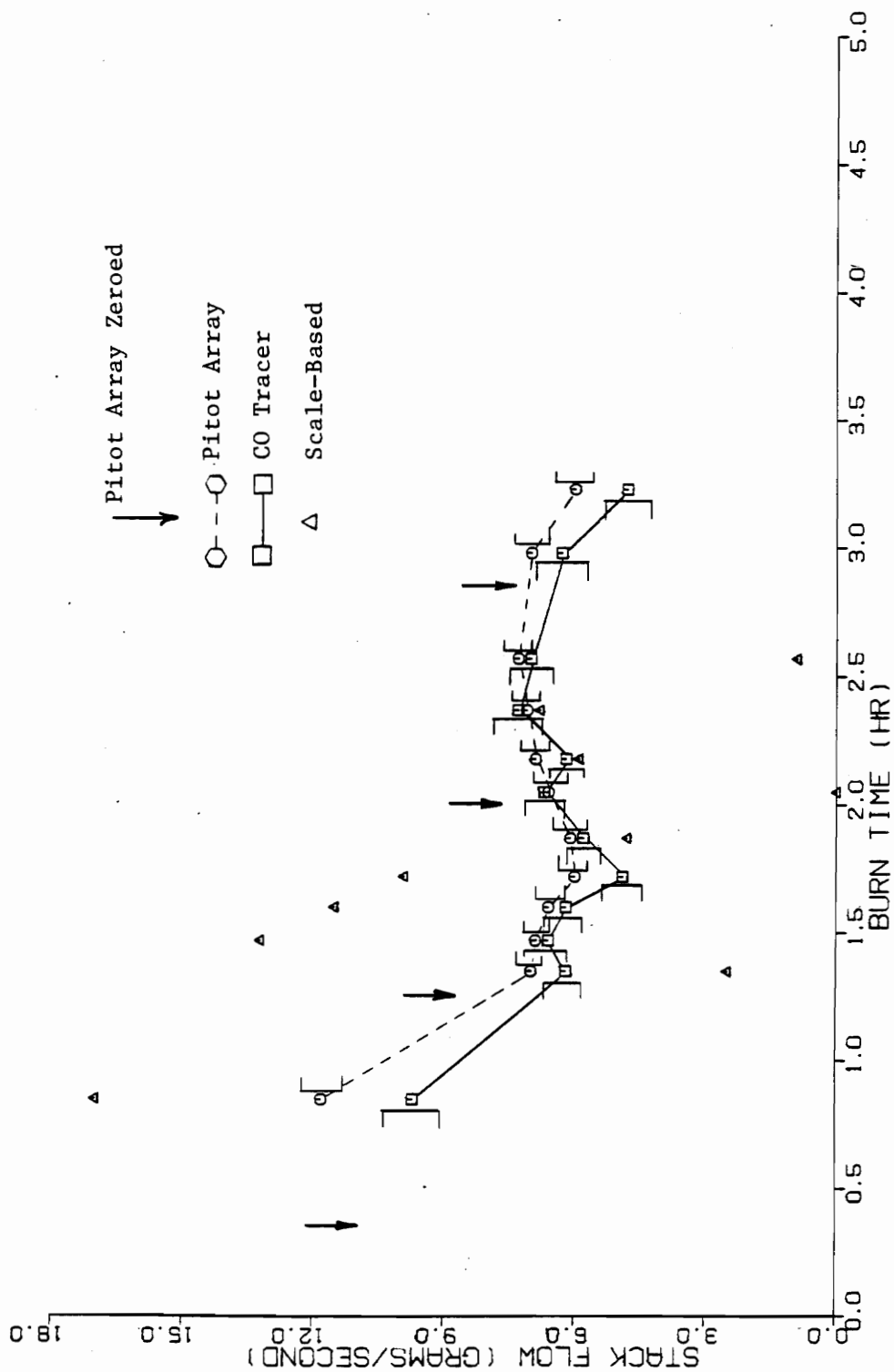


Figure 31. Comparison of Stack Flows Measured During Run 5

agree well with the CO tracer or pitot array. This would indicate that the burn rate for the scale-based method needs to be measured over a longer time interval than 3 to 5 minutes. Using a central difference technique with the scale plots of runs 4 and 5, the burn rates over a 10-15 minute time period were used to recalculate the scale-based flow measurements. These recalculated scale-based flow measurements are plotted versus the CO tracer and pitot array in Figs. (32-33). The improvement in agreement with the other methods in Fig. 33 was not as good as that in Fig. 32 due to the low density of scale recordings for run 5.

Due to an oversight, the temperature at the pitot array was not measured. The stack temperature was measured with the thermocouple array. Therefore, it was necessary to estimate the flue gas temperature drop through the 2m insulated section between the pitot array and the thermocouple array. This estimate was based on the measurements of the flue gas temperature drop through the 2m insulated section performed during runs 1 and 2. The temperature drop was estimated to be 15 percent of the recorded array temperature and the temperature at the pitot array location was calculated based on this estimate.

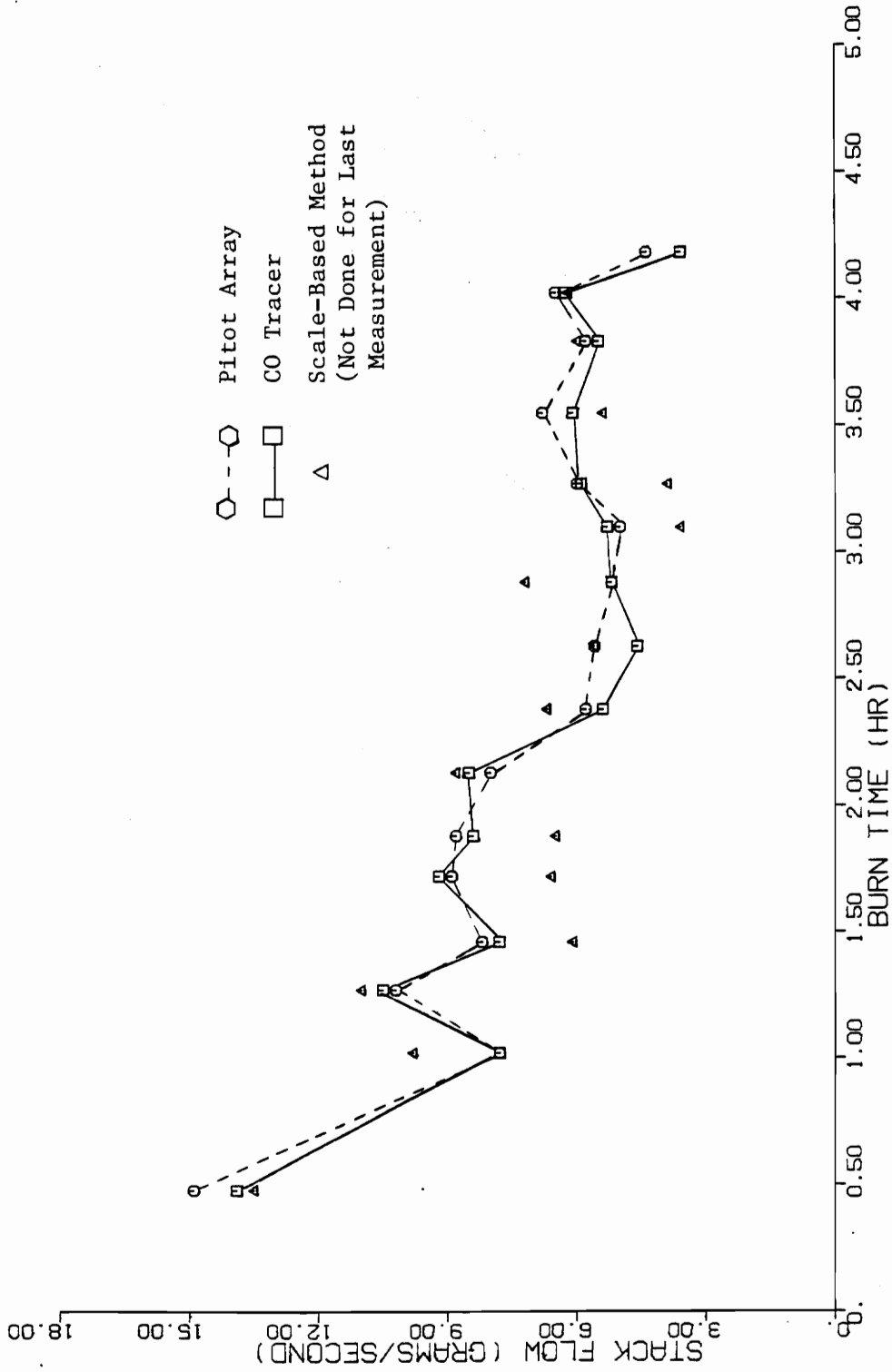


Figure 32. Comparison of Stack Flow for Run 4 with a Recalculated Scale-Based Flow

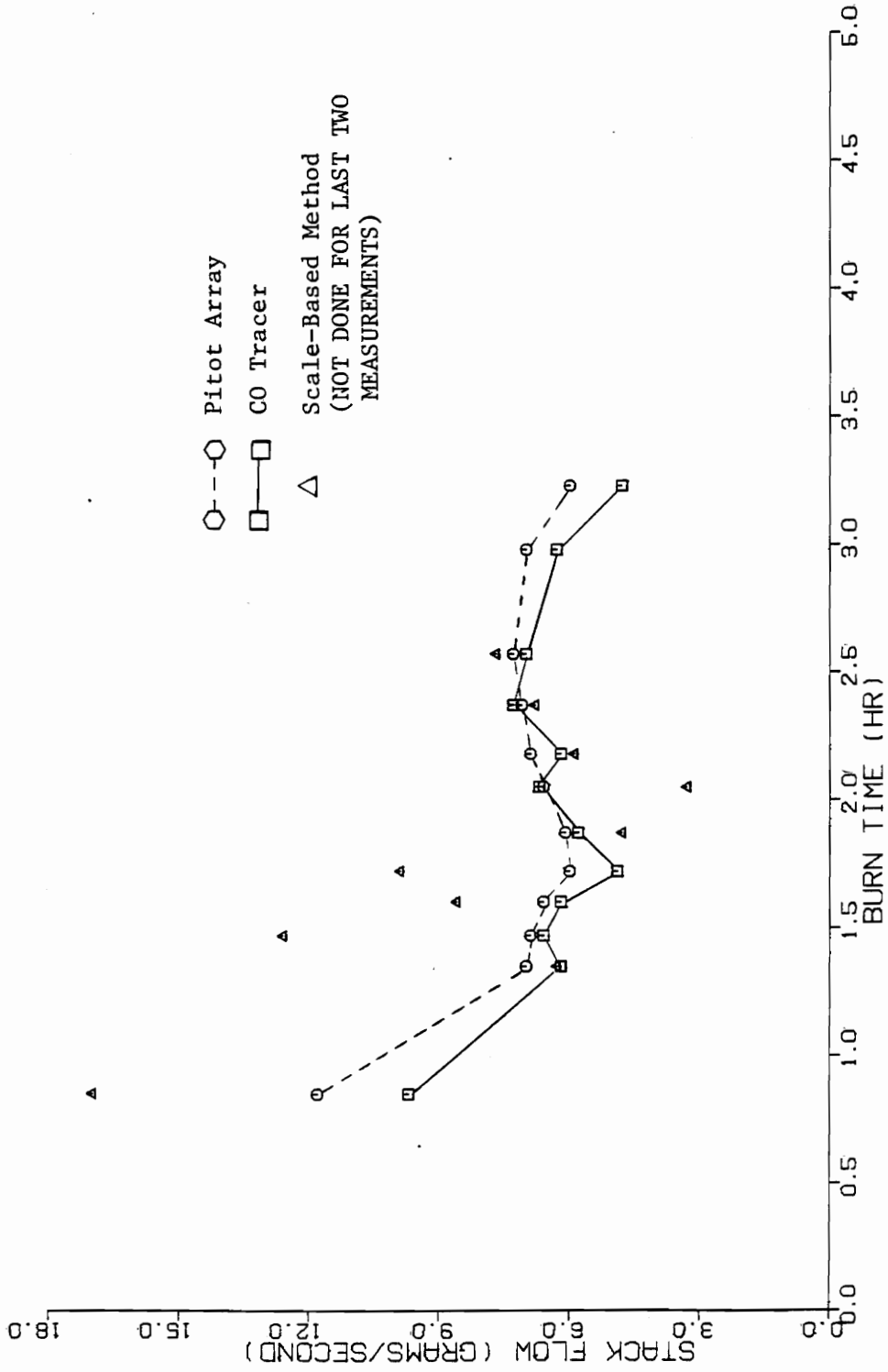


Figure 33. Comparison of Stack Flows for Run 5 with a Recalculated Scale-Based Flow

5. DISCUSSION

5.1 Temperature Profiles

Calculation of the instantaneous sensible energy loss of a stove requires measurement of the instantaneous stack bulk temperature, whereas many methods use only the centerline stack temperature to calculate the sensible energy loss. The bulk temperature is defined as the energy-average flue gas temperature across the duct. This one point temperature measurement would give the stack bulk temperature only if radial velocity and temperature differences did not exist in the flue. To estimate the error associated with using only the centerline temperature to calculate the instantaneous sensible energy loss, the temperature profile data of runs 1 and 2 were used to calculate bulk temperatures. Each bulk temperature was then used to determine the percent error in the sensible energy loss calculated when the centerline temperature was used as a representation of the bulk temperature. An error in the measurement of the sensible energy loss is of concern since the sensible energy loss is used in the calculation of the overall efficiency. The overall efficiency is defined as the useful heat output divided by the wood energy input. The useful heat output can be expressed in terms of the wood energy input and the energy losses (sensible, chemical, and latent).

To calculate the bulk temperature from the profile data, a flat velocity profile was assumed (this may not be an accurate assumption) along with a constant specific heat and a constant density across the stack. The equations used to calculate the bulk temperature are shown

Table III. Calculated Error in Sensible Energy Loss Using the Centerline Stack Temperature.

Centerline Stack Temperature (°C)	Array-Calculated Bulk Temperature ² (°C)	Error in Sensible Energy ¹ (%)
96	94	3
120	116	4
128	123	5
153	148	3
155	151	3
216	209	4

¹Based on an Ambient Temperature of 27°C and data measured during test Runs 1 and 2

²Based on a flat velocity profile in flue

in Appendix C. Table (III) shows the differences in the instantaneous sensible energy loss based on a room temperature of 27°C. Calculation of the instantaneous sensible energy loss using the centerline temperature overestimated the loss by 3 to 5 percent. The sensible energy loss is usually 10 to 50 percent of the total energy input to the stove. Thus a systematic error of 5 percent in the sensible energy loss might account for an error of 0.5 to 2.5 percentage points in overall efficiency.

The "true" bulk temperature was never measured since the velocity at each thermocouple location was not measured. Therefore, the validity of this discussion depends on the accuracy of the assumptions made for the bulk temperature. The assumption of constant density and constant specific heat across the duct is justified since the temperature gradients across the duct are not significant. The accuracy of the velocity profile assumption is unknown since the stack Reynolds numbers are in the transition region and either turbulent or laminar velocity profiles could exist. If a laminar velocity profile existed, then the assumption of a flat velocity profile would underestimate the velocity at most of the thermocouple locations on the array and therefore tend to underestimate the bulk temperature. If a turbulent velocity profile existed, then the assumption of a flat velocity profile is fairly accurate since the local velocity does not change more than 15 percent from the average velocity.

There may be times when the flue gas temperature drops rapidly and an influx of thermal energy from the stack walls to the flue gas occurs. If the influx of energy in the section between the stove and

the temperature measurement location was large enough, then the gases near the wall would be hotter than the gases in the center of the stack. This situation would cause an underestimate of the instantaneous sensible energy loss when the centerline temperature was used as a representation of the bulk temperature. If the average sensible energy loss for a run was calculated from the instantaneous values, then it may be possible for the errors (both overestimating and underestimating) of measuring the sensible energy loss with a centerline temperature to be compensating. However, the probability of a thermal influx to the gas large enough to have a reversed profile at the temperature measurement location, i.e. the flue gas at the wall being hotter than at the centerline, would be small. The section between the stove and the stack temperature measurement location is uninsulated except for the last 30 cm. Thus most of the energy stored in the stack wall would probably go to the room instead of the flue gas. In this study no reversed profiles were measured with the array.

The temperature measurements in this study were performed for only one stove and stack. Stack radial temperature differences for other stoves and stacks may differ. Radial temperature differences may be influenced by thermostatic cycling which would vary with each stove. Stoves that release hotter flue gases may have larger gradients in the stack. Radial temperature differences are also influenced by the chimney. Stacks with a large thermal mass will require longer response times to changes in the flue gas temperature and therefore create a favorable condition for radial temperature differences to exist. Diameter of the stack will also affect the radial temperature gradients, especially in an uninsulated section.

Probable radiation errors for unshielded thermocouple measurements were calculated using a worst case, simplified energy balance. The assumptions for the energy balance are that the shape of the bead is spherical, conduction from the bead through the wire can be neglected, the radiation shape factors were unity, and no-flow conditions existed (Nusselt number of 2.0). The temperature of the thermocouple bead was taken to be the recorded stack centerline temperature. The stack wall temperature was estimated to be 10°C cooler than the temperature recorded on the outer radius of the thermocouple array (1.6 cm from the wall). Radiation errors on the order of 3 to 14°C were calculated for the data taken with the array during runs 1 and 2. Using an ambient temperature of 27°C , the radiation errors in the temperature measurement would result in a 3 to 5 percent error in the sensible energy loss. This error in the sensible energy loss could result in an error of 0.3 to 2.5 percentage points in the overall efficiency.

The temperature measured using a suction pyrometer was available for some runs as the standard to which the thermocouple readings could be compared to. The radiation error of the suction pyrometer was assumed to be negligible. The pyrometer was positioned 1.8 cm from the centerline and 5 cm above the array junction as shown in Fig. (5). The reading of the pyrometer was compared to the average of the temperatures measured by the three array thermocouples 1.8 cm from the centerline. The readings of the pyrometer and the thermocouples are shown in Fig. (34). This plot shows the radiation errors to be largest at the beginning of the run when the temperatures are the highest and larger radial differences exist. Near the end of the run, the temperatures

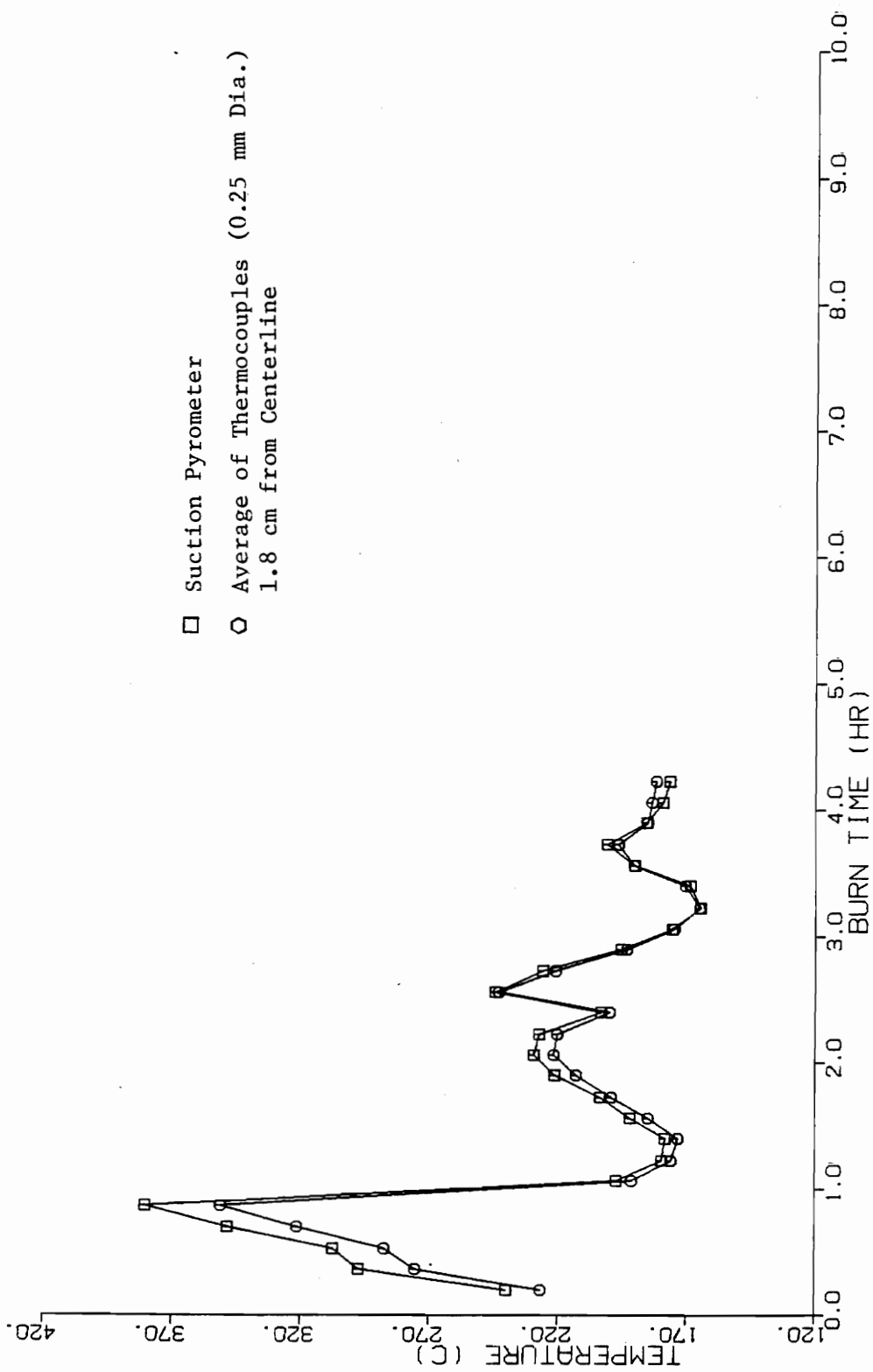


Figure 34. Comparison of Aspirated and Non-Aspirated Thermocouple Readings

measured by the suction pyrometer were slightly lower than the average temperatures of the three thermocouples. This may be caused by temperature differences due to the measurement location of the pyrometer and the three thermocouples being different. Temperatures measured 1.8 cm from the centerline by the three thermocouples were generally within 3°C of each other. Therefore, any temperature difference due to location would probably not be noticed until the end of the run when the radiation errors decrease and thermocouple measurement approaches the pyrometer measurement.

A plot of calculated versus measured temperature differences is shown in Fig. (35). Comparing the measured temperature difference to the calculated difference, it appears that the calculations underestimate the radiation errors (10.8°C calculated versus 27°C measured for the fourth data point). This underestimation may be due to a cooler inner wall temperature than was used and/or neglecting the radiation absorbed and emitted by such gases as CO₂, CO, and H₂O in the flue gas. Also, the creosote build-up on the thermocouple bead was neglected which would increase the size of the bead and thus possibly increase the radiation error.

In an attempt to reduce the radiation error, a thermocouple probe formed from 0.088 mm wire was used. As shown by comparing Fig. (34) to Fig. (36), the radiation errors of the fine gage probe are generally smaller for stack temperatures above 280°C. However, at lower temperatures the radiation errors of the fine gage probe were 10°C or less which was also the case for the array thermocouples. Further testing is needed to verify the apparent radiation errors of the

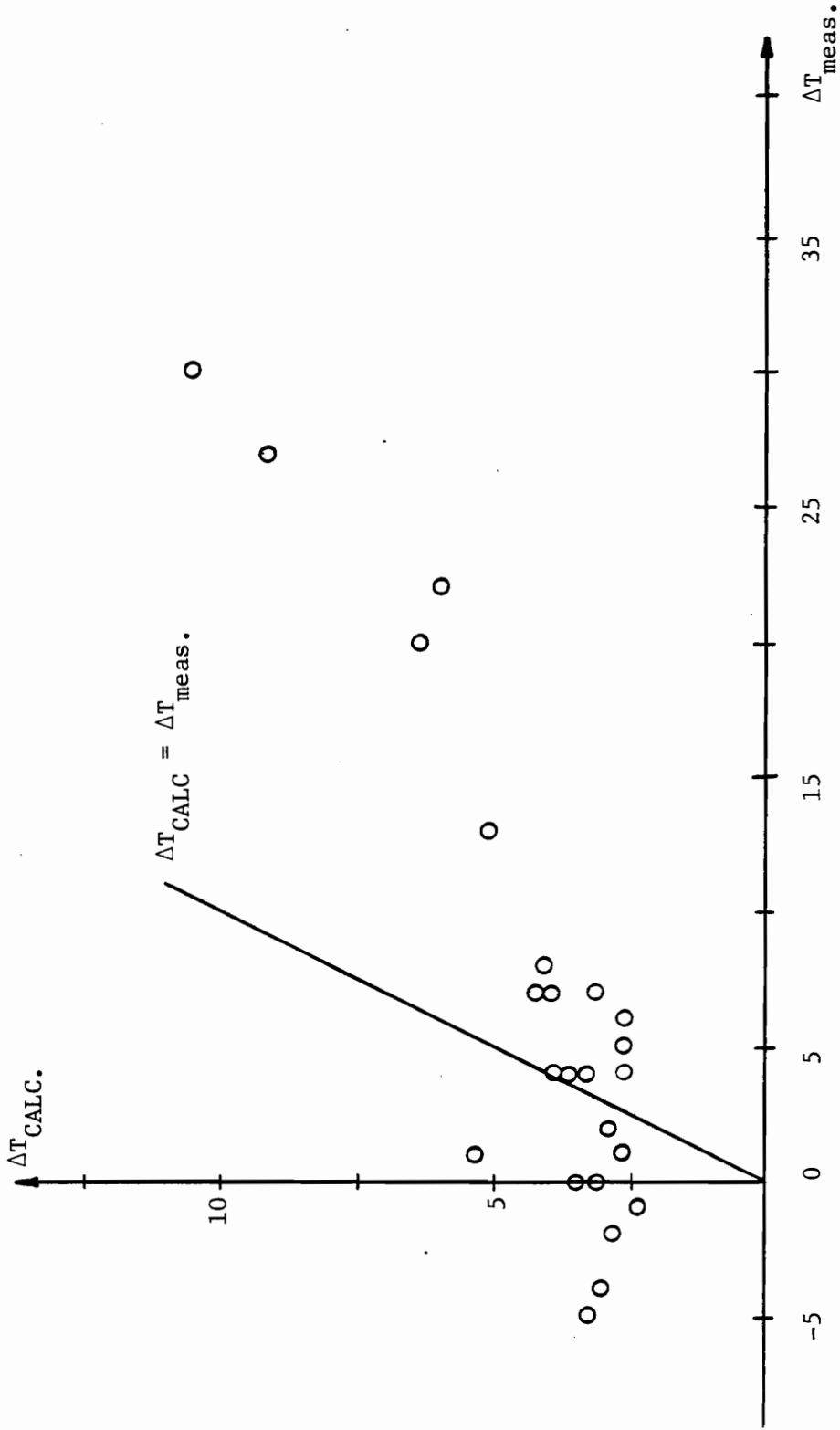


Figure 35. Comparison of Measured and Calculated Temperature Differences

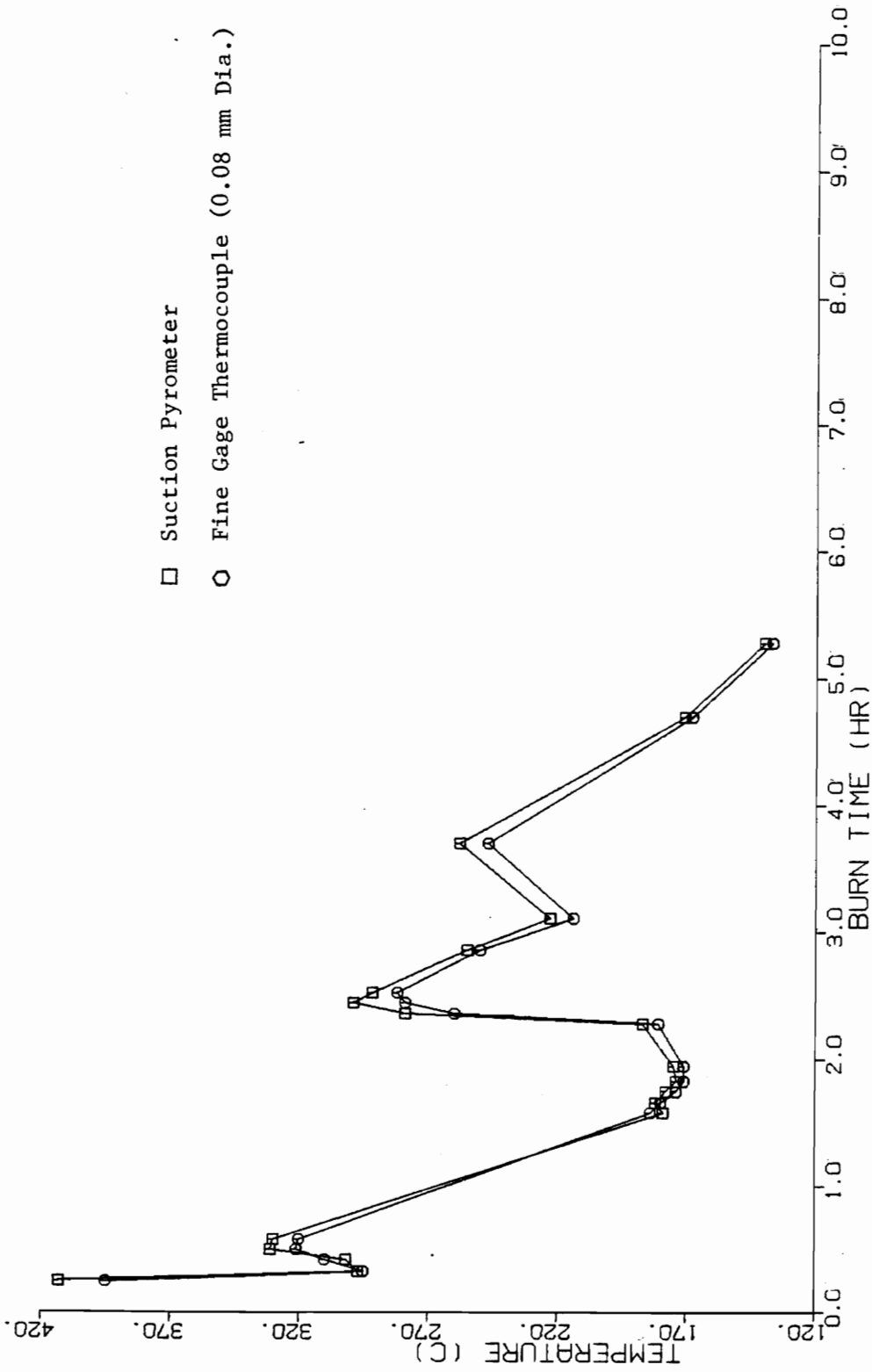


Figure 36. Comparison of Aspirated and Non-Aspirated Fine Gage Thermocouple Readings

thermocouple measurements due to the possible errors in the data (i.e., the pyrometer temperature sometimes was lower than the average thermocouple temperature). If the data taken in this study are correct, then this would imply that unshielded thermocouples are appropriate if flue gas temperatures remain below 250°C. If hotter temperatures are encountered, then shielded thermocouples may be required.

5.2 Flow Measurements

The agreement between the CO tracer and the pitot array flow measurements was usually good, i.e., the flows differed by less than 10 percent. However, poor agreement between the two methods was observed whenever there was an abrupt change in the stack flow rate. Although this phenomena was observed in all three runs, it was most noticeable during run 3 when the agreement between the two methods changed drastically after the damper was closed. The reason for this poor agreement is unknown, but several possible reasons exist.

One possible explanation for the observed differences could be hysteresis in the pitot array pressure transducer. Hysteresis effects would cause the pitot flow measurement to be high when the stack flow decreased rapidly and low when the stack flow increased rapidly. This trend can be observed in the data from all three runs. The stack conditions in run 3 did not change much except at the beginning and end of the run. Hysteresis in the pressure transducer would help explain why the pitot flow is much higher than the CO tracer at the two times when the stack flow decreased rapidly. (Although not shown by the figure, the stack flow decreased rapidly at the beginning of a run.

This was due to the stack temperature decreasing after the main load was added - see in Fig. 24.) The stack flow fluctuated more frequently in runs 4 and 5 than in run 3 and therefore hysteresis effects would cause a more random difference between the pitot and CO tracer measurement (i.e., pitot higher than the CO tracer at times and lower at other times).

The uncertainty in both the CO tracer and the pitot array flow measurement could explain part of the disagreement. The estimated uncertainty for the CO tracer flow measurement ranged from 6 to 11 percent while the pitot array had an estimated uncertainty of 4 to 7 percent in its flow measurement. Appendix B shows the derivation of the uncertainty estimates.

Figure (37) shows that the differences between the two methods do not appear to be a function of the stack CO concentration. However, Fig. (38) shows that the differences tend to increase for dilution tunnel CO concentrations less than 0.05 percent. This may indicate that the CO analyzer was inaccurate at low concentrations. A test using a primary standard calibration gas with 0.050 percent CO indicated that the low pressure calibration curve for the CO analyzer was 8 percent low at this concentration. This would make the CO tracer underestimate the actual flow by 8 percent when low CO concentrations in the range of 0.05 were being measured. No corrections were made to the data because it is unclear when/if the instrument calibration changed.

Another possible reason for the disagreement may be due to calibrating the pitot array at room temperature instead of normal operating temperatures of 100 to 300°C. To determine if the calibration

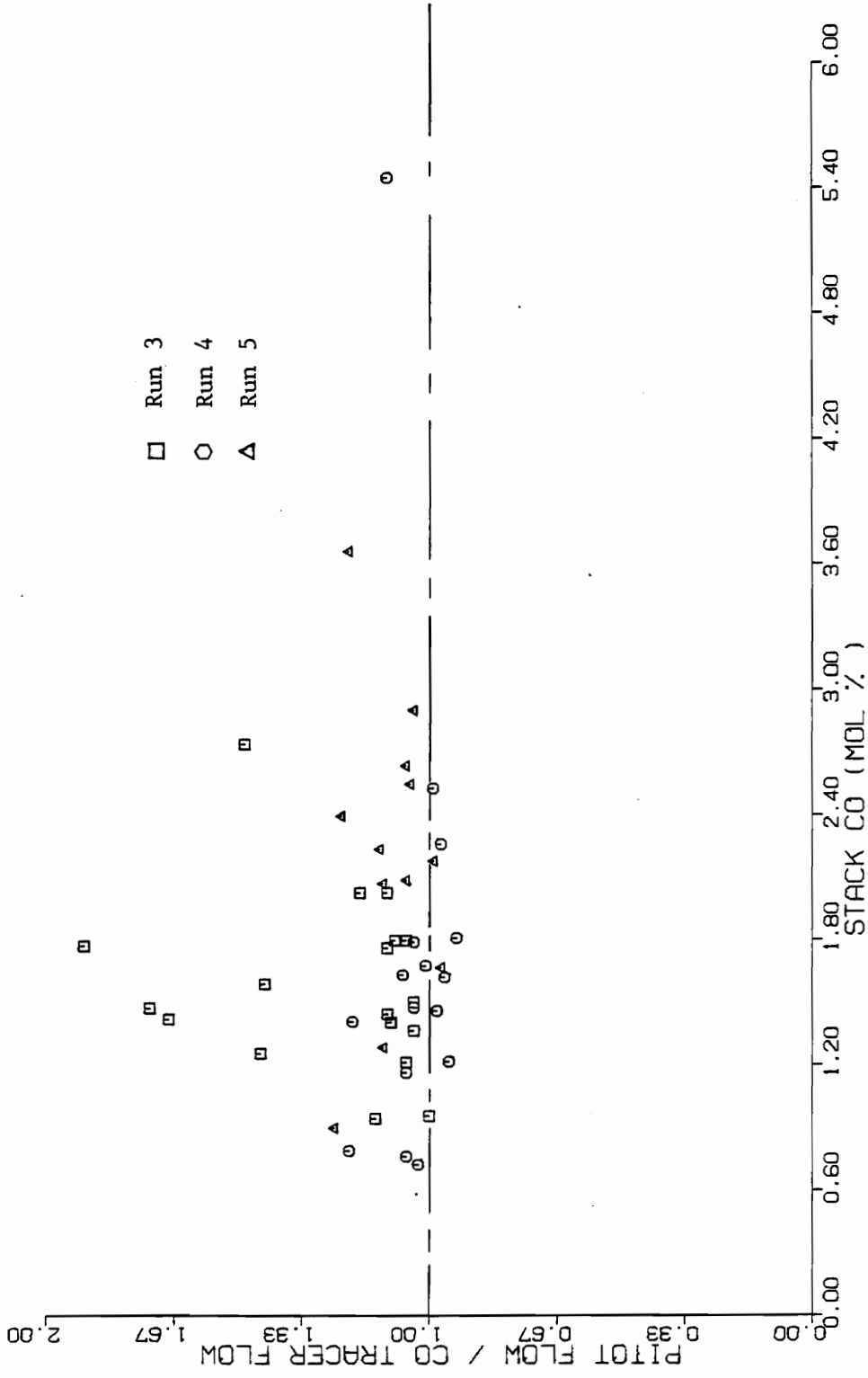


Figure 37. The Effect of Stack CO Concentrations on Flow Measurements

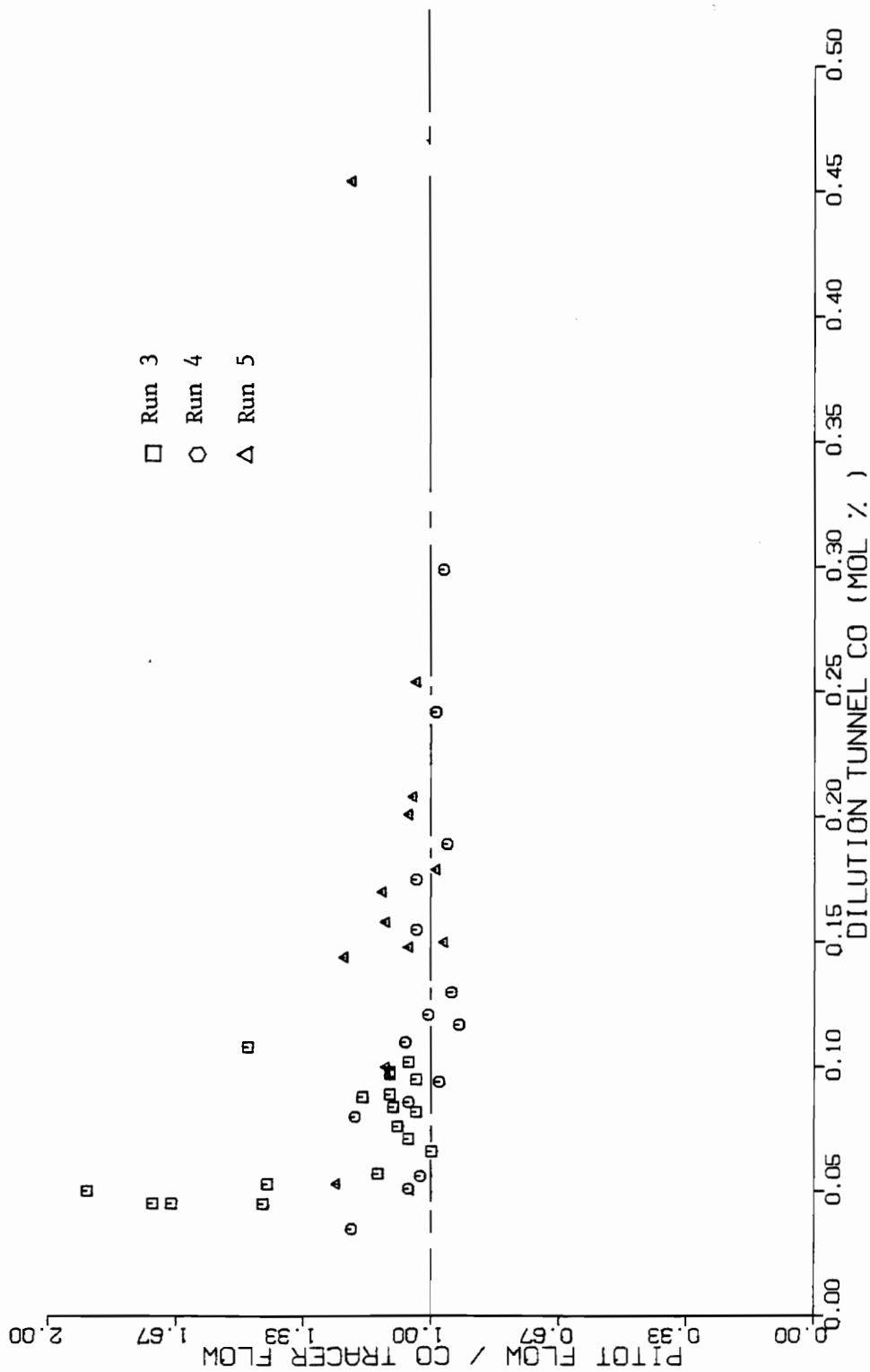


Figure 38. The Effect of Dilution Tunnel CO Concentrations on Flow Measurements

coefficient was influenced by the stack temperatures, the ratio of the pitot array to the CO tracer flow measurements are plotted versus stack temperature as shown in Fig. (39). This figure showed that the differences did not appear to be a function of temperature. An increase in the differences were observed at temperatures below 120° but this increase may be due to low stack flows. Low stack flows usually occur with low stack temperatures.

The accuracy of the pitot array flow measurement may be affected by the velocity profile in the stack. As mentioned in Section 3.3.2, the flow through the impact tubes would be greater for a laminar velocity profile than a turbulent profile. Therefore, the differences between the two methods are plotted versus stack Reynolds numbers as shown in Fig. 40. Note that the stack Reynolds number was based on the CO tracer flow. The disagreement between the methods tended to increase for Reynolds number below 1800. If transition from turbulent to laminar flow occurred near a Reynolds number of 2300, then this would indicate that the pitot array measurement may have been affected by a laminar velocity profile. This would cause an uncertainty in the pitot array measurement. Further testing is required to determine if this increase in disagreement is due to transition.

Of particular interest is the reason for the abrupt change in agreement between the two methods when the damper was closed in run 3. After the damper was closed, the CO concentration in the dilution tunnel was in the range of 0.05 percent. As discussed earlier, the CO analyzer was found to be off in this range. If the CO tracer flow was corrected, this would make the disagreement between the two methods smaller by 8

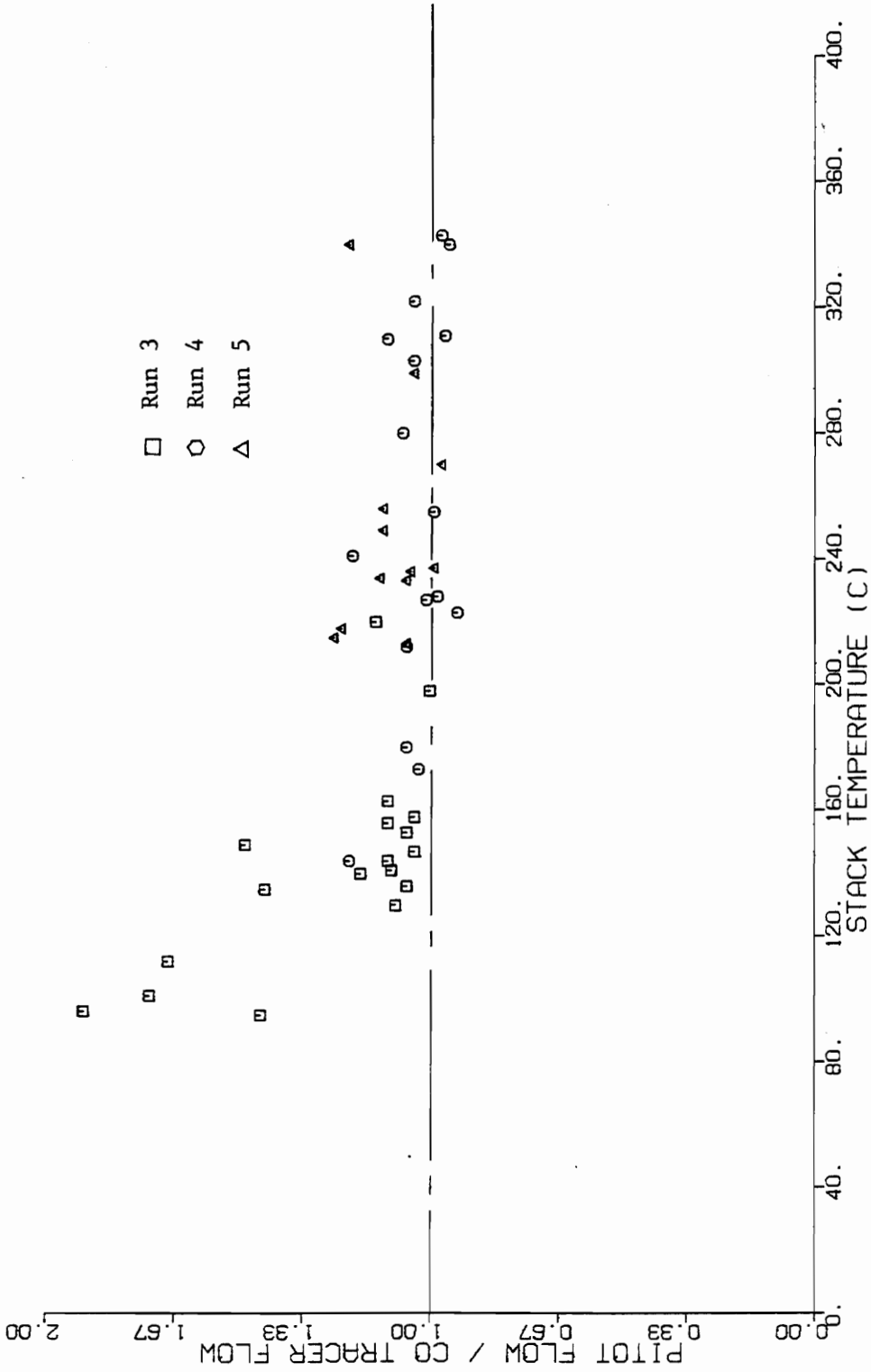


Figure 39. The Effect of Temperature on Flow Measurements

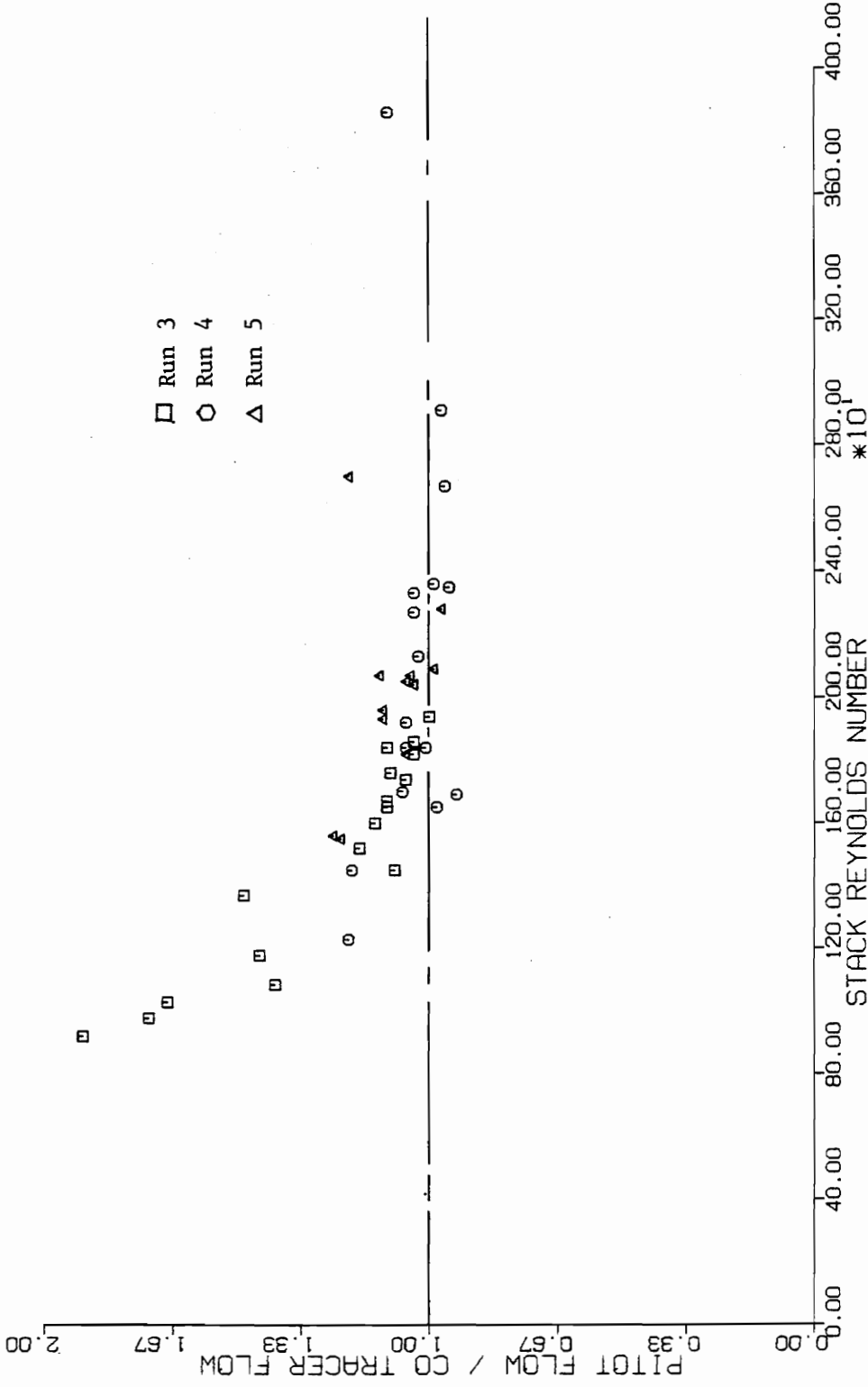


Figure 40. The Effect of Stack Reynolds Number of Flow Measurements

percent. The transducer used with the pitot array was checked for zero drift during the time period of these large disagreements and was found to have drifted +0.03 volts which represented a 12 percent uncertainty in the differential pressure measurement. However, this would only be a 3.5 percent uncertainty in the flow measurement due to the square root relationship between flow and differential pressure. Combining the uncertainty of both methods would reduce the difference by 11 percent, however the disagreement is still between 20 to 40 percent. Probable reason(s) for the poor agreement could be hysteresis in the transducer and/or the transition from turbulent to laminar flow once the damper was closed (Reynolds number decreased from 1900 to 1100).

The scale-based method did not agree well with the other flow measurements for the majority of the tests performed. The differences in flow measurements compared to the pitot ranged from 5.6 to 90 percent. This disagreement could in theory be caused by errors in gas concentration measurements (CO , CO_2 , O_2), errors in measuring the burn rate during the test, and the assumptions of the algorithm.

The sensitivity of the scale-based flow to gas concentration measurements was determined by using concentration data from the runs. The concentration data was used as the base case and the CO , CO_2 , and O_2 concentrations were varied one at a time by 0.2 percentage points from the base-case value. Table (IV) shows that the flows calculated from the algorithm changed less than 6 percent. Thus the algorithm tended to be insensitive to small errors in the gas concentration measurement.

Any error in the measurement of the burn rate will cause an equal error in the measured flow. The resolution of the electronic scale used

Table IV. Sensitivity of Scale-Based Flow to Concentration Measurement Errors

Air/Fuel Ratio (Mass Basis)	Dry Basis Concentrations			Measured Instantaneous Burn Rate (kg/hr)	Stack Flow (g/s)	Percent Error
	%CO	%CO ₂	%O ₂			
5.9	1.71	13.60	6.24	3.5	7.18	--
5.7	1.91	13.60	6.24		6.9	3.9
5.6	1.71	13.80	6.24		6.9	3.9
5.7	1.71	13.60	6.44		7.0	2.5
4.4	2.99	15.24	4.70	7.5	11.5	--
4.2	3.19	15.24	4.70		11.3	1.7
4.2	2.99	15.44	4.70		11.2	2.6
4.2	2.99	15.24	4.90		11.2	2.6
11.2	1.98	7.40	12.68	0.8	2.61	--
10.6	1.28	7.40	12.68		2.49	4.6
10.4	1.08	7.60	12.68		2.44	6.5
10.6	1.08	7.40	12.88		2.50	4.2

* Data taken from Runs 4 and 5

for the scale based method is 20 g during a 3 to 5 minute period. Typical mass changes recorded during the tests ranged from 20 to 600 g. As a result of the resolution of the scale, an error of 3 to 100 percent in the measured burn rate is possible. Several weight increases of the fuel charge were recorded during the runs. The weight increase was believed to be caused by the scale reading being sensitive to the location of the fuel in the stove, and thus any shift in the fuel charge would cause the scale reading to change even though the mass of the fuel remained the same. The stack also had four sample lines connected to it and this may have affected the scale readings. A comparison of the burn rate recorded during run 4 for the first ten flow measurements and the average burn rate over a slightly longer time period measured from Fig. (25) is shown in Table (V). The use of a longer time interval to determine the burn rate resulted in the flow measurements agreeing better with the other methods as shown in Figs. (32) and (33). Thus it is believed that the lack of obtaining an accurate "instantaneous" burn rate for the scale-based method caused a large percentage of the disagreement in flow rates.

There is always the possibility that the calibration gases used in this study were bad (i.e., the percent CO in the calibration gas is not what it is supposed to be). If this happened, then the flow measurement of the CO tracer would still be correct. The calibration curve for the analyzer would be off everywhere by the same percentage so the ratio of the stack and dilution tunnel CO concentrations would remain the same. As described in Appendix A, the pitot array was calibrated using two CO analyzers. If the calibration curves of these analyzers were bad, then

Table V: Comparison of "Instantaneous" Burn Rates Measured for Run 4

Flow Measurement No.	Burn Rate (kg/hr)	
	Scale-Based Data	Scale Data From Fig. 25
1	12.1	15.5
2	9.5	6.4
3	3.5	7.8
4	18.1	3.4
5	2.7	3.4
6	4.7	3.4
7	4.9	4.9
8	6.4	3.6
9	-7.1	2.3
10	2.8	1.2

two of the four stack flow measurements used in calibrating the pitot array would be wrong. Two flows are measured using the ratio of CO concentrations in the stack and dilution tunnel and therefore would not be affected by bad calibration gases. The other two flows are measured using the stack CO concentration measurement which would be wrong if the calibration gas was bad. If the error due to the bad calibration gas was large, then poor agreement between the four flows would result. Only small errors due to the bad calibration gas (± 4 percent disagreement between any of the four measured flows) would go unnoticed. Therefore, bad calibration gases should not affect the comparison of the flow measurement between the pitot array and CO tracer. The scale-based method would also be affected by bad calibration gases since the calibration curves for the CO and CO₂ analyzers would be off. The effect of bad calibration gas on the flow measurement would be different for the scale-based method than with the other methods and therefore the comparison of the scale-based method with the other methods would be affected.

5.2.1 CO Tracer

The CO tracer technique has potential as a means for accurate flow measurement. The advantages of this method are the flow measurement is independent of the stack velocity profile, real time flow measurements are possible, and only one calibration of the system may be necessary.

Total cost of the system used in this study is approximately \$8000 with the majority of the cost being the analyzer. The analyzer used in this study had a separate detector cell to compensate for water

interference in the CO measurement. This made the analyzer more expensive than most non-dispersive infrared analyzers. It may be possible to use a dry basis CO concentration and still have accurate results if water concentration data is available to correct the dry basis measurement to a wet basis one. A single-detector, non-dispersive analyzer costing around 3000 dollars can be used if the concentrations are done on a dry basis.

Response time of the CO analyzer and sampling system must be considered if only one analyzer is multiplexed between the stack and the dilution tunnel. If nearly real time flow measurements are desired, then a flow measurement is needed about every minute. This requires a response time of 30 seconds or less since two concentration measurements are needed. The flue gas CO concentration must be steady over the flow rate measurement period so that the CO concentration measurements only differ due to dilution with room air. (If the stack concentration changes rapidly, the stack concentration measurement would not be "compatible" with the dilution tunnel measurement.) The use of two analyzers would allow a continuous stack flow measurement. However, the response time of each sampling system (stack and dilution tunnel) needs to be about the same so that the concentration measurements would coincide with each other. The transit time for the gas to travel from the stack probe (located at the top of the stack) to the dilution tunnel probe must also be considered. The transit time was estimated to be about 2 seconds for this study, but it will vary depending on the probe locations and the velocities in the stack and tunnel. Very rapidly changing gas concentrations would cause problems even with the two

analyzer system, but such conditions would be encountered only momentarily during reloading of the appliance.

Several possible conditions exist where the CO tracer system may not work well in measuring the flow. Clean burning wood stoves produce low levels of CO (0.1 mole percent or less in some cases), and once diluted in the dilution tunnel the CO concentrations may be too low for accurate measurement. In this case, a CO₂ tracer system would work better since CO₂ concentrations would be high enough to measure accurately. Another concern is that all the stack emissions must be drawn into the dilution tunnel. In this study, the collection hood is positioned low enough over the stack to insure collection of all stack emissions. For efficiency tests an induced draft will alter the stove performance, and careful sizing and positioning of the collection hood is thus required to insure collection of all the stove emissions without altering the stove performance. If water condensed between the stack sampling probe and the dilution probe, the CO concentration would increase due to the decrease in water vapor concentration. This would cause errors in flow measurement, since the increase in the CO concentration between sample probes would result in an apparent flow increase. Water condensation generally would not occur in the dilution tunnel if dilution is adequate. Water condensation in the stack could occur, and therefore the sample probe needs to be located near the top of the stack to minimize the possibility of water condensing before the gas reaches the dilution tunnel. An additional advantage of the probe being near the top of the stack is that the stack gases are well mixed at this point.

5.2.2 Pitot Array

The pitot array has the advantage giving a continuous real time output. The other methods, as practiced in this study, did not have this feature although the CO tracer could with some design changes. Other advantages include ease of operation, and very quick response time to changing flow conditions. The sensitivity of the calibration coefficient to stack Reynolds numbers is lower than most other flow measuring devices as shown in Table I. The cost of the pitot array system used in this study is approximately 4000 dollars, the differential pressure transducer being about 75 percent of the cost.

As shown in Appendix A, the calibration curve shifted by one to two percent each time the stove was fired. Particulate accumulation on the array was believed to have caused this shift. These calibration shifts require the pitot array to be calibrated after each stove firing. This is a disadvantage of the system. Noise in the transducer signal can be a problem with obtaining an output signal that represents the average velocity in the stack. To correct this problem, the signal was electrically filtered. A time constant of 15 seconds was found to be necessary in order to obtain a signal which is virtually free of noise.

The stack operates in the transition region, and therefore in theory either a laminar or a turbulent velocity profile could exist in the stack. For a given mass flow, the differential pressure measured with the array would be different for a turbulent velocity profile than it would be for a laminar velocity profile. Even when the flow through the impact tubes of the array is considered, the differential pressures for the two types of velocity profiles would still differ. Therefore,

two different mass flows would be measured with the array even though the mass flow for both profiles is the same. This gives an uncertainty in the measured flow. However, if one considers the flow disturbances in a stove pipe (creosote build-up on the walls and several pipe joints), then there is a high probability that these flow disturbances will trip the flow into turbulence when in the transition region. If this is true, then a turbulent velocity profile would exist for most of a run and an accurate flow measurement could be achieved provided the array is calibrated using turbulent flow.

5.2.3 Scale-Based Method

The scale-based method has the advantage of using equipment which has historically been required to conduct an efficiency test. The cost of the three analyzers and the electronic scale used for the scale-base method in this study is about \$15,000. However, it is possible to use an ORSAT analyzer and reduce the cost to \$4,000. Data from the literature has shown that the sum of dry basis CO, CO₂ and O₂ concentrations usually ranges between 20 and 22 percent. Therefore, if two concentrations are measured then a third concentration can be obtained using the fact that the sum should be about 21 percent. Another advantage is that no additional calibrations other than those for the analyzers are needed. The disadvantage of this method is that flow measurements are time-averaged and not real time. If the test time intervals are shortened then problems with measuring the burn rates accurately may occur, as experienced in this study.

6. CONCLUSIONS

The following conclusions are based on the results of this study. They may not be true for a full range of appliances and operating conditions.

Comparison of the sensible energy losses calculated from the centerline and bulk temperatures show that the centerline temperatures overestimate the sensible energy losses by 3 to 5 percent. This would result in an error of 1.5 to 2.5 percentage points in the overall efficiency for appliances with a sensible energy loss around 50 percent of the total input energy. For this type of appliance, a thermocouple array would be necessary. The true bulk temperature is never calculated from the profile data since the velocity profiles in the stack had to be assumed. Therefore, there is a possibility that the bulk temperature calculated from the array data could be wrong.

The comparison between the aspirated and non-aspirated thermocouple readings is questionable for both tests performed since the aspirated thermocouple temperature was sometimes lower than the non-aspirated thermocouple temperature. If the results are correct, then an unshielded fine gage thermocouple array is more appropriate for high stack temperature measurement (above 250°) than the thermocouple array used in this study. Further testing is needed to verify the radiation errors measured in this study.

Good agreement between the CO tracer and the pitot array (i.e., flows differ by less than 10%) was usually observed. Sometimes poor agreement (i.e., flows differ by more than 15%) was observed, especially at the beginning and end of a run or following an abrupt change in the

flow rate. The reason(s) for this poor agreement are unknown, but possible reasons are:

1. Hysteresis in the pitot array transducer.
2. Laminar flow in the stack could increase the errors in the pitot array measurement due to flow through the impact tubes.
3. Inaccuracy of the CO analyzer at CO concentrations around 0.05 percent.

The author believes that reasons 1 and 2 are the most probable for the observed poor agreement.

The scale-based method is hampered by noisy scale readings which prevented an accurate measurement of the burn rate over short-time intervals. The use of a longer time interval improves the scale-based flow measurement but the agreement with the other methods is still poor. The most probable reason for the poor agreement for the recalculated flows is obtaining an accurate burn rate from the scale plots of runs 4 and 5.

7. RECOMMENDATIONS

Based on the need to develop accurate stack flow and temperature measurement techniques for stack loss efficiency tests, the author makes the following recommendations.

1. Further measurement of radial temperature profiles for different stoves and chimneys needs to be done to determine if the profiles measured in this study are typical for other appliances.
2. Measurement of the radiation errors should be done with the suction pyrometer and the unshielded thermocouple being at essentially the same location in the stack. This would eliminate any uncertainty in the temperature differences measured due to the location of the pyrometer and the thermocouple being different.
3. Testing of the thermal mass flowmeter and the CO₂ tracer.
4. A test method to validate a flow measurement system is needed to determine if any of the flow methods indicates the true stack flow. A method using an air-tight gaseous fuel combustor, in which the fuel and air input are measured, could be used to test whether the pitot array, CO₂ tracer, and the thermal mass flowmeter indicate the true stack flow.
5. Calculate the errors due to flow through the impact tubes of the pitot array using a method similar to that presented by Gasiorrek [17]. The calculations should be done for both laminar and turbulent flows since both may exist in the stack during a run.

8. REFERENCES

1. Test Protocol for Indirect Measurement of the Heating Performance of Wood-Fired, Closed Combustion-Chamber Heating Appliances, (Wood Heating Alliance. Washington, D.C.), 1982.
2. Personal conversation with Jay Shelton, Shelton Energy Research, Santa Fe, New Mexico.
3. Tiegs, P., "Efficiency and Emission Testing for Residential Wood-Fired Appliances," Omni Environmental Services, Inc., Beaverton, OR.
4. Staab, J., H. Klingenberg, and D. Schurmann, "Strategy for the Development of a New Multicomponent Exhaust Emissions Measurement Technique," Paper No. 830437, Society of Automotive Engineering, Warrendale, PA, 1983.
5. Macumber, D. W., and D. R. Jaasma, "Efficiency and Emissions of a Hand Fired Residential Coalstove," in Residential Solid Fuels, (J. Cooper and D. Malek, eds.), Oregon Graduate Center, Beaverton, OR, 1982.
6. Thomas, C. C., "The Measurement of Gases," Journal of the Franklin Institute, Vol. 172, pp. 1191.
7. Zinsmeister, G. E., "Applications and Analysis of Thermal Flowmeters," Ph.D. Thesis, Purdue University, 1965.
8. Richards, A. M., and F. W. Kuether, "A New Velocity Probe for Sensing Pulsatile Blood Flow," IRE Transactions on Medical Electronics, Vol. ME-6, 1959.
9. Barnett, S. G., and D. Shea, "Effects of Woodstove Design and Operations on Condensable Particulate Emissions," in Residential Solid Fuel, Loc. Cit.
10. Laub, J. H., "Measuring Mass Flow with the Boundary-Layer Flowmeter," Control Engineering, Vol. 4, No. 3, 1957.
11. Butcher, S. S., and M. J. Ellenbecker, "Particulate Emission Factors for Small Wood and Coal Stoves," in Residential Solid Fuels, Loc. Cit.
12. "Standard Method of Test for Average Velocity in a Duct (Pitot Tube Method)," ASTM Test Code D 3 154-72,
13. Burton, C. L., "Quantitation of Stack Gas Flow," Journal of the Air Pollution Control Association, Vol. 22, 1972.

14. Brown, N., "A Mathematical Evaluation of Pitot Tube Traverse Methods," ASHRAE Transactions, Part 1, 1975.
15. Preston, M. A. "The Three-Quarter Radius Pitot Tube Flow Meter," The Engineer, Oct. 27, 1950.
16. Ma, V. H. L., "The Averaging Pressure Tubes Flowmeter for the Measurement of the Rate of Airflow in Ventilating Ducts and for the Balancing of Airflow Circuits in Ventilating Systems," Journal of the Institution of Heating and Ventilating Engineers, Vol. 34, 1967.
17. Gasiorek, J. M., "The Use of Inter-connected Pitot-Static Tubes for Air-Flow Measurement," Building Services Engineer, Vol. 41, 1974.
18. Jaasma, D. R., "Wood Stove Efficiency Determination Using Stack-Loss Method: Sensitivity to Measurement Errors and Assumed Elemental Analysis," ASHRAE Transactions, Vol. 88, Part 2, 1982.
19. Shelton, J. W., L. Graeser, and D. R. Jaasma, "Sensitivity Study of Traditional Flue Loss Methods for Determining Efficiencies of Solid Fuel Heaters," ASME Paper No. 84-WA/Sol-39.
20. Hubble, B. R., and J. B. L. Harkness, "Results of Laboratory Tests on Wood-Stove Emissions and Efficiency," Conference on Wood Combustion Environmental Assessment, New Orleans, LA, Feb. 21-24, 1981.
21. Pierce, T. L., and D. R. Jaasma, "Use of Sensitized Fluorescence and Total Incompletely Oxidized Carbon For Measurement of Non-Criteria Emissions from Residential Woodstoves," Proceedings: Measurement and Monitoring of Non-Criteria (Toxic) Contaminants in Air, (E. R. Fredrick, ed.), Air Pollution Control Association, Pittsburgh, PA, March 1983.
22. Standard Measurement Guide: Section on Temperature Measurements: ASHRAE Standard 41.1-74.
23. "Temperature Measurement." ASME Power Test Code PTC 19.3-1961.
24. Dutt, M., "On the Measurement of Average Temperature in Circular Ducts," Advances in Test Measurement, Vol. 5, Proceedings of the 5th Annual ISA Test Measurement Symposium, NY, Oct. 28-31, 1968.
25. Mackenzie, D. M., and W. E. Kehret, "Review of Temperature Measurement Techniques," Part I & II, Instrumentation Technology, Sept., 1976.
26. Improving the Efficiency, Safety, and Utility of Wood Burning Units, Quarterly Report No. WB-6, Dept. of Mechanical Engineering, Auburn University (Auburn, AL, 1979.).

27. Powell, R. L., W. J. Hall, C. H. Hyink, Jr., and L. L. Sparks, "Temperature Reference Tables Based on the IPTS-68," NBS Monograph 125, 1974.
28. Holman, J. P., Experimental Methods for Engineers, McGraw-Hill Book Company, 1978.

9. APPENDIX A CALIBRATION PROCEDURES

A.1 Calibration of the Pitot Array

The pitot array was calibrated at room temperature using a CO tracer technique. To induce a flow through the stack, the stove was slightly pressurized using a compressed air line. Pure CO was injected into the stove pipe at the breech of the stove. The CO flow rate was measured using a dry gas meter. Two CO analyzers were used to measure the CO concentrations. These analyzers were simultaneously multiplexed between the stack and the dilution tunnel. The stack flow was determined by

$$\dot{m}_S = MW_S \dot{n}_{DT} \frac{[CO]_{DT}}{[CO]_S} \quad (33)$$

The dilution tunnel molar flow rate was determined using the orifice. The stack flow was also determined by

$$\dot{m}_S = \dot{m}_{IR} / [CO]_S \quad (34)$$

where

$$\dot{m}_{IR} = \text{mass flow rate of injected CO, kg/s}$$

The stack flow was calculated using Eq. (33) and (34) with the data from each CO analyzer, thus a total of four stack flows were calculated. These four stack flows were then averaged. The average

stack flow was used to calculate the flow coefficient of the pitot array, which is given by:

$$C_{DP} = \frac{\dot{m}_{ave}}{A_S \left(\frac{2\Delta P_{PA}}{RT_S} \right)^{1/2}} \quad (35)$$

where

$$\dot{m}_{ave} = \text{Average stack flow, kg/s .}$$

The calibration was done for a range of stack flows. CO concentrations used for these calibration tests ranged from 1.1 to 2.5 percent in the stack and 0.1 to 0.3 percent in the dilution tunnel. The greatest difference between the average stack flow and the four stack flows from which the average flow was calculated from was less than 2 percent.

The calibration coefficient calculated from Eq. (35) is plotted versus the indicated mass flow (i.e. the mass flow calculated from the pitot signal assuming a coefficient of unity) and this plot is shown in Fig. (40). The calibration curves shown in this figure were used to obtain the calibration coefficients used for data reduction. (Due to a shift in the calibration coefficients each time the stove was fired, these calibration curves were fit mid-way between the pre-test and the post-test calibration curves.) A stack mass flow was then calculated based on the indicated mass flow and the calibration coefficient.

The raw data used to calibrate the pitot array is given in Tables (A.1-A.3). The curve fits to the calibration curves of the analyzer are given in Table A.4.

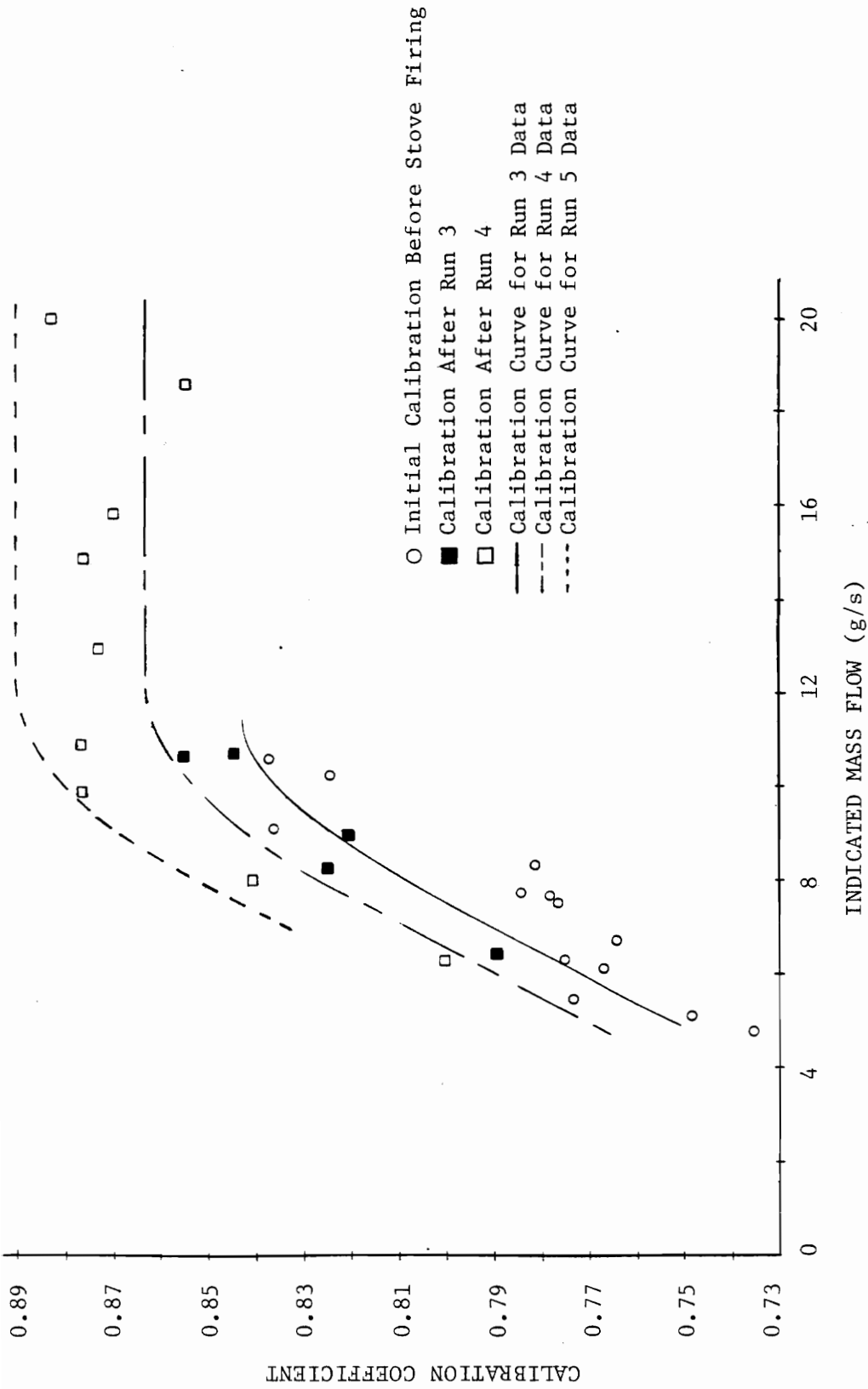


Figure 41. Calibration Data for Pitot Array

Table A.1: Initial Pitot Array Calibration Data

C _{OR}	ΔP_{OR} ("H ₂ O)	Stack		Dilution Tunnel		CO Injection Rate ^{**} ($\mu\text{/s} \times 10^{-2}$)	Pitot Array [*] Volts	C _{DP}
		V _{OUT} ¹	V _{OUT} ²	V _{OUT} ¹	V _{OUT} ²			
0.694	1.35	5.27	0.614	0.910	0.0480	8.26	0.165	0.773
	1.34	5.53	0.657	0.915	0.0483	8.29	0.142	0.748
	1.34	5.76	0.692	0.913	0.0484	8.29	0.124	0.735
	1.34	5.03	0.576	0.916	0.0485	8.27	0.202	0.767
	1.35	4.81	0.538	0.915	0.0490	8.26	0.243	0.764
	1.35	4.53	0.491	0.923	0.0491	8.28	0.304	0.776
0.701	1.42	4.00	0.420	0.890	0.0480	8.46	0.450	0.836
	1.46	4.29	0.466	0.869	0.0465	8.47	0.378	0.781
	1.45	4.48	0.496	0.880	0.0469	8.53	0.320	0.784
	1.44	3.80	0.389	0.881	0.0470	8.48	0.572	0.824
	1.40	4.93	0.563	0.880	0.0465	8.31	0.215	0.775
	1.38	4.43	0.492	0.873	0.0470	8.37	0.320	0.777
	1.38	3.57	0.363	0.873	0.0468	8.29	0.618	0.837

1 CO Tracer Analyzer (AIA)

2 PIR 2000 Analyzer

* 0.001" H₂O Range

** Based on 27°C, 95 kPa

Table A.2: Post Run 3 Pitot Array Calibration Data

C _{OR}	ΔP_{OR} (¹ H ₂ O)	Stack		Dilution Tunnel		CO Injection Rate** ($\ell/s \times 10^{-2}$)	Pitot Array* Volts	C _{DP}
		V _{OUT} ¹	V _{OUT} ²	V _{OUT} ¹	V _{OUT} ²			
0.706	1.36	4.37	0.475	1.170	0.0675	12.16	0.628	0.884
	1.36	3.83	0.384	0.966	0.0515	9.09	0.620	0.855
	1.37	4.24	0.451	0.965	0.0516	9.20	0.435	0.820
	1.37	5.10	0.595	0.966	0.0523	9.18	0.224	0.789
	1.36	4.38	0.480	0.960	0.0519	9.15	0.364	0.825

1 CO Tracer Analyzer (AIA)

2 PIR 2000 CO Analyzer

* 0.001 " H₂O Range

** Based on 24°C, 94.5 kPa

Table A.3: Post Run 4 Pitot Array Calibration Data

C _{OR}	ΔP_{OR} ($"H_2O$)	Stack		Dilution Tunnel		CO Injection Rate** ($\ell/s \times 10^{-2}$)	Pitot Array* Volts	C _{DP}
		V _{OUT} ¹	V _{OUT} ²	V _{OUT} ¹	V _{OUT} ²			
0.701	1.35	3.36	0.316	1.105	0.0622	11.04	0.454	0.869
	1.34	3.80	0.378	1.127	0.0633	11.04	0.306	0.873
	1.33	3.85	0.340	1.133	0.0635	11.05	0.277	0.879
	1.32	3.24	0.285	1.037	0.0635	11.08	0.630	0.854
	1.36	2.83	0.245	1.039	0.0580	9.93	0.697	0.884
	1.35	4.95	0.565	1.750	0.120	21.92	0.400	0.876
	1.35	5.41	0.637	0.730	0.122	22.00	0.282	0.876
	1.35	4.28	0.457	1.750	0.122	21.97	0.733	0.882

1 CO Tracer Analyzer (AIA)

2 PIR 2000 CO Analyzer

* 0.001 " H₂O Range

** Based on 24°C, 94.5 kPa

Table A.4: CO Analyzer Calibration Curve Equations

AIA CO ANALYZER

<u>VOLTAGE RANGE</u>	<u>EQUATION</u>
$0 < V_{OUT} < 0.33$	$\%CO = 1.530 \times 10^{-4} + 0.09408 V_{OUT}$
$0.33 < V_{OUT} < 0.54$	$\%CO = 0.1133 V_{OUT} - 0.006400$
$0.54 < V_{OUT} < 0.96$	$\%CO = 0.1418 V_{OUT} - 0.02175$
$0.96 < V_{OUT} < 1.15$	$\%CO = 0.1750 V_{OUT} - 0.05333$
$1.15 < V_{OUT} < 1.71$	$\%CO = 0.2411 V_{OUT} - 0.12923$
$1.71 < V_{OUT} < 2.27$	$\%CO = 0.2873 V_{OUT} - 0.2091$
$2.27 < V_{OUT} < 2.82$	$\%CO = 0.3764 V_{OUT} - 0.4113$
$2.82 < V_{OUT} < 3.30$	$\%CO = 0.4604 V_{OUT} - 0.6484$
$3.30 < V_{OUT} < 3.80$	$\%CO = 0.5533 V_{OUT} - 0.9550$
$3.80 < V_{OUT} < 5.46$	$\%CO = 0.7213 V_{OUT} - 1.6586$
$5.46 < V_{OUT} < 6.02$	$\%CO = 0.8902 V_{OUT} - 2.5255$
$6.02 < V_{OUT} < 6.54$	$\%CO = 1.1339 V_{OUT} - 4.00634$
$6.54 < V_{OUT} < 7.39$	$\%CO = 1.2352 V_{OUT} - 4.6788$
$7.39 < V_{OUT} < 8.38$	$\%CO = 1.4937 V_{OUT} - 6.6078$
$8.38 < V_{OUT} < 9.52$	$\%CO = 1.8947 V_{OUT} - 9.9480$

PIR 2000 Analyzer

$$\%CO = 2.206 \times 10^{-5} + 0.0211 V_{OUT} + 2.192 \times 10^{-4} V_{OUT}^2 - 1.073 \times 10^{-6} V_{OUT}^3 + 1.774 \times 10^{-8} V_{OUT}^4$$

A.2 Calibration of Dilution Tunnel Orifice

A 7.6 cm diameter orifice was used to measure the dilution tunnel flow rate. Calibration of the orifice plate was performed with a CO₂ tracer. The injection rate of the tracer needs to be high because of the high flow in the dilution tunnel. Therefore CO was not used due to its poisonous nature. The CO₂ was injected 3 m above the orifice plate to insure adequate mixing before reaching the orifice. The injection rate of CO₂ was measured with a dry gas meter (Singer AL-425).

The diluted CO₂ concentration was measured downstream of the orifice with a CO₂ analyzer. Using the conservation of CO₂, the molar flow rate of the dilution tunnel is given by

$$\dot{n}_{DT} = \dot{n}_{CO_2} \frac{[CO_2]_{sup}}{[CO_2]_{DT}} \quad (36)$$

where

$[CO_2]_{sup}$ = mole fraction of CO₂ in supply bottle, 0.998.

$[CO_2]_{DT}$ = mole fraction of CO₂ in tunnel minus the CO₂
concentration of room air

CO₂ concentrations in the dilution tunnel were typically around one percent. Problems with supply bottle regulator icing prevented the use of higher CO₂ concentrations. The CO₂ in room air was measured prior to the calibration test and this concentration was subtracted from the measured CO₂ concentration of the dilution tunnel.

The dilution tunnel temperature was measured along with the pressure drop across the orifice plate. The discharge coefficient of

the orifice is determined from

$$C_{OR} = \frac{MW_{DT} \dot{n}_{DT}}{A_{OR} \left(\frac{2 \Delta P_{OR} P}{R T_{DT}} \right)^{1/2}} \quad (37)$$

The molecular weight and density were determined by the following

$$MW_{DT} = (MW Y)_{H_2O} + (MW Y)_{CO_2} + (MW Y)_{DA} \quad (38)$$

and

$$\rho_{DT} = (\rho Y)_{H_2O} + (\rho Y)_{CO_2} + (\rho Y)_{DA} \quad (39)$$

where

- MW_{H_2O} = molecular weight of H_2O , 18.01 kg/kmol
- MW_{CO_2} = molecular weight of CO_2 , 44.09 kg/kmol
- MW_{DA} = molecular weight of dry air, 28.97, kg/kmol
- Y_i = mole fraction of species i
- ρ_i = density of species i

Three data sets were taken for each calibration test run. A discharge coefficient was calculated for each data set and an average of the three was used. A total of 31 calibration tests were performed for this study of which the mean coefficient is 0.698. The standard deviation was 0.0066 which showed that very good agreement between calibration tests was achieved and that the particulate build up on the orifice was not

large enough to appreciably change the coefficient. The flow in the dilution tunnel typically varied between 79 and 86 g/s during a test. The flow in the tunnel was typically around 86 g/s during a calibration test and therefore the flows are similiar enough not to have an appreciable effect on the discharge coefficient.

10. APPENDIX B UNCERTAINTY ANALYSIS

The uncertainty analysis applied to the CO tracer and the pitot array methods is described herein. This uncertainty analysis considers only random errors. The uncertainty of a function $F = F(x,y,z)$ can be written as:

$$E_F = \left[\left(e_x \frac{\partial F}{\partial x} \right)^2 + \left(e_y \frac{\partial F}{\partial y} \right)^2 + \left(e_z \frac{\partial F}{\partial z} \right)^2 \right]^{1/2} \quad (40)$$

where

E_F = the uncertainty in the function F

e = uncertainty in the independent variables of F .

An estimate on e_x , e_y , etc. is made based on experience and judgement. Some errors may be small compared to others and are usually neglected. This method of calculating the uncertainty is detailed in reference (27).

The flow rate measured from the CO tracer is calculated from:

$$\dot{m}_S = \dot{n}_{DT} MW_S \frac{[CO]_{DT}}{[CO]_S} \quad (41)$$

A separate error analysis is first required for the dilution tunnel flow measurement. The dilution tunnel molar flow rate is given by

$$\dot{n}_{DT} = \frac{C_{OR}^A}{MW_{DT}} \left(\frac{2\Delta P_{OR} P}{R T_{DT}} \right)^{1/2} \quad (42)$$

Error in the measurement of ΔP_{OR} , T_{DT} , P , and C_{OR} , are considered. The partial derivatives required are:

$$\frac{\partial \dot{n}_{DT}}{\partial C_{OR}} = \frac{A_{OR}}{MW_{DT}} \left(\frac{2\Delta P_{OR} P}{R T_{DT}} \right)^{1/2} \quad (43)$$

$$\frac{\partial \dot{n}_{DT}}{\partial \Delta P_{OR}} = \frac{1}{2} \frac{C_{OR}}{MW_{DT}} \left(\frac{2 P}{R T_{DT} \Delta P_{OR}} \right)^{1/2} \quad (44)$$

$$\frac{\partial \dot{n}_{DT}}{\partial T_{DT}} = -\frac{1}{2} \frac{C_{OR} A_{OR}}{MW_{DT}} \left(\frac{2\Delta P_{OR} P}{R} \right)^{1/2} T_{DT}^{-3/2} \quad (45)$$

$$\frac{\partial \dot{n}_{DT}}{\partial P} = \frac{1}{2} \frac{C_{OR} A_{OR}}{MW_{DT}} \left(\frac{2\Delta P_{OR}}{R T_{DT}} \right)^{1/2} \quad (46)$$

The estimated errors associated with each measurement and the typical value of the measurement encountered during testing are:

$$C_{OR} = 0.698$$

$$e_{C_{OR}} = 0.0135 \quad ; \text{ two times the standard deviation of the average calibration coefficient}$$

$$\Delta P_{OR} = 336 \text{ Pa}$$

$$e_{\Delta P_{OR}} = 4.98 \text{ Pa} \quad ; \text{ accuracy of manometer plus ability to read fluctuating signal}$$

$$T_{DT} = 30^\circ\text{C}$$

$$e_{T_{DT}} = 1^\circ\text{C} \quad ; \text{ estimate of dilution tunnel temperature measurement}$$

$$P = 94.8 \text{ kPa}$$

$$e_P = 0.169 \text{ kPa} \quad ; \text{ accuracy of barometer plus changes in room pressure during a test}$$

The calculated uncertainty for the dilution tunnel flow measurement is 2.3 percent. The main contribution to the uncertainty is the ΔP_{OR} while the least was the room pressure measurement. The uncertainty in the tunnel flow can now be used in the uncertainty analysis of the stack flow measurement. The partial derivatives required for these calculations are:

$$\frac{\partial \dot{m}_S}{\partial \dot{n}_{DT}} = \frac{[CO]_{DT}}{[CO]_S} MW_S \quad (47)$$

$$\frac{\partial \dot{m}_S}{\partial [CO]_{DT}} = \dot{n}_{DT} MW_S \left(\frac{1}{[CO]_S} \right) \quad (48)$$

$$\frac{\partial \dot{m}_S}{\partial [CO]_S} = - \dot{n}_{DT} MW_S [CO]_{DT} \left(\frac{1}{[CO]_S} \right)^2 \quad (49)$$

The estimated error associated with each measurement and the range of values typically encountered during testing are:

$$\dot{n}_{DT} = 2.73 \times 10^{-3} \text{ to } 2.96 \times 10^{-3} \text{ kmol/s}$$

$$e_{\dot{n}_{DT}} = 6.14 \text{ to } 6.66 \times 10^{-5} \text{ kmol/s} \quad ; \text{ based on previously calculated uncertainty of 2.3\%}$$

$$\%CO_{DT} = 0.45 \text{ to } 0.04\%$$

$$e_{\%CO_{DT}} = 0.024 \text{ to } 0.004 \quad ; \text{ based on an uncertainty of 5\% of the reading due to the possible inaccuracy of the calibration curve at low concentrations plus "dead space" on strip recorder}$$

$$\%CO_S = 3.6 \text{ to } 0.8\%$$

$$e_{\%CO_S} = 0.077 \text{ to } 0.021$$

; represents 2% of the reading due to the uncertainty in the calibration curve at higher concentrations plus "dead space" on strip recorder

The error values for $[CO]_S$ and $[CO]_{DT}$ will vary with the magnitude of these measurements. The estimated uncertainty for the CO tracer flow measurement is calculated to be between 6 and 11 percent. The main contribution to the uncertainty is the dilution tunnel concentration measurement.

The flow rate measured from the pitot array is calculated from:

$$\dot{m}_S = C_{DP} A_S \left(\frac{2\Delta P_{PA} P}{R T_S} \right)^{1/2} \quad (50)$$

and

$$\Delta P_{PA} = \left(248.9 \frac{\text{Pa}}{\text{H}_2\text{O}} \right) (0.001 \text{ H}_2\text{O}) (V_{out}) \quad (51)$$

where

V_{out} = equivalent voltage output of manometer on 0.001"H₂O range

Substituting Eq. (50) into (51)

$$\dot{m}_S = C_{DP} A_S \left(\frac{2(0.2489) V_{out} P}{R T_S} \right)^{1/2} \quad (52)$$

Error in the measurement of C_{DA} , A_S , V_{out} , T_S , and P are considered.

The partial derivatives required for the analysis are:

$$\frac{\partial \dot{m}_S}{\partial A_S} = C_{DP} \left(\frac{2(0.248) V_{out} P}{R T_S} \right)^{1/2} \quad (53)$$

$$\frac{\partial \dot{m}_S}{\partial C_{DP}} = A_S \left(\frac{2(0.248) V_{out} P}{R T_S} \right)^{1/2} \quad (54)$$

$$\frac{\partial \dot{m}_S}{\partial T_S} = -\frac{1}{2} C_{DP} A_S \left(\frac{2(0.248) V_{out} P}{R} \right)^{1/2} T_S^{-3/2} \quad (55)$$

$$\frac{\partial \dot{m}_S}{\partial V_{out}} = \frac{1}{2} C_{DP} A_S \left(\frac{2(0.248) P}{R T_S V_{out}} \right)^{1/2} \quad (56)$$

$$\frac{\partial \dot{m}_S}{\partial P} = \frac{1}{2} C_{DP} A_S \left(\frac{2(0.248) V_{out}}{R T_S P} \right)^{1/2} \quad (57)$$

The estimated errors associated with each measurement and the range of values typically encountered during testing are:

$$A_S = 0.01824 \text{ m}^2$$

$$e_{A_S} = 1.8 \times 10^{-4} \text{ m}^2 \quad ; \text{ one percent change due to thermal expansion of the stove pipe section.}$$

$$C_{DP} = 0.77 \text{ to } 0.89$$

$$e_{C_{DP}} = 0.023 \text{ to } 0.034 \quad ; \text{ accounts for scatter of calibration data points and shift in calibration curve. Varies between 3.0 and 3.9 percent of the calibration coefficient.}$$

$$T_s = 82 \text{ to } 292^{\circ}\text{C}$$

$e_{T_s} = 8^{\circ}\text{C}$; estimate of stack temperature measurement error

$$V_{\text{OUT}} = 0.23 \text{ to } 0.60 \text{ V}$$

$e_{V_{\text{out}}} = 0.020 \text{ V}$; ability to obtain the average output voltage during the flow measurement interval from the strip chart recorder

$$P = 94 \text{ kPa}$$

$e_p = 0.169 \text{ kPa}$; accuracy of barometer plus change in room pressure during a test

The estimated uncertainty for the pitot array varied between 4 and 7 percent depending on the magnitude of the flow rate. The main contribution to the uncertainty is the V_{OUT} measurement and the smallest contribution was the room pressure measurement.

11. APPENDIX C TEMPERATURE ANALYSIS

C.1 Temperature Modeling

An analytical model was developed to predict the insulated length of stove pipe required for an initial radial temperature gradient to disappear. If the insulated section was perfectly adiabatic, then the bulk temperature (i.e., the energy-averaged temperature) would remain constant. This would allow the measurement of the bulk temperature to be made where the radial gradients no longer exist, and therefore the measurement would be trivial. The place where uniform temperature profiles exist would also be the ideal location for placement of flowmeters which are affected by temperature gradients. For example, the thermal mass flowmeter requires the measurement of the bulk temperature upstream and downstream of the heater.

The following assumptions were made for the analytical model:

1. The heat transfer is one dimensional
2. The walls are adiabatic
3. The initial temperature profile is parabolic
4. Plug flow exists

If the velocity of the gas is known, then distance can be related to time. The governing equation can be written as:

$$\frac{1}{r} \frac{\partial}{\partial r} \left(r \frac{\partial \theta}{\partial r} \right) = \frac{\rho C_P}{k} \frac{\partial \theta}{\partial t} \quad (58)$$

where

$$\theta(r,t) = T(r,t) - T_{ave}$$

r = radius in duct

The initial condition and boundary condition are the following:

$$\text{IC: } \theta(r,0) = \theta(R_w,0) + [\theta(0,0) - \theta(R_w,0)][1 - (r/R_w)^2]$$

$$\text{BC: at } R = R_w \frac{\partial \theta(R_w, t)}{\partial r} = 0$$

$$\text{BC: at } R = R_w \frac{\partial \theta(0, t)}{\partial r} = 0$$

The solution of the governing equation via separation of variables yields:

$$\frac{d\tau}{dt} + \alpha\lambda^2\tau = 0 \quad (59)$$

and

$$\frac{d}{dr} \left[r \frac{d\phi}{dr} \right] + r\lambda^2\phi = 0 \quad (60)$$

where

$$\theta(r,t) = \phi(r,t) \tau(t)$$

$$\alpha = k/\rho C_p$$

λ = separation constant

Solving for $\theta(r,t)$ gives:

$$\theta(r,t) = b_o + \sum b_n J_o(\lambda_n r) \exp[-\alpha \lambda_n^2 t] \quad (61)$$

where

$$b_o = \frac{1}{2} [\theta(0,0) + \theta(R_w,0)]$$

$$b_n = \frac{-4[\theta(R_w,0) - \theta(0,0)]}{\lambda_n^2 R_w^2 J_o(\lambda_n R_w)}$$

The time required for both the centerline ($T(0,t)$) and the wall ($T(R_w,t)$) temperature to approach the average temperature can now be calculated. The following conditions were used:

$$T(0,0) = 343 \text{ C}$$

$$T(R_w,0) = 316 \text{ C}$$

$$\alpha = 7.5 \times 10^{-5} \text{ m}^2/\text{s}$$

$$T_{AVE} = 330 \text{ C}$$

Using the first six terms of the summation, the temperature can be calculated as a function of time. A time period of 10 seconds is required before the difference between the average temperature and the temperature at either the wall or the centerline is less than 5°C. The

velocity of the stack gas in in the range of 0.2-1.4 m/s and thus the stack length required is 2-14 meters depending on the velocity. This indicates that significant radial temperature gradients will be present in the flow, even with a perfectly adiabatic stack.

C.2 Bulk Temperature Calculation

The bulk temperature in a duct or pipe is given by the following:

$$T_b = \frac{\int u \rho C_p T 2\pi r dr}{\int u \rho C_p 2\pi r dr} \quad (62)$$

Assuming a flat velocity profile, a constant specific heat, and constant density across the duct, Eq. (62) can be written as

$$T_b = \frac{\int 2\pi r T dr}{\int 2\pi r dr} \quad (63)$$

The integrals can be approximated by partitioning the duct into several smaller areas and then assume that the temperature in each of these smaller areas is constant.

$$T_b = \frac{A_1 T_1 + A_2 T_2 + \dots + A_n T_n}{A_1 + A_2 + \dots + A_n} \quad (64)$$

where

n = number of temperature measurement locations.

If the temperatures are measured with an equal area arrangement, then the area in the numerator of Eq. (64) can be factored out.

12. APPENDIX D FLOW MEASUREMENT DATA AND RESULTS

Table D.1: Summary of Flow Measurements from Run 3

Flow Measurement <u>No.</u>	CO Tracer <u>(g/s)</u>	Pitot Array <u>(g/s)</u>	Difference* <u>%</u>
1	3.4	5.1	32.3
2	4.2	4.6	10.1
3	3.8	4.5	15.5
4	3.7	4.0	8.5
5	5.0	5.3	6.1
6	4.8	5.3	10.1
7	5.2	5.4	3.7
8	5.3	5.9	10.2
9	5.3	5.6	4.1
10	5.0	5.5	8.8
11	5.0	5.3	6.0
12	5.1	5.9	12.7
13	5.8	5.8	-0.2
14	2.9	4.1	30.0
15	2.7	4.6	40.5
16	2.6	4.5	42.3
17	3.1	4.4	30.5
18	2.4	4.6	47.4

* Based on Pitot Array Flow Measurement

Table D.2: Summary of Flow Measurements from Run 4

Flow Measurement No	CO Tracer (g/s)	Scale- Based (g/s)	Pitot Array (g/s)	Difference* (CO Tracer) %	Diff.* (Scale) %
1	13.9	13.5	14.9	6.7	5.9
2	7.9	9.9	7.8	- 0.87	- 25.9
3	10.5	11.0	10.3	- 2.6	- 7.5
4	7.9	6.2	8.2	4.1	24.6
5	9.3	6.7	8.9	- 4.1	25.0
6	8.4	6.6	8.8	4.6	- 25.4
7	8.5	8.8	8.1	- 5.3	- 8.8
8	5.5	6.7	5.9	6.6	- 14.7
9	4.7	5.7	5.7	16.8	- 0.8
10	5.3	7.0	5.2	- 1.7	- 38.5
11	5.4	3.6	5.3	- 7.1	- 27.4
12	5.9	3.9	6.1	2.0	35.3
13	6.1	5.4	6.9	11.2	21.5
14	5.5	6.0	5.9	6.1	- 3.4
15	6.4	6.2	6.6	2.6	4.9
16	3.7	N/D	4.4	17.2	N/D

¹ Recalculated Scale-Based Flow

* Based on Pitot Array Flow Measurement

N/D Not done

Table D.3: Summary of Flow Measurements From Run 5

Flow Measurement No.	CO Tracer (g/s)	Scale- ¹ Based (g/s)	Pitot Array (g/s)	Difference* (CO Tracer) (%)	Difference* (Scale) (%)
1	9.8	17.0	11.9	17.6	-43.6
2	6.2	6.3	7.1	12.1	10.6
3	6.7	12.7	7.0	4.5	-81.7
4	6.3	8.7	6.6	5.6	-31.2
5	4.9	9.9	6.1	18.8	-62.8
6	5.8	4.8	6.2	5.8	22.1
7	6.7	3.3	6.7	0.5	51.3
8	6.2	5.9	7.0	10.6	15.1
9	7.4	6.8	7.1	3.1	4.6
10	7.1	7.7	7.3	3.3	- 5.2
11	6.3	N/D	7.1	10.4	N/D
12	4.8	N/D	6.0	19.8	N/D

¹Recalculated Scale-Based Flow

*Based on Pitot Array Flow Measurement

N/D Not Done

TABLE D. 4: RAW DATA OF RUN3

NO.	STACK ARRAY TEMP. (C)	DILUTION TUNNEL TEMP. (C)	ORIFICE Δ P DROP (H2O)	STACK CO (%)	DILUTION CO (%)	PITOT (VOLTS)	PITOT COEFF.
1	149.50	29.00	1.39	2.7400	0.1080	0.3150	0.7800
2	144.00	28.00	1.37	2.0340	0.0974	0.2640	0.7700
3	140.00	28.50	1.38	2.0270	0.0887	0.2500	0.7690
4	130.00	28.00	1.37	1.7960	0.0758	0.2000	0.7550
5	153.50	30.00	1.39	1.7960	0.1026	0.3420	0.7840
6	156.50	30.00	1.37	1.7600	0.0977	0.3500	0.7840
7	158.50	30.00	1.37	1.3640	0.0822	0.3630	0.7820
8	163.00	31.00	1.36	1.4430	0.0886	0.4200	0.7940
9	147.50	30.00	1.31	1.5010	0.0950	0.3700	0.7890
10	141.50	30.00	1.32	1.4060	0.0836	0.3600	0.7880
11	136.00	29.00	1.32	1.2120	0.0711	0.3310	0.7840
12	220.00	33.00	1.32	0.9440	0.0571	0.4650	0.7930
13	198.00	33.50	1.31	0.9550	0.0659	0.4400	0.7930
14	135.50	28.50	1.32	1.5870	0.0534	0.2100	0.7580
15	112.00	27.00	1.32	1.4210	0.0452	0.2400	0.7700
16	101.50	26.50	1.32	1.4790	0.0446	0.2250	0.7680
17	95.50	26.00	1.32	1.2550	0.0454	0.2210	0.7680
18	96.50	26.00	1.33	1.7680	0.0499	0.2360	0.7710

TABLE D.5: RAW DATA OF RUN 4

NO.	STACK ARRAY TEMP. (C)	DILUTION TUNNEL TEMP. (C)	ORIFICE ΔP DROP (H ₂ O)	STACK CO (%)	DILUTION TUNNEL CO (%)	PITOT ¹ (VOLTS)	PITOT COEFF.
1	310.00	78.50	1.21	5.4470	1.0040	2.9750	0.8630
2	255.00	51.00	1.32	2.5270	0.2421	0.7800	0.8420
3	343.00	61.50	1.27	2.2610	0.2994	1.4760	0.8620
4	303.00	56.50	1.27	1.7900	0.1757	0.9200	0.8460
5	311.00	58.50	1.26	1.6200	0.1890	1.0800	0.8540
6	322.50	60.00	1.28	1.4760	0.1553	1.0800	0.8530
7	340.00	60.00	1.28	1.2160	0.1295	0.9510	0.8450
8	280.50	50.50	1.28	1.6310	0.1102	0.4960	0.8100
9	241.00	45.00	1.29	1.4070	0.0804	0.4330	0.8060
10	228.00	44.50	1.29	1.4610	0.0939	0.3680	0.7950
11	223.00	42.50	1.30	1.8070	0.1177	0.3460	0.7910
12	227.00	42.00	1.29	1.6780	0.1207	0.4780	0.8130
13	212.00	43.50	1.30	1.1660	0.0864	0.5800	0.8280
14	179.50	41.00	1.30	0.7630	0.0506	0.4120	0.8100
15	173.50	41.00	1.28	0.7250	0.0563	0.4950	0.8220
16	144.00	37.00	1.28	0.7930	0.0350	0.2340	0.7800

1. Voltage converted to equivalent 0.15 Pa range

TABLE D. 6: RAW DATA OF RUN5

NO.	STACK ARRAY TEMP. (C)	DILUTION TUNNEL TEMP. (C)	ORIFICE Δ P DROP (H ₂ O)	STACK CO (%)	DILUTION TUNNEL CO (%)	PITOT ¹ (VOLTS)	PITOT COEFF.
1	340.00	68.00	1.28	3.6590	0.4543	1.8490	0.8900
2	234.00	43.50	1.28	2.2370	0.1700	0.6000	0.8530
3	236.50	42.00	1.28	2.5490	0.2083	0.5940	0.8520
4	233.00	41.50	1.29	2.6380	0.2010	0.5390	0.8450
5	218.00	39.50	1.28	2.3980	0.1444	0.4530	0.8340
6	213.50	39.00	1.28	2.0920	0.1479	0.4600	0.8350
7	237.00	39.00	1.27	2.1790	0.1793	0.5520	0.8450
8	256.00	42.00	1.28	2.0710	0.1576	0.6070	0.8520
9	270.00	43.50	1.28	1.6670	0.1504	0.6530	0.8530
10	299.00	47.00	1.27	2.9000	0.2541	0.7160	0.8560
11	249.00	43.00	1.27	1.2840	0.1001	0.6200	0.8530
12	215.50	38.00	1.28	0.8990	0.0529	0.4440	0.8340

1. Voltage converted to equivalent 0.15 Pa range

VITA

The author was born on May 14, 1961 in Miami, Florida. After graduating from Wade Hampton High School in Greenville, SC, he entered Virginia Tech in September of 1979. In June of 1983 he received a Bachelor of Science degree with honors in Mechanical Engineering. Continuing his studies at Virginia Tech, he entered the Master of Science program in September of 1983. In September of 1984 he was married to Kimberly Hope Gilstrap. After completing his Master of Science degree he will return to Greenville and work for CRS Serrine Inc.


Robert M. Bell